Environmental Factors Affecting the Whale Shark Aggregation site in the South Central Red Sea

Dissertation by

Aya Hozumi

In Partial Fulfillment of the Requirements

For the Degree of

Doctor of Philosophy

King Abdullah University of Science and Technology

Kingdom of Saudi Arabia

EXAMINATION COMMITTEE APPROVALS FORM

The dissertation/thesis of Aya Hozumi is approved by the examination committee.

Committee Chairperson: Dr. Burton Jones

Committee Members: Dr. Stein Kaartvedt

Dr. Pei-Ying Hong

Dr. Michael Berumen

Dr. Xabier Irigoen

ABSTRACT

Environmental Factors Affecting the Whale Shark Aggregation site in the South Central Red Sea

Aya Hozumi

Motivation behind the spring whale shark (*Rhincodon typus*) aggregation in Al-Lith, on the Saudi Arabian coast of the South Central Red Sea, is uncertain. A plausible hypothesis is that whale sharks gather to feed on high prey density, leading to questions about the cause of the prey density. A bottom-up process fueled by nutrient input or accumulation from physical advection could create a peak in prey biomass. Wastewater discharged from an aquaculture facility could affect productivity or provide a chemosensory cue for whale sharks. Yet, basic physico-biological oceanography of this region is unresolved. Monthly profiles, long-term moorings, and spatial surveys were used to describe the temporal variability of potential prey biomass and water masses in this region for the first time. Plankton abundance of individuals larger than ~0.7 cm did not peak during whale shark season. Rather, a decrease coinciding the trailing end of whale shark detections was observed. Sites 180 m apart had differences in acoustic backscatter, suggesting small-scale biomass patchiness, supporting the small-scale variability in whale shark habitat selectivity. Red Sea Deep Water, a nutrient-rich water mass formed in the northern Red Sea, appeared in July at the same time the Tokar wind jet from the Sudanese mountain gap is the highest. Gulf of Aden Water, a nutrient-rich water mass from the Indian Ocean, arrived as episodes from May to September, contrary to previous expectations that the water arrives continuously. It is unlikely that these

natural nutrient sources are directly responsible for the high prey density attracting the whale sharks. The aquaculture plume, observed at the aggregation site, had a distinct seasonality from the ambient waters. The plume's highest salinity (>48) approached the extreme limits of coral tolerances. Nutrient concentrations (nitrate, nitrite, phosphate, silica), suspended particulate matter, phytoplankton biomass, bacteria and cyanobacteria cell counts, total nitrogen, and relative abundance of genera associated with opportunistic pathogenic species (e.g., *Arcobacter*) were significantly higher in the plume. This study was the first to estimate the nutrient flux and spatial variability of the aquaculture plume.

ACKNOWLEDGEMENTS

I am grateful for the opportunities, support and enthusiasm Prof. Burt Jones has given me throughout my PhD.

I thank all my committee members, Prof. Xabier Irigoien, Prof. Michael Berumen, Prof. Pei-Ying Hong, and Prof. Stein Kaartvedt, for their time, encouragement, and constructive feedback on my thesis. A special thank you to Pei-Ying for her help in the microbial work and feline companionships, and to Stein for guidance, moral support, and help in the acoustics.

I thank Anders Røstad for teaching me acoustics in the field and on the computer, and for all his patience. I thank Ingrid Solberg and Rita Amundsen for their help in plankton sampling and identification. I thank Mohd Ikram Ansari for his help in lab analysis. I thank Malika Kheireddine for her expert help, moral support, and mentoring. And I thank Isabelle Schulz for her company and help in the field.

Without Jesse Cochran, Amr Gusti, Ahmed Shibl, Fernando Cagua, Pedro De La Torre, and Joseph DiBattista, generously taking their time to drive me down to Al-Lith and help in the field, this thesis would have never happened. Thank you.

I am indebted to Ioannis Georgakakis, Ajay Sancheti, Lloyd Smith, Francis Mallon, Brian Hession, Gazi Aljehdali, Waleed Aljehdali, and Abdullah Aljehdali for all their efforts and preparations to help with my fieldwork. And I cannot emphasize enough the support and friendship the R/V Thuwal captain and crew gave me. I also appreciate the KAUST Coastal and Marine Resources Core Lab,and Dream Divers for their help in logistics and permits.

I am thankful to have learned from the best and meet my classmates at the Maine Ocean Optics course.

I thank KAUST for funding my PhD and people at the RSRC for their support and company.

I thank my grandparents and my parents for all the love and support they send me from afar. And thank you to my friends for keeping my spirits high.

TABLE OF CONTENTS

LIST OF ABBREVIATIONS

ADCP acoustic Doppler current profiler

AUV automated underwater vehicle

BAM Bab al Mandeb strait

chla chlorophyll *a*

CMRCL Coastal and Marine Resources Core Lab

c_p particulate beam attenuation coefficient

CTD conductivity temperature depth

D1 Deployment One

D2 Deployment Two

DF dilution factor

FFT Fast Fourier Transform

EKE eddy kinetic energy

FLNTUB fluorometer and turbidity sensor with battery

GAIW Gulf of Aden Intermediate Water

GASW Gulf of Aden Surface Water

GAW Gulf of Aden Water

HPLC high-performance liquid chromatography

LISST laser in-situ scattering and transmissometry

MDS multidimensional scaling

MLD mixed layer depths

N^2 stratification

OMP Optimum multiparameter

OTU operational taxonomic units

PAR photosynthetic available radiation

PSD particle size distribution

REMUS remote environmental measuring units 100

RSDW Red Sea Deep Water

SCRS South Central Red Sea

SLA sea level anomaly

SPM suspended particulate matter

SSH sea surface height

SST sea surface temperature

SW Surface Water

TS target strength

WET Labs Western Environmental Technologies

LIST OF ILLUSTRATIONS

LIST OF TABLES

INTRODUCTION

The main objective of this dissertation is to describe the oceanography of the coastal waters by Al-Lith. Al-Lith is a coastal town in the Saudi Arabian coast of the South Central Red Sea (SCRS). It is an interesting region for two reasons. First, the whale sharks (*Rhincodon* typus) aggregate here in the spring from March to May at a nearshore submerged reef, Shi'b Habil. This aggregation site was scientifically discovered in 2009 and has been studied through tagging efforts, but the motivation behind the seasonal aggregation of the sharks is not yet understood. One of the largest integrated aquaculture facilities in the world discharges its untreated wastewater less than five km from Shi'b Habil. This wastewater could introduce nutrients, organic matter, harmful species, and physical stress to Al-Lith's coastal ecosystem but its properties are unknown. Much of the fundamental oceanography, biogeochemical processes, and natural variability in Al-Lith's coastal waters are undocumented despite its importance to studying these interesting phenomena (i.e. whale shark aggregation and aquaculture plume). My dissertation aims to define the annual oceanographic patterns at Al-Lith to provide basic understanding for processes in the region.

Whale sharks

The whale shark, *R. typus*, is the largest fish in the sea. Whale sharks are globally distributed in tropical to warm temperate waters (Figure 0.1) (Compagno, 2001). Whale sharks are opportunistic filter feeders that often forage on spatio-

temporally patchy food sources (Colman, 1997; Compagno, 2001; Freedman & Noakes, 2002). They filter water through five sets of porous pads before passing through its gills and external gill slits (Motta et al., 2010). Waters dominated by 0.7-0.8 mm fish eggs has been targeted by foraging whale sharks, suggesting they are able to sieve small particles as small as 0.7 mm (Hoffmayer & Franks, 2007). Research has shown that whale sharks at times aggregate in areas of enhanced productivity (Cárdenas-Palomo, Herrera-Silveira, Velázquez-Abunader, Reyes, & Ordoñez, 2014; Duffy, 2002; Iwasaki, 1970) and that they may time their movements and migrations to coincide with localized productivity events to enhance feeding opportunities (Wilson, Taylor, & Pearce, 2001). Sea surface temperature has been used to predict the distribution of whale sharks in the open Indian Ocean (Sequeira, Mellin, Rowat, Meekan, & Bradshaw, 2012).

Whale sharks possess an olfactory capsule that is spherical and moderately large, suggesting a capability to sense chemical cues (Martin, 2007). Recent advances on whale sharks in an aquarium setting have shown whale sharks respond to chemosensory cues (Dove, 2015). Whale sharks displayed foraging behavior, changed swimming speed, and revisited the patch of plume when they were exposed to plumes of dimethyl sulfide (released by phytoplankton when grazed upon) and homogenized krill (prey). This suggests chemosensory cues are an important signal for foraging. It will be of interest to study other chemosensory cues that provoke foraging behaviors and examine whether they can use traces of the cue to navigate to high prey densities.

Life history characters of the whale sharks are little known, mostly owing to low encounter rates of pregnant females and pups. A single pregnant female specimen in Taiwan revealed 231 embryos developing at various stages, at least 90% of them fathered by a single male (Joung, Chen, Clark, Uchida, & Huang, 1996; Schmidt et al., 2010). Sperm storage and fertilization over time is suspected to be the case instead of pair-bonding with the single male or fertilized egg dormancy (Rowat & Brooks, 2012). Discovery of mating grounds would help advance our knowledge on their reproduction.

Currently 16 seasonal aggregation sites of whale sharks are known worldwide (none are mating grounds or parturition sites). These aggregation sites provide opportunities for biological studies that are otherwise logistically difficult for these epipelagic species, yet also provide opportunities for fisheries to exploit whale shark populations (V. Y. Chen & Phipps, 2002). Aggregations of whale sharks have been reported to coincide with coral spawning events at Ningaloo Reef in Western Australia (Taylor, 1996), red crab (*Gecarcoidae natalis*) spawning off Christmas Island in the Indian Ocean (Colman, 1997), copepods (*Acartia clausi*) swarms in the Sea of Cortés (Clark & Nelson, 1997), and snapper species (*Lutjanus cyanopterus* and *Lutjanus joci*) spawning off Belize (Heyman, Graham, Kjerfve, & Johannes, 2001). Hydrologic and oceanographic features may also influence seasonal distribution of whale sharks (e.g., Loop Current, river plume, convergent zones, upwelling, and temperature discontinuities) (Burks & Mullin, 2006).

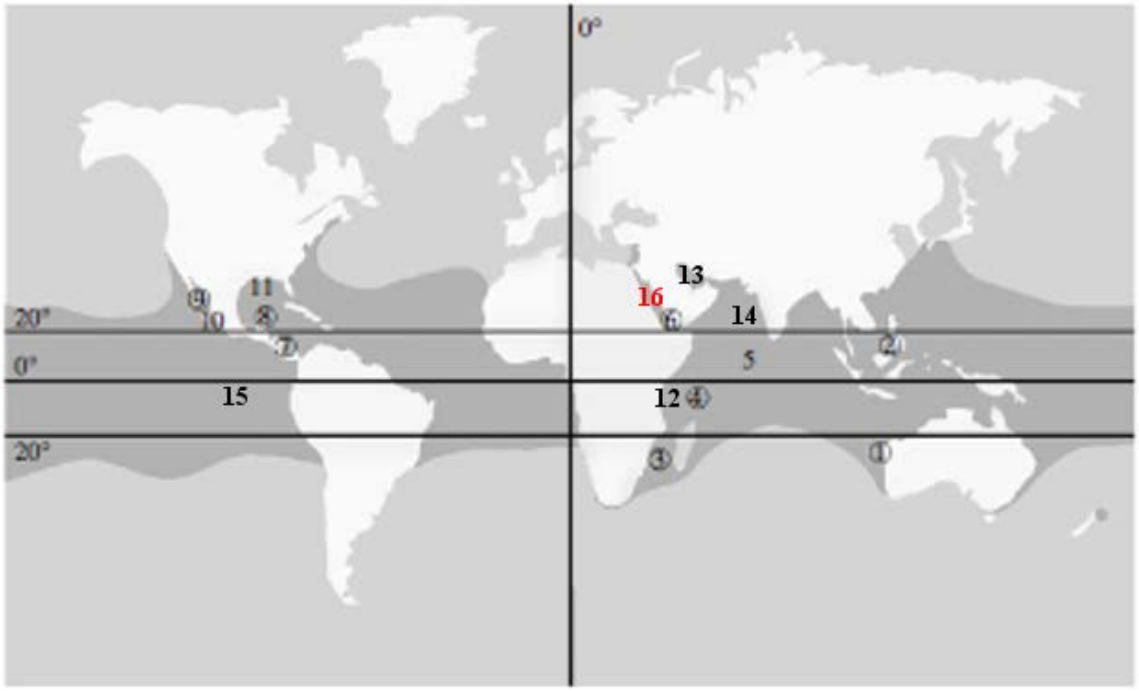

Figure 0.1. Reprinted with permission from Rowat and Brooks (2012) and modified. Global range of *R. typus* distribution (darker shade of gray) with currently known aggregation areas: 1, Ningaloo, Australia; 2, Philippines; 3, Mozambique, Madagascar; 4, Seychelles; 5, Maldives; 6, Djibouti; 7, Belize; 8, Holbox, Mexico; 9, Northern Gulf of California; 10, Southern Gulf of California; 11, Northern Gulf of Mexico; 12, Tanzania; 13, Qatar; 14, Gujarat, India; 15, Galapagos, Ecuador; 16, Shi'b Habil, Saudi Arabia. Circled numbers indicate areas with *R. typus* tourism activities.

Whale shark aggregation at Shi'b Habil, Red Sea

Recently a whale shark aggregation site has been discovered at Shi'b Habil, on the coast of Al-Lith in the South Central Red Sea (SCRS) (Figure 0.2). Whale sharks aggregate at this nearshore submerged reef between March to May and has been confirmed by recent studies based on visual sightings, passive acoustic monitoring, and satellite tracks of tagged whale sharks (Berumen, Braun, Cochran,

Skomal, & Thorrold, 2014). Of the 47 sharks tagged with satellite tags, 39 stayed in the southern Red Sea from summer to winter, three traveled to the northern Red Sea, and five left the Red Sea to the Gulf of Aden into the Indian Ocean. Their distribution in the spring was concentrated near Al-Lith and some kept returning to Shi'b Habil in subsequent years. Individuals actively feed at the surface. Active surface ram-feeding is an energetically costly behavior typically performed in high prey density waters (Rowat & Brooks, 2012). It is therefore hypothesized that the most probable motivation for their aggregation is high prey density. However, the shark's target prey has not been identified and no spatio-temporal time-series of potential prey population have been obtained in this region. Nothing is known about the seasonal variability of potential prey (zooplankton and nekton) biomass.

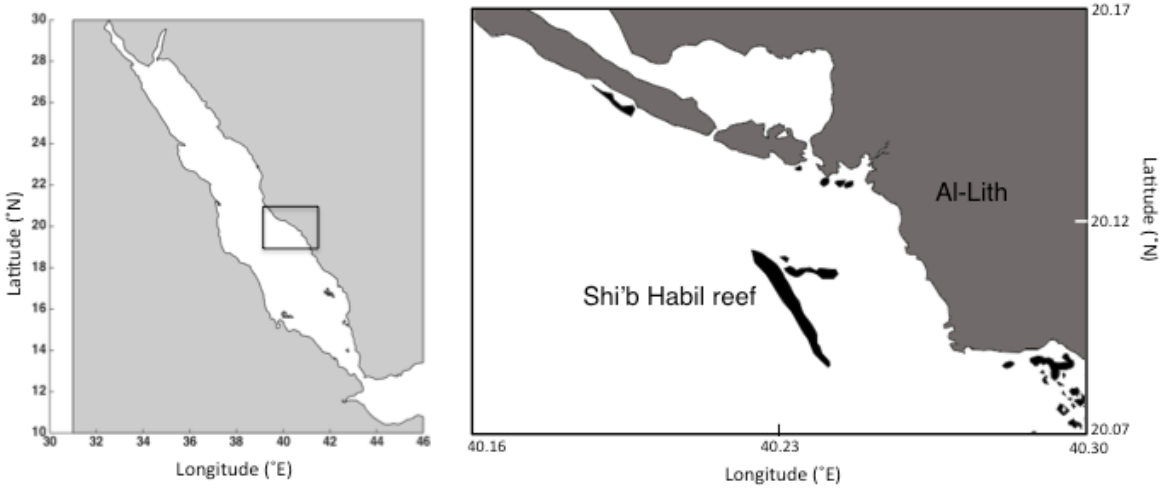

Figure 0.2. A map of the Red Sea with a close-up view of Al-Lith's coastline showing Shi'b Habil. The black regions in the inset are submerged features.

Foraging behavior has only been observed at the surface in Al-Lith but the whale sharks could be foraging subsurface as well. Current tagging efforts cannot reveal if the individual is feeding or not. Tagged individuals spent most (~70%) of their time above 50 m depth but little time (16.7%) in surface layers (0-2 m) (Berumen et al., 2014). This suggests that subsurface prey is a significant source of their diet. In Tanzania, tagged whale sharks inhabited subsurface waters during "off-seasons" without visual sightings of individuals at the surface (E Fernando Cagua et al., 2015). This shift towards deeper waters is speculated to relate to movements or changes in prey populations. On the other hand, fish spawning periods, following the lunar cycle, influenced diving depths of tagged whale sharks off Belize (Graham, Roberts, & Smart, 2006). In Belize, whale sharks had shallower dives (< 200 m) at nighttime and deeper dives (200- 1000 m) at daytime. Their diving patterns could have been following the local prey diel vertical migration, however, prey populations were not observed to explore this hypothesis. Dive behavior of a tagged whale shark in Mozambique showed 79.1% of epipelagic (50-200 m) dives occurred during the nighttime; the individual stayed in shallow waters during the daytime (Brunnschweiler & Sims, 2011). This diel cycle of vertical movement was related to foraging behavior. These studies revealed whale sharks spend time in the subsurface waters, and suggested they interact with prey populations in these deeper depths, possibly performing diel vertical migrations.

The whale sharks at Shi'b Habil certainly could be foraging subsurface, interacting with diel vertical migration of the prey. However, data on subsurface prey abundance, diel vertical distribution, their seasonality, and any relation to the

whale shark detections are not available. In addition an anthropogenic plume from a land-based aquaculture facility in Al-Lith is discharged less than 5 km from Shi'b Habil. This wastewater plume could provide a chemosensory cue, increase productivity, or introduce microbial species, with subsequent influence on their aggregation. No study on the plume's chemistry, seasonal variability, or biological properties exists. A deeper understanding of the site's biogeochemistry is needed to improve conservation of these species and their spring habitat. In particular, understanding the seasonal abundance of prey populations, their vertical migratory patterns, and the nutrient inputs that may lead to high prey density, might unveil the mechanisms responsible for making Shi'b Habil a whale shark aggregation site.

Objectives

The environmental conditions controlling whale shark aggregation still remain largely unknown. Here, in my study, I will examine the physico-biological processes (e.g., upwelling, advection, mixing, anthropogenic input, fronts) at Shi'b Habil to study the potential factors triggering a bottom-up process that motivates the whale shark aggregation (Figure 0.3).

The studies conducted for my PhD dissertation are designed to address the following questions:

i) What bio-physical processes could play a role in a bottom-up process at Shi'b Habil? (shown in blue in Figure 0.3)

ii) Does the aquaculture plume affect and modify the coastal region of Al-Lith? (shown in red in Figure 0.3)

iii) What is the seasonal variability of plankton biomass at this whale shark aggregation site? (suggested food chain in Figure 0.3)

My dissertation is organized as follows. The first chapter describes relevant background information of the study area in relation to our objectives. Then our approach to answer the objectives is summarized. In the second chapter, I present the seasonal variability of the three potential nutrient inputs (Red Sea Deep Water (RSDW), Gulf of Aden Intermediate Water (GAIW), and aquaculture effluent) in this region (Figure 0.4). In the third chapter, I characterize the aquaculture effluent's physical, biological (plankton and microbial), and chemical properties and its trajectory. The fourth chapter focuses on a method to study the seasonal variability of prey abundance larger than ~0.7 cm (copepods, fish larvae, etc.). The Overall Conclusions summarizes the findings from this work and presents perspectives for continued work in Al-Lith.

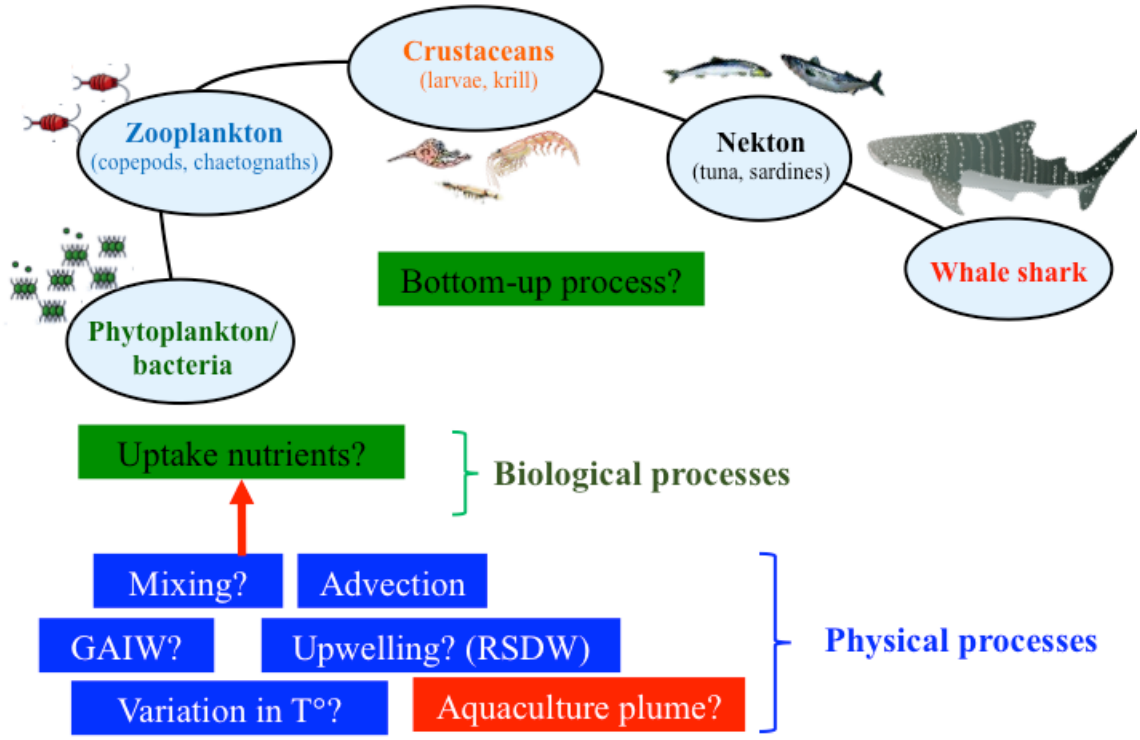

Figure 0.3. A schematic diagram of the bottom-up process that is potentially a motivating factor for whale sharks aggregating at Shi'b Habil in the spring. The physical processes that could be influencing the supply of nutrients to contribute to this bottom-up process are shown as well. My research interests are to define the variability of these physical processes (natural = blue; anthropogenic = red) and reveal seasonal variability in biomass of animals involved in the bottom-up process.

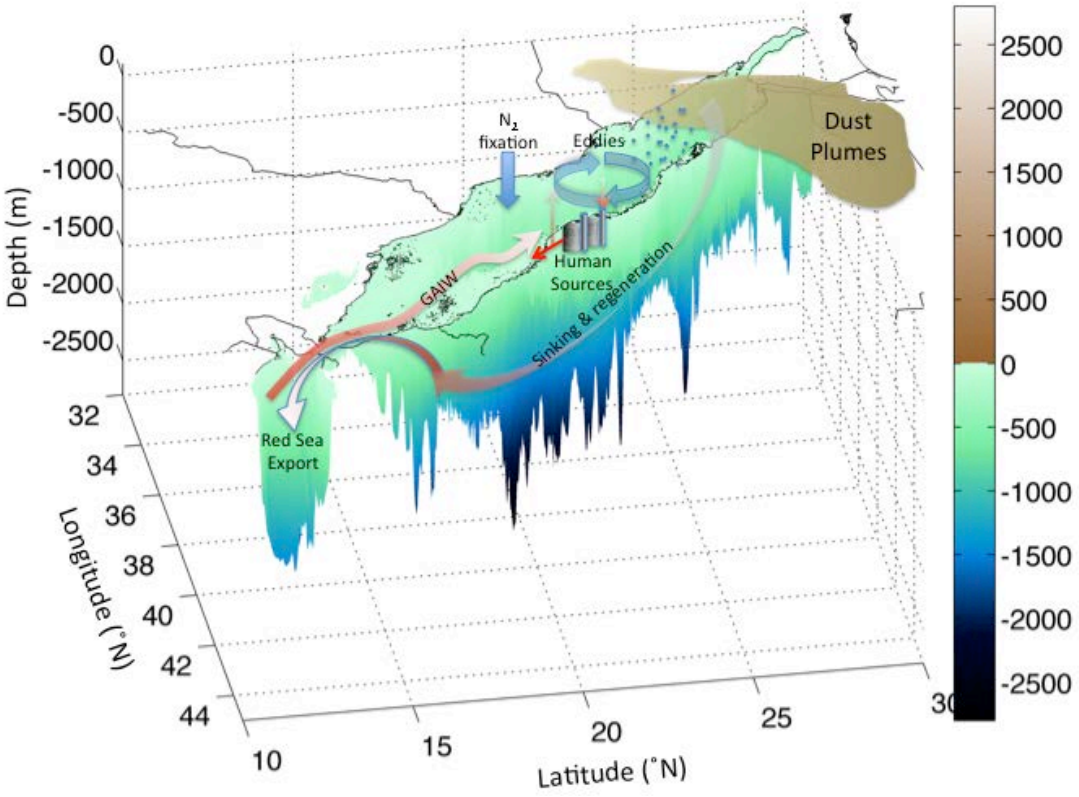

Figure 0.4. Extracted from B. Jones Red Sea CCF Proposal. A schematic of the fate of the nutrients are illustrated (aerosol dust input, atmospheric nitrogen-fixation, formation of deep water, anthropogenic pollution, eddy-driven up and downwelling, exchange with the open ocean) for the Red Sea. The colors show the bathymetry of the basin.

CHAPTER 1. RELEVANT BACKGROUND INFORMATION

1.1 Importance of the Red Sea's biogeochemistry

The Red Sea is a geologically young semi-enclosed basin between Africa and the Arabian Peninsula (Bosworth, Huchon, & McClay, 2005). It is a notably saline, warm, and oligotrophic sea. This is due to the region's high evaporation rates exceeding precipitation rates. Furthermore, the Red Sea has no freshwater input from rivers and negligible terrestrial runoff. The only large-scale water mass exchange with the global waters is from the Indian Ocean by atmospheric forcing, an estimated mid-summer inflow of 0.36×10^6 m^3s^{-1} (Maillard & Soliman, 1986; D. Smeed, 1997). The Red Sea is thus a semi-isolated basin representing a high-temperature and high-salinity marine ecosystem that provides a natural laboratory to investigate impacts of global climate change (Berumen et al., 2013; Voolstra et al., 2015). The skeletal growth of the coral *Diploastrea heliopora* decreased 0.12 mm for every 0.2 ˚C increase in summer sea-surface temperature since the mid-1970s in the Red Sea (Cantin, Cohen, Karnauskas, Tarrant, & McCorkle, 2010). Thus, understanding the biogeochemistry of the Red Sea can contribute to protecting and managing marine ecosystems worldwide, as it could be a predictive model for other regions where rising sea temperatures are expected to cause biological adaptations and ecosystem shifts.

The Red Sea has high economic value but is at risk of degradation. The basin provides oil, fisheries, ecotourism, aquaculture, fresh water through desalination, and potential mining the deep brine basins. However, marine resources are

exploited with minimal regulations on fishing and wastewater discharge (Tesfamichael & Pitcher, 2007). For example, fisheries devastate shark populations, even targeting nurseries, despite the illegality of fishing and selling shark in Saudi Arabia (Spaet, Jabado, Henderson, Moore, & Berumen, 2015). In Jeddah, Saudi Arabia, a city of 3.5 million people, 70% of households are not connected to sewage pipelines and more than 270 pipes were found dumping untreated wastewater along its coast (Sharif, 2008). Algal blooms and mangrove degradation were observed (Basaham, Rifaat, El-Mamoney, & El-Sayed, 2009). The sewage outlet was shifted south and outside of Ghorab lagoon, where it was located before. Heavy metal concentrations (Al, Fe, Mn, Cu, Zn, Cr) in sediments at this new site doubled, while concentrations inside the lagoon, where the outlet used to be, significantly decreased. Taking into account the Red Sea's low flushing rate, the growing anthropogenic influences will contribute significant levels of nutrients, organic matter, diseases, heavy metals, toxins, and invasive species that threaten its economic benefits.

Recent genetic surveys have uncovered higher biodiversity and unique evolutionary lineages in the Red Sea (DiBattista et al. 2013; DiBattista et al. 2015a; DiBattista et al. 2015b). Studies also found biogeographic boundaries for reef fish that have yet to be explained (Froukh & Kochzius, 2007; Nanninga, Saenz-Agudelo, Manica, & Berumen, 2014; C. M. Roberts, Shepherd, & Ormond, 1992). Long-term tagging projects of filter-feeding megafauna, namely whale sharks (*Rhincodon typus*) and manta rays (*Manta alfredi* and *Manta birostris*), intend to study their aggregations, behavioral patterns, and spatio-temporal distributions in the region

(Braun, Skomal, Thorrold, & Berumen, 2014; in press). Much of the biology of these species is unknown, and new insights are vital for improving conservation of these charismatic organisms.

Despite its biogeochemical significance, the Red Sea has been an understudied marine environment, compared to reef systems like the Great Barrier Reef and Caribbean (Berumen et al., 2013). Studies on oceanographic processes that interact with the biogeochemistry of the Red Sea have been limited to infrequent cruises providing snapshots (e.g., Churchill, Bower, Mccorkle, & Abualnaja, 2014; Sofianos & Johns, 2007), remote sensing data revealing surface processes (Racault et al., 2015; Raitsos, Pradhan, Brewin, Stenchikov, & Hoteit, 2013), and models (Triantafyllou et al., 2014; Yao, Hoteit, Pratt, Bower, Kohl, et al., 2014; Yao, Hoteit, Pratt, Bower, Zhai, et al., 2014). Hence the annual cycle and mesoscale variability of basic oceanography is essential to fully understand and appreciate the region's biogeochemistry. This data, however, is lacking.

1.2 Atmosphere-sea interface of the Red Sea

Wind-sea surface interaction shapes the Red Sea's oceanographic circulation, which governs spatio-temporal patterns of nutrient sources and areas of biological hotspots. The Red Sea is bordered by mountain ranges that channel the winds along the central axis of the basin. The northern half of the basin experiences a dominant northwesterly wind all year round, while the southern half switches from northwesterly in the summer (June-October) to southeasterly in the winter (November-May), influenced by Indian monsoon winds (Pedgley, 1972; Sofianos,

Johns, & Murray, 2002; Sofianos & Johns, 2003). The change in wind direction occurs near 19°N, where the converged wind escapes the basin westward through the Tokar Gap in Sudan (Figure 1.1; Jiang et al. 2009).

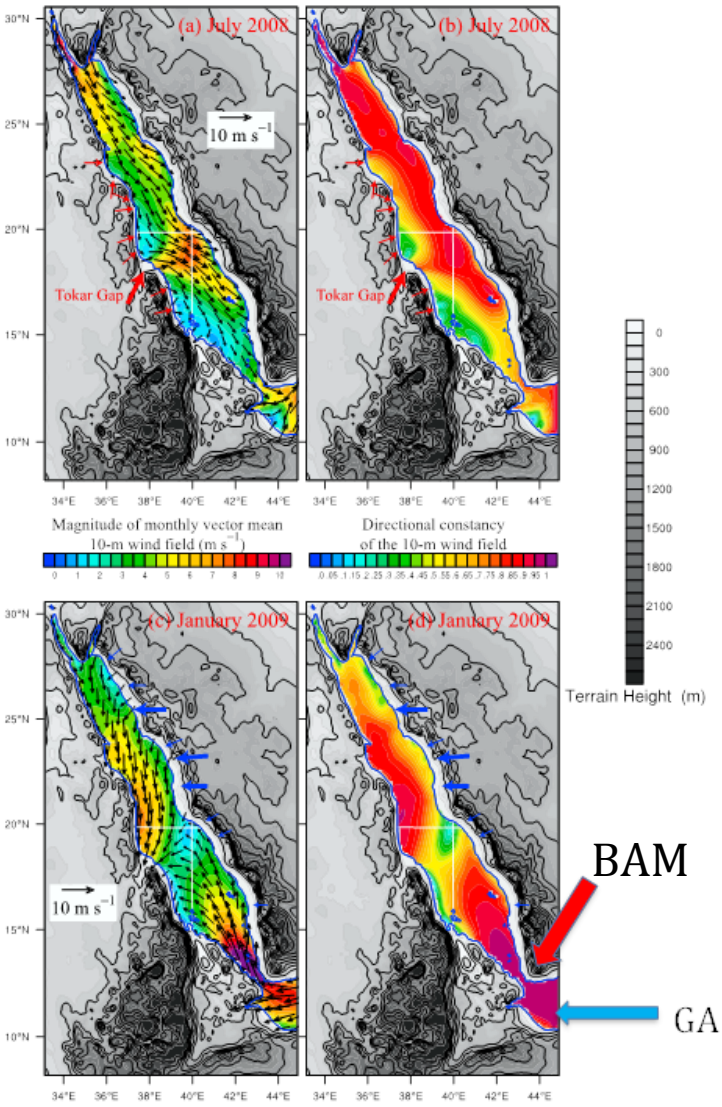

Figure 1.1. Reprinted with permission from Jiang et al. (2009). Vector fields and contour maps showing the monthly mean surface (10 m) wind magnitude (ms^{-1}) (left) and directional constancy from model output (right). July 2008 and January 2009 are shown to represent the summer and winter surface wind patterns. The

Bab al Mandeb strait (BAM) connects the Gulf of Aden (GA) in the south of the Red Sea.

The Tokar Gap is a break in the Eastern Desert mountain range in Sudan, creating zonal wind jets that give the predominant north-south wind a cross-basin component (Jiang et al., 2009; Zhan, 2013). In winter, easterly winds that escape the winter wind convergence towards Sudan recur every 10-20 days and lasts for several days (Zhai & Bower, 2013). This easterly zonal wind blows toward the Tokar Gap and may induce upwelling in the eastern SCRS. Coastal upwelling from these wind jets could resuspend sediments and uplift nutrient-containing waters from below the pycnocline into the upper water column. On the other hand, from mid-June to mid-September, westerly Tokar wind jets enter the basin as regularly as everyday (Jiang et al., 2009). This generates a zonal wind stress curl and is speculated to create dipole eddies and Ekman convergence and divergence in the basin (Jiang et al., 2009; Zhai & Bower, 2013).

High evaporation rates at the air-sea interface drive a northward buoyancy flux at the surface. Buoyancy forcing leads to vertical convective mixing and is especially important in forming mixed layers and RSOW in the north. This northward flow driven by the buoyancy flux forms an eastern intensified boundary current and is suspected to cause downwelling in the east, except south of 16°N where it transitions to an intensified western boundary current (Sofianos & Johns, 2003). Differences in the surface circulations change the mixed layer depths and thus the biology of the water column. These atmospheric interactions with sea surface are crucial in determining locations of biological hotspots and biogeographic

boundaries.

1.3 Nutrient sources in the oligotrophic Red Sea

Various nutrient sources including dust plumes, nitrogen fixation, eddy circulations, anthropogenic discharges, nutrient rich deep-water, and intrusion of high nutrient water from the Gulf of Aden, are thought to contribute to the productivity of the Red Sea. Nutrient enrichment will lead to an increase in primary productivity by phytoplankton, which will fuel secondary producers contributing to a sufficient food supply for larger marine organisms, such as whale sharks. Ocean currents and upwelling events introducing different water masses and circulations to a region have been related to aggregations in coasts of Japan, Australia, and Mexico (Cárdenas-Palomo et al., 2014; Iwasaki, 1970; Wilson et al., 2001). Therefore, resolving spatio-temporal variability of water masses and circulations at the whale shark aggregation site will provide insight into their aggregation.

The South Central Red Sea (SCRS), which includes Al-Lith, has two major natural marine-sourced nutrient inputs: the Red Sea Deep Water (RSDW) that forms in the northern tip of the basin, and the Gulf of Aden Intermediate Water (GAIW) that enters the Red Sea through the Bab al Mandeb (BAM) strait. Wind-driven oceanographic circulations can cause upwelling of the RSDW coupled with horizontal and vertical nutrient transport (Acker, Leptoukh, Shen, Zhu, & Kempler, 2008; Raitsos et al., 2013). Models and remote sensing observations highlight the importance of mesoscale eddies to the circulation and biological processes in the Red Sea. Mesoscale anti-cyclonic eddies are “enhanced feeding stations” for higher

trophic marine life due to the passive transport and accumulation of dense lower trophic level biomass to its periphery (Godø et al., 2012). In addition, they can upwell nutrients of the RSDW into the euphotic zone along its periphery and concentrate food sources that may trigger biological hotspots.

The other natural nutrient source, the GAIW intrusion, is seasonally limited by the exchange between the Gulf of Aden and the Red Sea waters at BAM. During the winter (November-May), the strait has a two-layer exchange with the Indian Ocean, where the Surface Water (SW) from the Gulf of Aden flows into the Red Sea and Red Sea Overflow Water (RSOW) flows out of the basin (Figure 1.2; Cromwell & Smeed, 1998). In the summer (June-October), northwesterly winds dominate the entire basin, forcing GASW to exit out BAM. At this time, the Indian monsoon upwells GAIW to a depth shallower than BAM's sill, causing inflow of the GAIW into the Red Sea (Patzert, 1974; D. A. Smeed, 2004). A three-layer exchange occurs, with the SW and RSOW flowing out sandwiching the inflowing GAIW tongue at a depth of 60-150 m (Figure 1.2; Cromwell & Smeed, 1998). This restricts GAIW intrusion to the summer months, or at least to times when upwelling occurs in the Gulf of Aden. Upon entry into the Red Sea, GAIW has temperature <17.8 ˚C, salinity <36 psu (Sofianos & Johns, 2007), oxygen levels of ~1.0 mL L^{-1}, phosphate concentration 2.0 μmol L^{-1} (Patzert, 1974) and estimated nitrite and nitrate concentrations of 17 μmol L^{-1} (Churchill et al., 2014), compared to nitrate-rich (>30 μM) Antarctic Intermediate Water in the South Atlantic (Hansen book). Therefore, GAIW is high in nutrients, fresher, colder, and less oxygenated than SW or RSOW. Following its diminishing but significant signatures, GAIW have been observed north of 22°. But

no *in-situ* data has been able to describe the magnitude and timing of GAIW in the southern coastal reefs. Understanding the magnitude and seasonality of this intrusion in the reefs will improve our knowledge on the reef systems and their resilience to varying oceanographic conditions.

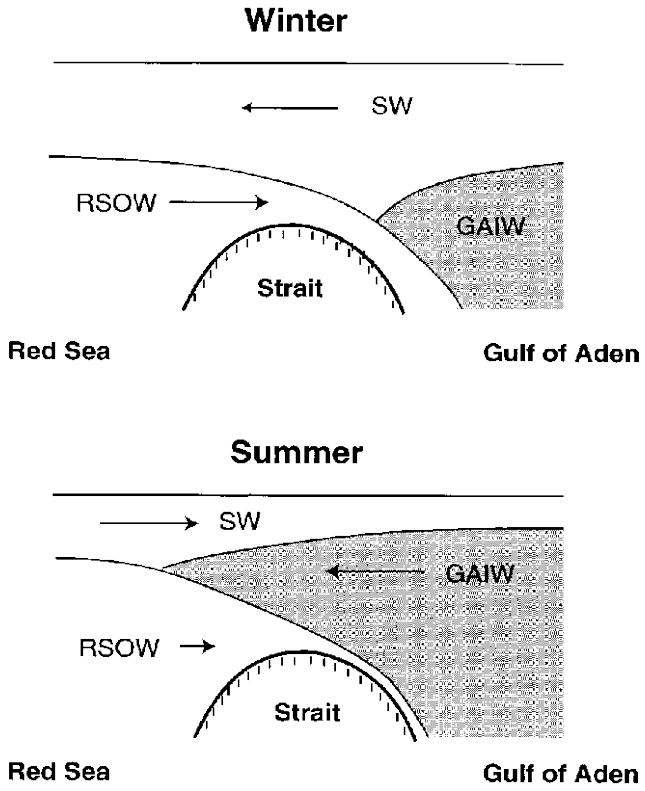

Figure 1.2. Reprinted with permission from Cromwell and Smeed (1998). A schematic illustration showing the two different exchange patterns between the Red Sea and Gulf of Aden at Bab al Mandeb sill. SW is the Surface Water, RSOW is the Red Sea Outflow Water, and GAIW is the Gulf of Aden Intermediate Water.

Terrestrial nutrient sources in the Red Sea include coastal effluents from urban areas (Ansari, Harb, Jones, & Hong, 2015; Risk, Sherwood, Nairn, & Gibbons, 2009), aquaculture, and aerosol inputs from dust (Y. Chen et al., 2007). One of the

largest aquaculture facilities in the world is located in Al-Lith on the coast of the Saudi Arabian coast of the SCRS (20.15˚N, 40.25˚E). The reef is 410 km north from the Farasan Islands, home to myriad coral reefs patches, and the wastewater outfall from the aquaculture facility is less than 5 km away from the whale shark aggregation site. During the course of my study, the facility's main product was prawn, but it also produces sea cucumber, beta-carotene, algae, and offshore cage farming of Asian seabass (N. Ayaril & M. Villarreal Ricord, pers. comm.). Allegedly, the pond farms are stocked for harvest from April for three cycles until the last harvest in February. Wheat bran, molasses, urea and di-ammonium phosphate are added to the ponds to trigger a plankton bloom before they are stocked with shrimp. Feed pellets composed of 34-40% crude protein and 9-11% fat are produced at the facility and are fed to the shrimp. In between the cycles, ponds are flushed to remove accumulation on the bottom and to aerate the sediments. During harvest, ponds are flushed out and it is at this time that wastewater discharge and contamination are suspected to be highest. The discharge could provide sufficient organic matter (e.g., shrimp feed) to alter the plankton community structure and abundance with subsequent impacts on the coastal ecosystem. This in turn could affect the distribution of whale sharks or impact their health with toxins or pathogens. Finally, timing of dust inputs is sporadic and its seasonality has not been resolved in the SCRS. The biological response and impact on the whale sharks from these various terrestrial nutrient inputs needs to be investigated.

METHODS OVERVIEW

For my dissertation, I used a combination of different strategies to tackle the complex physico-biological processes in Al-Lith (Figure M.1).

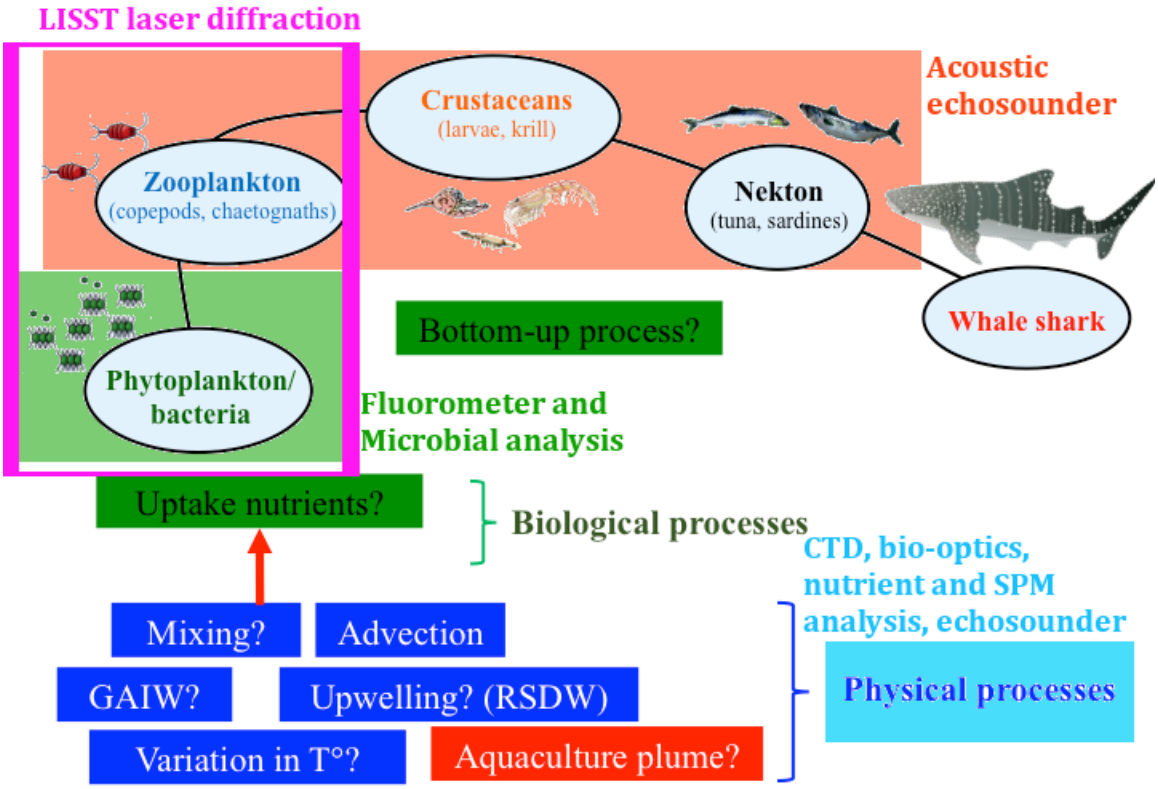

Figure M.1. Schematic summarizing the methods applied to observe the various aspects of the physico-biological processes in Al-Lith. Physical processes are observed using CTD, bio-optics, echosounder, nutrient and SPM analysis (blue). Phytoplankton and bacteria are quantified by fluorometer and microbial analysis (green). Phytoplankton (not including pico-phytoplankton), smaller zooplankton, and aggregates are measured using the LISST via the particle size distribution using laser diffraction method (pink). The larger zooplankton, crustaceans, nekton, etc. are observed using the acoustic echosounder (orange).

We had a time-series effort to provide the first annual cycle of basic oceanography at a nearshore-reef in the South Central Red Sea (SCRS) and spatial surveys to capture the horizontal and vertical variability. Fixed moorings were deployed to measure physical and biological variables (temperature, salinity, depth, chlorophyll *a* fluorescence (chla), backscattering) at Shi'b Habil. These measurements provided high temporal resolution data from May 2013 to July 2015. Battery deaths and set-up failure interrupted the time-series. Monthly cruises were made from January 2014 to January 2015 (except October 2014) to complement the mooring data by providing vertical profiles of the water column (temperature, salinity, depth, chla fluorescence, turbidity, particulate beam attenuation coefficient, particle size distribution) at 17 stations around Shi'b Habil and the aquaculture discharge outfall. This effort provided monthly snapshots of areas away from the mooring instruments fixed on Shi'b Habil. Water samples were taken for lab analysis (microbial, nutrient, suspended particulate matter, chla extraction). This revealed biogeochemical properties of the aquaculture discharge such as bacteria and cyanobacteria cell counts, microbial assemblages, nitrate, nitrite, silica, and phosphate concentrations, particulate load, and phytoplankton biomass. An echosounder with two frequencies (120 kHz and 333 kHz) equipped with battery and computer was deployed as a bottom-mounted upward-facing mooring at the northern end of Shi'b Habil. The aim was to record the acoustic backscatter (a proxy for biomass larger than 0.7 cm) at the location with the highest whale shark detections during whale shark season (March to May). We collected the acoustic backscatter data of the water column from January 15, 2014 to April 30, 2014.

Spatial surveys were conducted using an automated underwater vehicle (REMUS 100) measuring temperature, salinity, depth, chla fluorescence, turbidity, and water velocity. The REMUS sampling was conducted in May, June, September, October, and December of 2013 and was intended to continue monthly through 2014; however, the REMUS was sent for factory calibration and was not returned until the end of 2014. The manual profiling at 17 stations were employed as a substitute. We also applied a 200kHz frequency echosounder mounted on the side of a boat to measure acoustic backscatter with the aim of characterizing the path of the plume from the aquaculture facility. The mapping with the echosounder survey to track the aquaculture plume and observe its dispersal was carried out January 15, 2014. Multiple approaches were combined in attempt to capture the oceanography of Al-Lith's coastal region and examine any correlations with the whale shark aggregation variability.

CHAPTER 2. SPATIO-TEMPORAL VARIABILITY OF WATER MASSES IN THE WHALE SHARK AGGREGATION SITE

Abstract

The spatio-temporal variability of water masses was resolved at a nearshore reef (Shi'b Habil) in the coastal coral reef systems in the South Central Red Sea. It has been hypothesized that a bottom-up process, such as nutrient input, may promote productivity in this region, attracting whale sharks in the spring. It is therefore important to understand the nutrient sources contributing to the primary productivity at this whale shark aggregation site. Based on monthly profiles and fixed mooring records, we observed Red Sea Deep Water signatures (high salinity and colder) on the offshore side of Shi'b Habil in July. This month coincided with the highest surface wind stress from the Tokar wind jets. For the first time, the Gulf of Aden Water signatures (colder and fresher) were observed at an inshore coastal reef in the Red Sea. This water intrusion reached the reef as episodes lasting 5 to 26 days from May to September rather than as a continuous supply. A major anthropogenic nutrient source, an aquaculture-associated plume, was tracked as a bottom-hugging layer, throughout the year at stations northeast of the reef. In early autumn, signatures of this discharge were seen 8.4 km from the outfall, on the exposed side of the reef at mid-water column. Timing of these three nutrient inputs does not coincide with the whale shark season and therefore are interpreted not to contribute directly to the whale shark aggregation that runs from March to May.

2.1 Introduction

From March to May, a seasonal whale shark aggregation occurs at Shi'b Habil, a nearshore submerged reef by Al-Lith, Saudi Arabia, located on the eastern coast of the South Central Red Sea (SCRS) (Berumen et al., 2014). Individuals at this aggregation site are sexually immature and are seen to actively feed at the surface, an energetically costly behavior associated with high prey densities (Colman, 1997; Stevens, 2007). Thus we hypothesize this region receives seasonal nutrient input to create a foraging hotspot for whale sharks in the spring. Shi'b Habil has higher whale shark detections than other reefs in the vicinity (Cochran, 2014). Detection of whale sharks is spatially variable along the 5 km length of the reef, where a north-south and exposed-sheltered gradient exists (Cochran, 2014). The spatio-temporal variability in whale shark detections indicates mesoscale abiotic or biotic variability that could promote this mesoscale habitat selectivity, which we suspect is dictated by prey density. For this study, we focus on sources of nutrient input, which is a key factor that affects prey populations.

An increase in nutrient concentration can promote primary productivity, subsequently supporting secondary productivity, which eventually could provide sufficient prey density to motivate the megaplanktivore aggregation. Red Sea Deep Water (RSDW), Gulf of Aden Intermediate Water (GAIW), and aquaculture-associated wastewater are all potential nutrient sources in Al-Lith. Sea level anomaly (SLA) from satellite data show that anticyclonic eddies are common in the Red Sea (Zhan, Subramanian, Yao, & Hoteit, 2014). Along-basin winds are channeled by the Eastern Desert mountain ranges lining the basin. However, a break in the

western wall, the Tokar Gap, exists in Sudan (~18° N), and results in cross-basin winds. This is called the Tokar wind jet and causes highest wind stress in the SCRS usually in July (Zhai & Bower, 2013). This interacts with the along-basin winds and regional orography to structure eddy seasonality and characteristics (Clifford, Horton, & Schmitz, 1997). Eddy Kinetic Energy (EKE) calculated from SLA illustrates a peak in January with a secondary peak in August (Zhan et al., 2014). Anticyclonic eddies in the SCRS, especially with high EKE, will tilt the pycnocline and lift nutrient-rich, colder (21.5 ˚C), saltier (40.6) RSDW into the upper layers of the coastal sea where there is sufficient light for primary productivity. Thus nutrient enrichment from upwelled RSDW could contribute to the primary productivity of the coastal ecosystem.

During the southwest monsoon (June – September), winds shoal the thermocline over the Bab al Mandeb strait (BAM) sill and a northward baroclinic pressure gradient drives the GAIW intrusion (Yao, Hoteit, Pratt, Bower, Zhai, et al., 2014) at an estimated rate of 0.36 x 10^6 m^3s^{-1} (Maillard & Soliman, 1986; D. A. Smeed, 2004). This colder, fresher, less oxygenated, high nutrient inflow (temperature<18 °C, salinity<36, oxygen<15 μmol kg^{-1} (Sofianos & Johns, 2007), 2.0 μmol L^{-1} (phosphate (Patzert, 1974)), 17 μmol L^{-1} (nitrite and nitrate (Churchill et al., 2014)) enters the Red Sea at mid-water column (60-150 m (Cromwell & Smeed, 1998)). Mixing occurs at the interface of GAIW and Red Sea water and the mixture in the upper layers form the Gulf of Aden Surface Water (GASW). This water is a warmer, saltier GAIW as result of mixing (Figure 2.1). Satellite and cruise observations suggest GAIW enters the eastern coastal reef system, including Al-Lith

(Churchill et al., 2014; Zhan, 2013). This could promote primary productivity, and subsequently grazing, as it travels through the complex coastal system (e.g., the Farasan Banks, an extensive network of coral reefs). Yet there have been no *in-situ* observations to confirm its presence in the coastal reef systems.

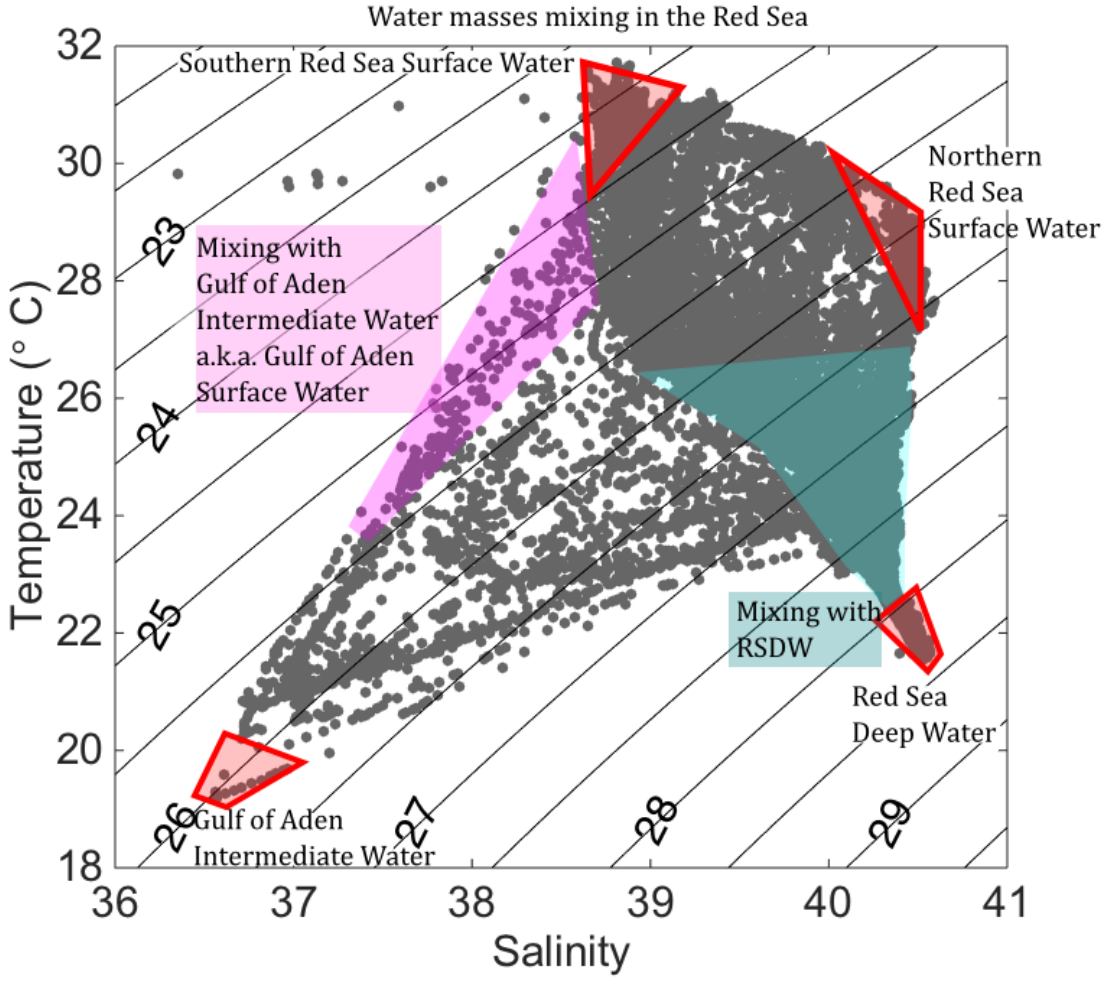

Figure 2.1. Temperature-salinity plot from the WHOI-KAUST cruise in September-October 2011 that captured water masses in the Red Sea. Southern Red Sea Surface Water, Northern Red Sea Surface Water, GAIW, and RSDW are indicated in red. The mixing between these water masses result in new water masses such as the GASW and RSDW-influenced water.

Wastewater from the coastal integrated aquaculture facility in Al-Lith is an anthropogenic nutrient source. The aquaculture ponds, which produced 13,000 t of prawn in 2014, are enriched with molasses, wheat bran, di-ammonium phosphate, and urea. These shrimp are fed pellets of crude protein and fat that, if unconsumed, contributes organic matter to the plume. The facility's wastewater passes through a settling basin before discharging into Al-Lith's coastal waters. The added fertilizers, the organic wastes (carcass, animal waste, uneaten feed), and the lack of tertiary wastewater treatment likely result in discharge water that has higher nutrient concentrations and suspended particles than the ambient coastal seawater (see Chapter 3). Sawall et al. (2014) suggested the aquaculture wastewater could contribute to blooms of chain-forming diatoms and filamentous Cyanobacteria (i.e., *Trichodesmium sp.*) that could be responsible for the observed reef deterioration. Kürten et al. (2014) observed higher abundance of potentially toxic algae (i.e., *T. erythraeum*, *Dinophysis miles* and *Gonyaulax spinifera*) in a field effort in September-October 2011. No difference in Fungiidae coral health was observed with distance from the outfall (Furby, Apprill, Cervino, Ossolinski, & Hughen, 2014). It is important to resolve the wastewater's water quality, seasonality, and trajectory to aid further environmental assessments of the aquaculture effluent.

In-situ observations are important to resolve the spatio-temporal variability in water masses at a nearshore coastal reef, such as those near Al-Lith, in SCRS. This information is fundamental in understanding the local ecosystem and the spatio-temporal patterns observed in places where whale sharks aggregate. Previously,

complex bathymetry prevented nearshore cruises and AUV efforts. Satellite data is available; however, the data provides little insight into the subsurface processes and cloud and aerosol coverage in the southern half of the Red Sea, especially during summer, often prevents ocean color image retrieval. Additionally, a lack of a regional algorithm for ocean color products and challenges posed by optically shallow waters, in which bottom heterogeneity and bottom reflectance must be corrected for (Bames et al, 2013), add uncertainty to satellite-derived data for this coastal regions.

Thus this study aims to bridge this gap in long-term observations to answer 1) when and where does RSDW, GAIW, and the aquaculture plume arrive at this whale shark aggregation site, and 2) does chlorophyll *a* (chla) and particulate backscatter (both biological proxies) vary with water mass? Characterization of the first spatio-temporal water mass variability at a nearshore reef in Al-Lith will provide timing and residence times of water mass intrusions. This will help determine if a bottom-up process from nutrient input causes the localized spring whale shark aggregation.

2.2 Method

Study site

Our study site, Shi'b Habil (20.1142˚ N, 40.2203˚ E), is a 5 km long and on average 600 m wide submerged reef located 4 km off the coast of Al-Lith, Saudi Arabia (Figure 2.2). The area has complex bathymetry with coral reefs, seagrass beds, and mangrove patches with associated fauna and flora. An integrated coastal

aquaculture facility in Al-Lith and its discharge outfall lay within 5 km of this reef. To capture the temporal and spatial variability of water masses, field efforts around this reef had two separate approaches: fixed long-term moorings and monthly spatial surveys.

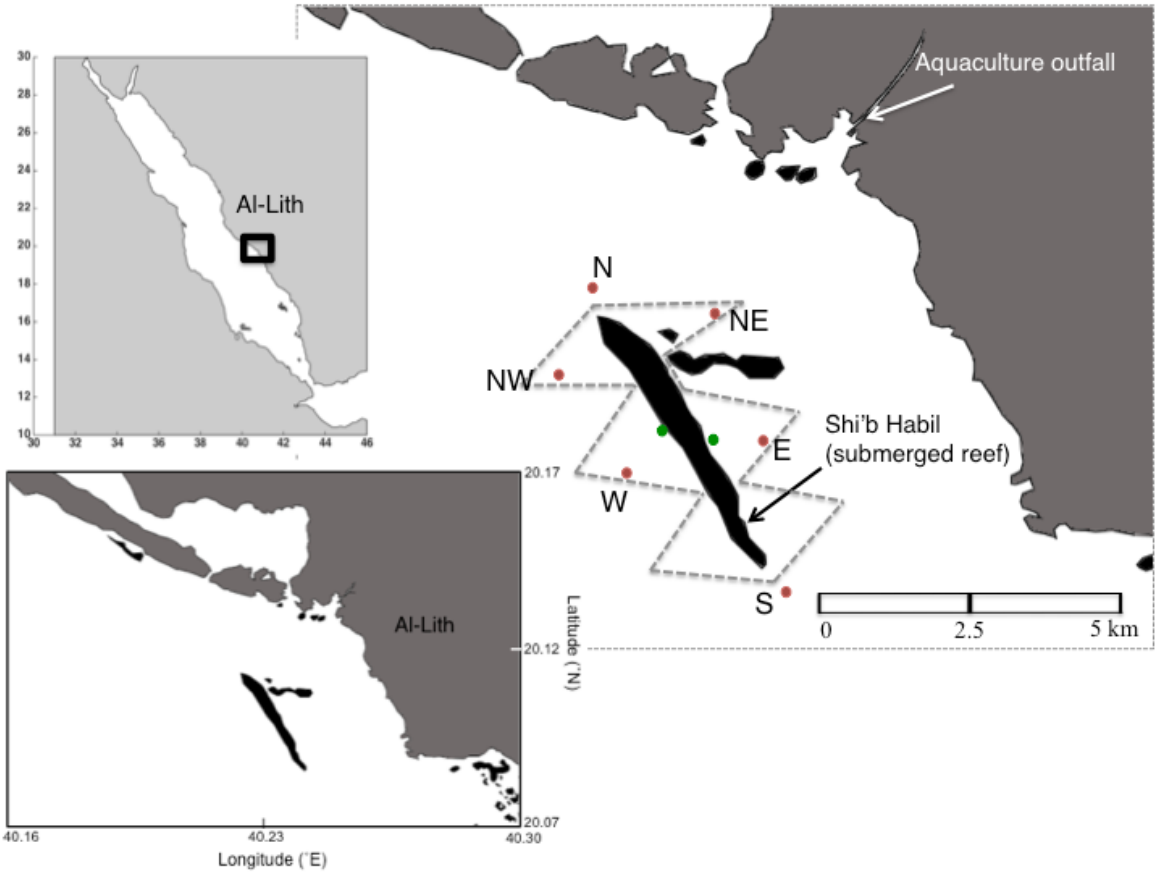

Figure 2.2. Map of the Red Sea and inset showing overview of Al-Lith. The position of the six monthly stations (red) and fixed moorings (green) on Shi'b Habil are labeled. The AUV survey line is shown as a grey dashed line. The predominant winds offshore of Shi'b Habil are from the northwest based on measurements in June-July 2011 (E. F. Cagua, Berumen, & Tyler, 2013).

Fixed moorings

Two moorings were fixed at ~10 m and ~6 m depth directly on the reef at exposed and sheltered sites, respectively, (Figure 2.2) for multiple deployment periods (Figure 2.3). CTDs (Microcat 37-SMP, Seabird, USA) were deployed from May 19, 2013 to January 28, 2015 to measure temperature, conductivity, and pressure every 40 seconds. From January 29, 2015 until June 8, 2015, the sampling frequency was reduced to every 120 seconds to prolong battery life. Fluorometers (FLNTUB, WETlabs, USA) were deployed from September 18, 2013 to April 30, 2015 to measure chla at excitation 470 nm/emission 685 nm, and turbidity at 700 nm for particulate backscatter every hour for 20 seconds at 1 Hz. Battery failure created gaps in data from March 11, 2014 to June 9, 2014 for all instruments (Figure 2.3). Fluorometers were serviced and therefore not deployed from June 9, 2014 to September 24, 2014.

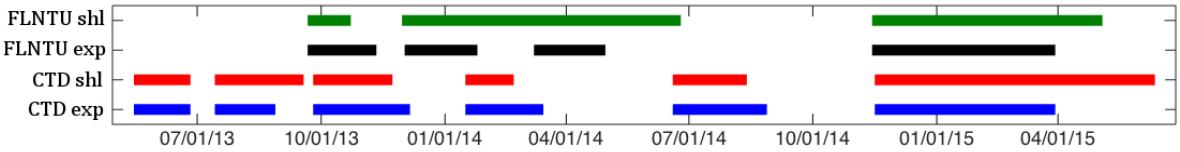

Figure 2.3. Deployment periods for the moored instruments, CTD and fluorometer (FLNTU), at exposed (exp) and sheltered (shl) sites on Shi'b Habil.

Monthly surveys

Two different survey approaches were utilized. The first used an automated underwater vehicle (AUV) (Remote Environmental Measuring UnitS 100 (REMUS), Kongsberg, Norway) equipped with CTD (Neil Brown Ocean Systems, USA), fluorometer (EcoPuck, WETlabs, USA) for chla fluorescence and optical turbidity,

and up- and down-looking 1200 kHz Acoustic Doppler Current Profiler (ADCP) (RD Instruments, USA). The REMUS was programmed to navigate around Shi'b Habil while profiling the water column (Figure 2.2). Preliminary surveys with the REMUS started in May 2013 (Appendix B), however, only data collected after October 2013 is presented because of the minimal overlap in the spatial coverage by the preliminary REMUS surveys with the surveys that followed. ADCP data is analyzed with caution because of uncertainties in data processing due to REMUS tilt, roll, and vertical and lateral movement (described further in Appendix C).

The second survey approach utilized a manual profiling package with CTD (Microcat 37SM, Seabird, USA or Ocean Seven 304, Idronaut, USA), fluorometer (FLNTUB, WETlabs, USA), and particle size analyzer (Laser in-situ Scattering and Transmissometry (LISST), Sequoia Scientific Inc., USA). The LISST measured particulate beam attenuation coefficient (c_p) as a proxy for suspended particulate matter and particle size distribution for 1.25 to 250 μm. This profiler was used to characterize water mass variability at six stations around Shi'b Habil (Figure 2.2) selected based on previous REMUS efforts (Appendix B). The REMUS was the preferred survey method due to high spatial resolution of data; however, the REMUS was unavailable from January 2014 for servicing so the manual profiling method was used instead for the rest of the operations. Sampling occurred from local time 6:00 to 17:00 (3:00-14:00 UTC) with some exceptions when sampling lasted until 21:00 (18:00 UTC) in January and April 2014 and when field days were cut short due to weather, i.e.. March and June 2014.

Data quality control

To check for fluorometer stability we measured air, dark, and Milli-Q® counts between deployments following instrument manual and Roesler (2011). We performed a 3-point dilution count for fluorescence with Diet Coke® (The Coca Cola Company) and 7UP® (Dr Pepper/Seven Up, Inc) (Cetinić, Toro-Farmer, Ragan, Oberg, & Jones, 2009; I. Walsh, pers. comm.). Milli-Q and FSW background counts for the LISST were taken prior and after deployments.

Data analysis

All data were manually screened for outliers. The CTD data was screened and values of salinity below 37.5 were considered contamination in conductivity cells. The FLNTUB chla data was crosschecked with chla values measured using a calibrated benchtop Turner Designs Trilogy fluorometer (Arar and Collins, 1997). Mixed layer depths (MLD) was calculated with density gradient criterion of 0.125 kg m^{-3} (Levitus, 1982) and potential temperature, practical salinity, and stratification (N^2) was calculated using Matlab GSW toolbox (McDougall & Barker, 2011) from the raw CTD data. For power spectral analysis, Fast Fourier Transform (FFT) was done after removing the best-fit linear trend (Trauth, 2010). Optimum multiparameter analysis (OMP) could not be used to test the ratios of water masses mixed in our data because we only measured two conservative tracers (temperature and salinity). For our study, nutrient concentrations are not conservative tracers because all of our data is coastal water in the euphotic zone and thus subject to

biological processes that will change nutrient concentrations unlike deep waters where OMP analysis is usually used.

2.3 Results

Seasonality of temperature and salinity

The temperature and salinity at Shi'b Habil demonstrated clear seasonality. Temperature reached a minimum (27 ˚C) in February (Figure 2.4), when the atmospheric temperature was also at its minimum. The temperature of the water column was homogenous at all stations during this minimum, a typical result of winter mixing. A secondary minimum in July was also observed when the temperature dropped below 29 ˚C (Figure 2.4). Here, the water column was stratified, as summer stratification occurred from May until it was homogenous again in November. During these stratified months (May to October), salinity was also lower (38.7 to 38.9; Figure 2.4). Salinity returned to higher levels (over 39.3) in November, but another drop in salinity was observed in December for both sampled years (REMUS survey and manual profiling effort). By January in both years, this drop in salinity had returned to levels observed in November.

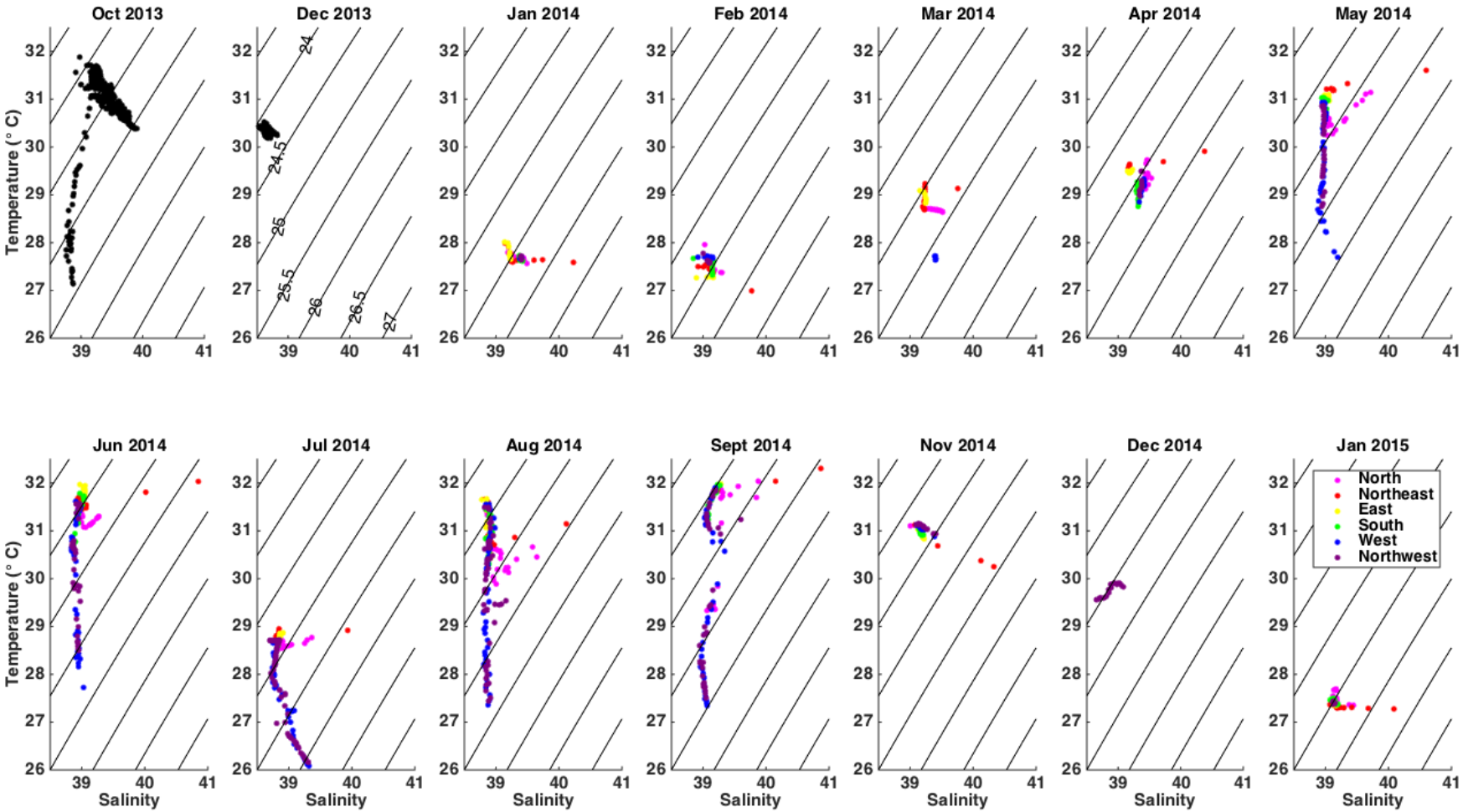
Oct 2013
Dec 2013
Jan 2014
Feb 2014
Mar 2014
Apr 2014
May 2014
Jun 2014
Jul 2014
Aug 2014
Sept 2014
Nov 2014
Dec 2014
Jan 2015
Temperature (° C)
Salinity
24
24.5
25
25.5
26
26.5
27
North
Northeast
East
South
West
Northwest

Figure 2.4. A series of temperature-salinity plots for each monthly survey from October 2013 to January 2015 in Shi'b Habil. The contour lines show the density and are consistent in all plots. Contour lines are labeled in the December 2013 plot to minimize clutter. Different stations are color-coded to illustrate the spatial variability in temperature-salinity data. October and December 2013 are not color-coded because these were continuous measurements by the REMUS, not single profiles.

Water mass variability

The monthly profiles and mooring measurements were examined to determine signatures of the different water masses. Monthly vertical profiles of all stations are provided in Appendix D. Vertical profiles at stations on the exposed side of the reef (NW and W) had high salinity (39.31) and lower temperature (26.1 ˚C) near the seafloor (~60 m) in July (Figure 2.5). The rest of the water column was relatively fresher (38.8) and colder (28.5 ˚C) homogenous water with a mixed layer depth of 30 m. The July temperature and salinity data plotted over the data collected during the Fall 2011 WHOI-KAUST cruise reveals how the colder, saltier water mass is consistent with the RSDW characteristics (Figure 2.6).

Salinity at all six stations on the reef measured below 39 at different time periods. Sheltered stations (NE, E) showed salinity signals, as low as 38.84 in July and August. In contrast, exposed stations (NW, W, N and S) showed salinity signals, as low as 38.7 from May to September (Figure 2.5). These stations had lowest salinity in June, July and August. The temperature at both exposed and sheltered moorings started to decrease in June and occasionally dropped below 29 ˚C until it started to increase in late August (Figure 2.7). This lower temperature coincided

with a period of lower salinity (below 39), indicating these are water mass signatures from the Gulf of Aden (Figure 2.7). These episodes of lower salinity water deviate towards the GAIW signatures observed by the WHOI-KAUST cruise; however are isothermal (Figure 2.8). This suggests this water mass is GASW that has been mixed with Red Sea water as it travelled northward to reach Shi'b Habil (Figure 2.1). The fresher, colder GAIW signatures are weaker in the GASW because of the mixing with the Red Sea water that is warmer and saltier. Regrettably, we did not measure oxygen levels and had difficulty distinguishing GAIW (lower oxygen) and GASW (higher oxygen). The isothermal, lower salinity, lower temperature water was categorized as GASW (Figure 2.8). Both monthly profiles and mooring time-series suggest GAW signatures were present at this reef from May to September.

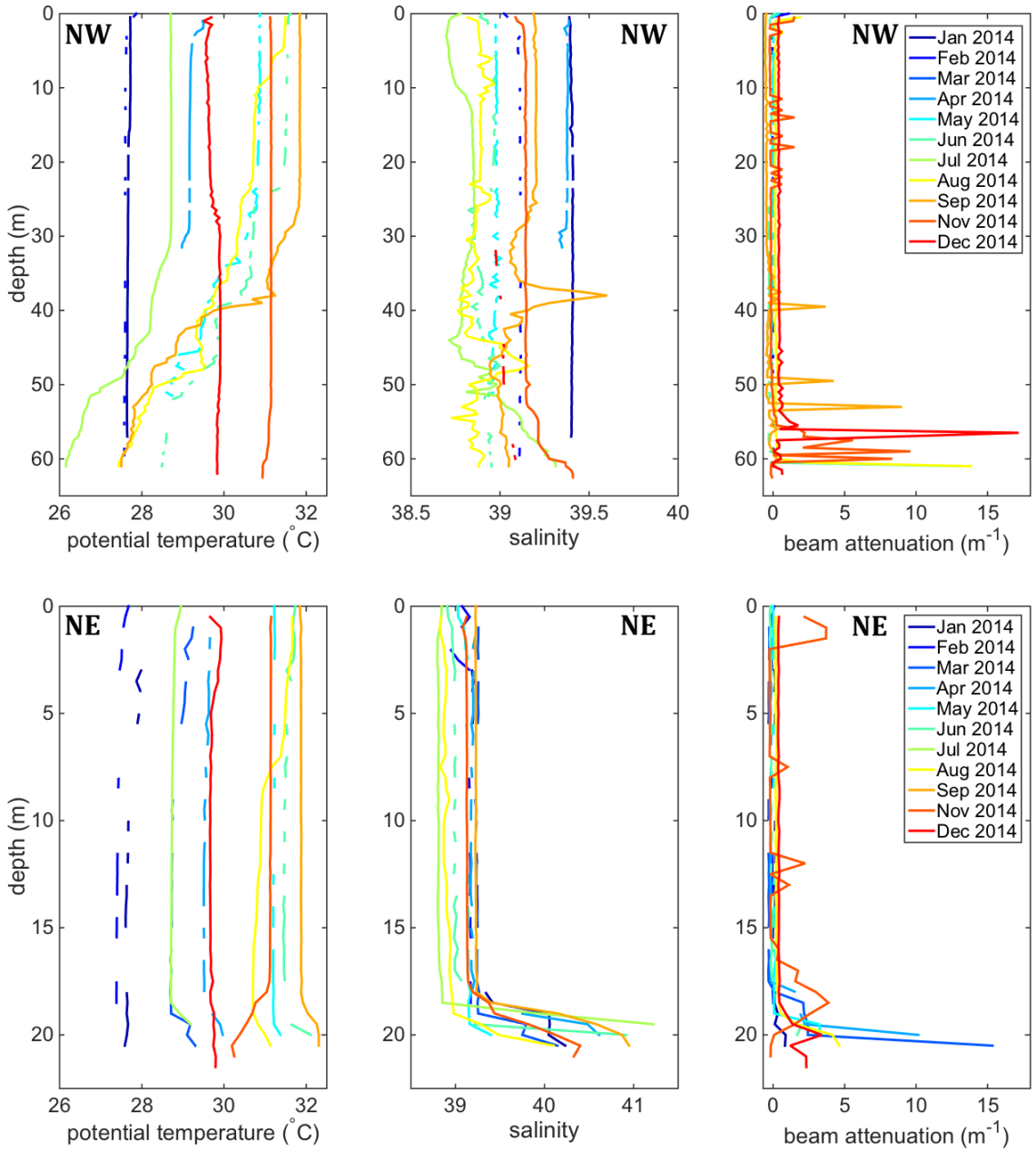

Figure 2.5. Potential temperature, salinity, and c_p profiles of all surveyed months (color-coded) at NW (top) and NE stations (bottom) in Shi'b Habil. The NW station is on the exposed northern side of Shi'b Habil, where whale shark detections are higher than the NE station, which is on the sheltered northern end of the reef.

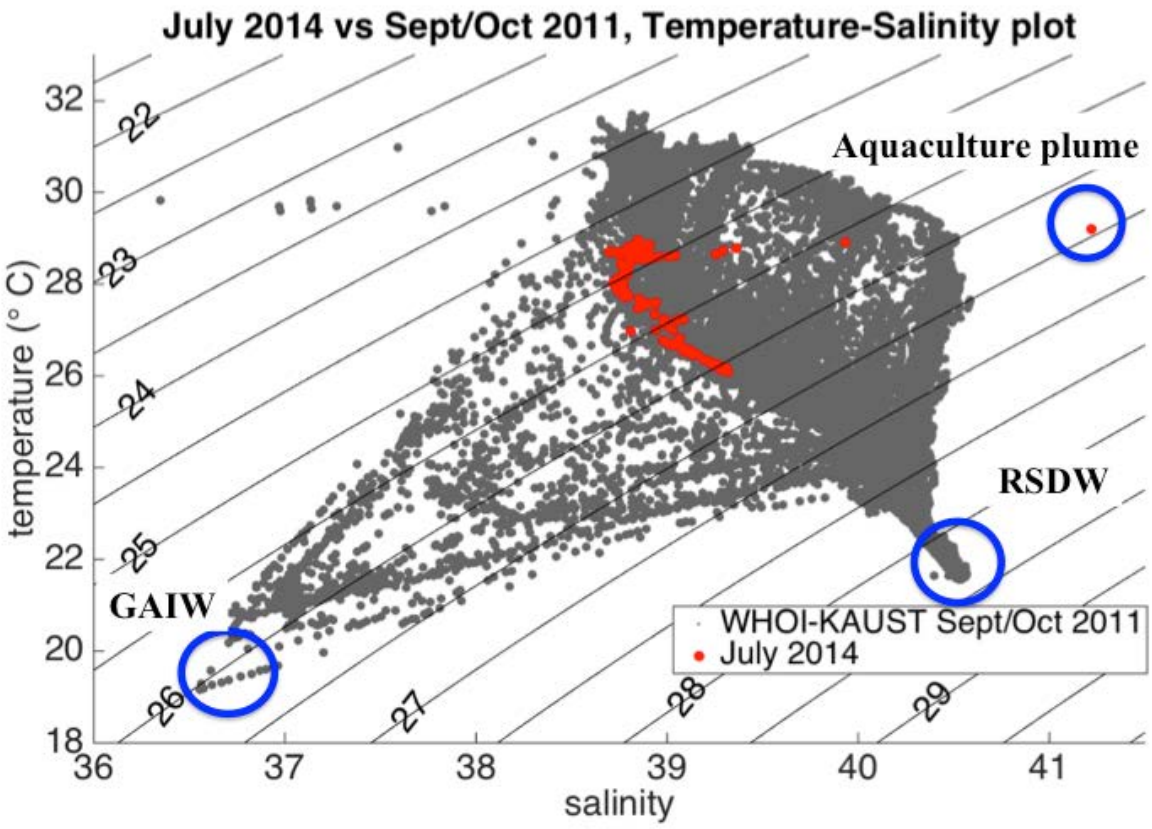

Figure 2.6. Temperature and salinity data collected in July by our efforts (red) plotted over the data collected during the Fall 2011 WHOI-KAUST cruise (gray). The temperature-salinity signatures of the RSDW, GAIW, and the aquaculture plume are indicated (blue circles). Density is shown as contour lines.

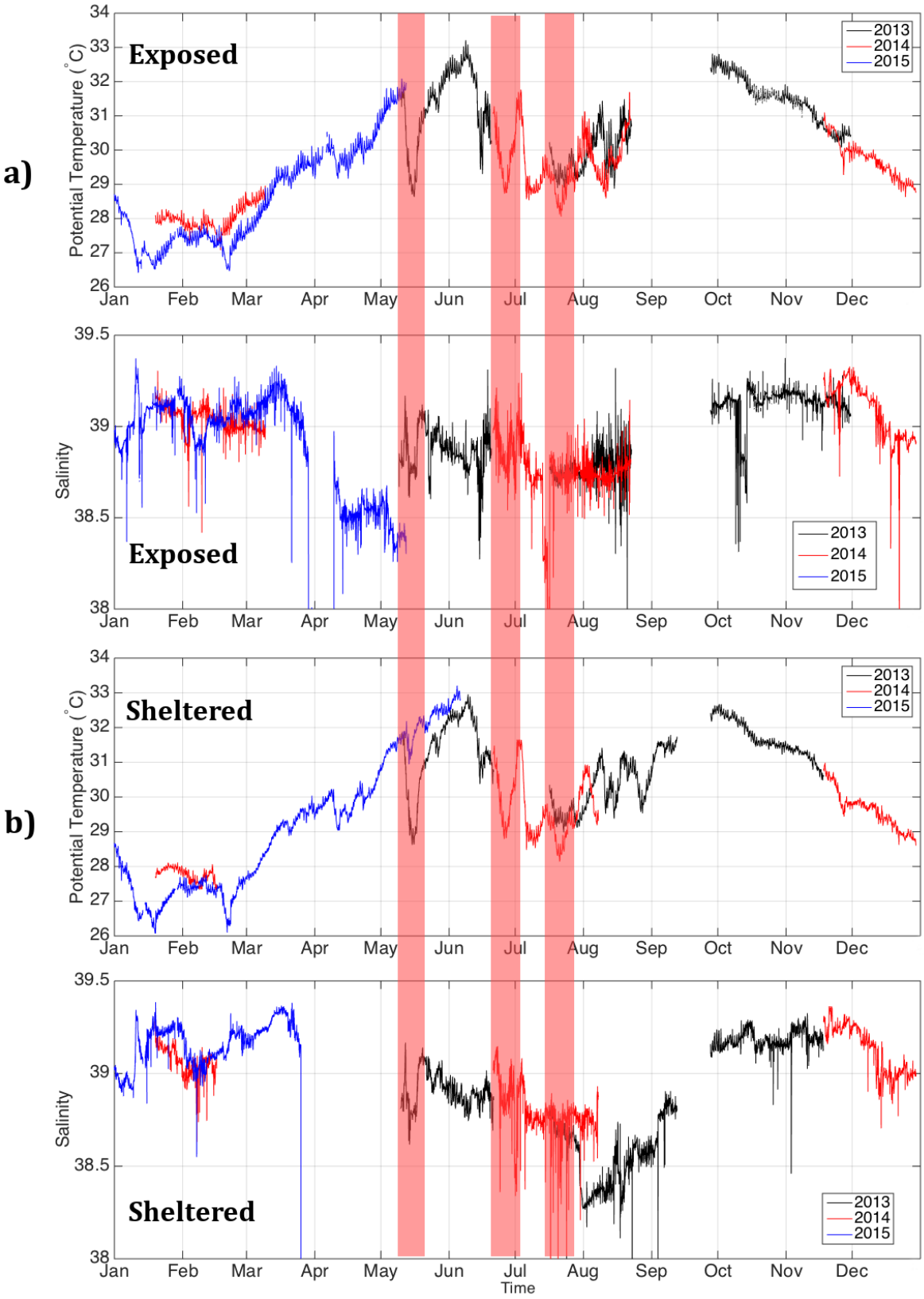
a)
Exposed
Potential Temperature (°C)
Salinity
Exposed
b)
Sheltered
Sheltered
2013
2014
2015
Jan
Feb
Mar
Apr
May
Jun
Jul
Aug
Sep
Oct
Nov
Dec
Time

Figure 2.7. Times series data of potential temperature and salinity from the a) exposed and b) sheltered moored instruments in Shi'b Habil. The highlighted periods correspond to the episodes of low salinity and low temperature water intrusion. Separate years are indicated by colors (2013 = black, 2014 = red, 2015 = blue).

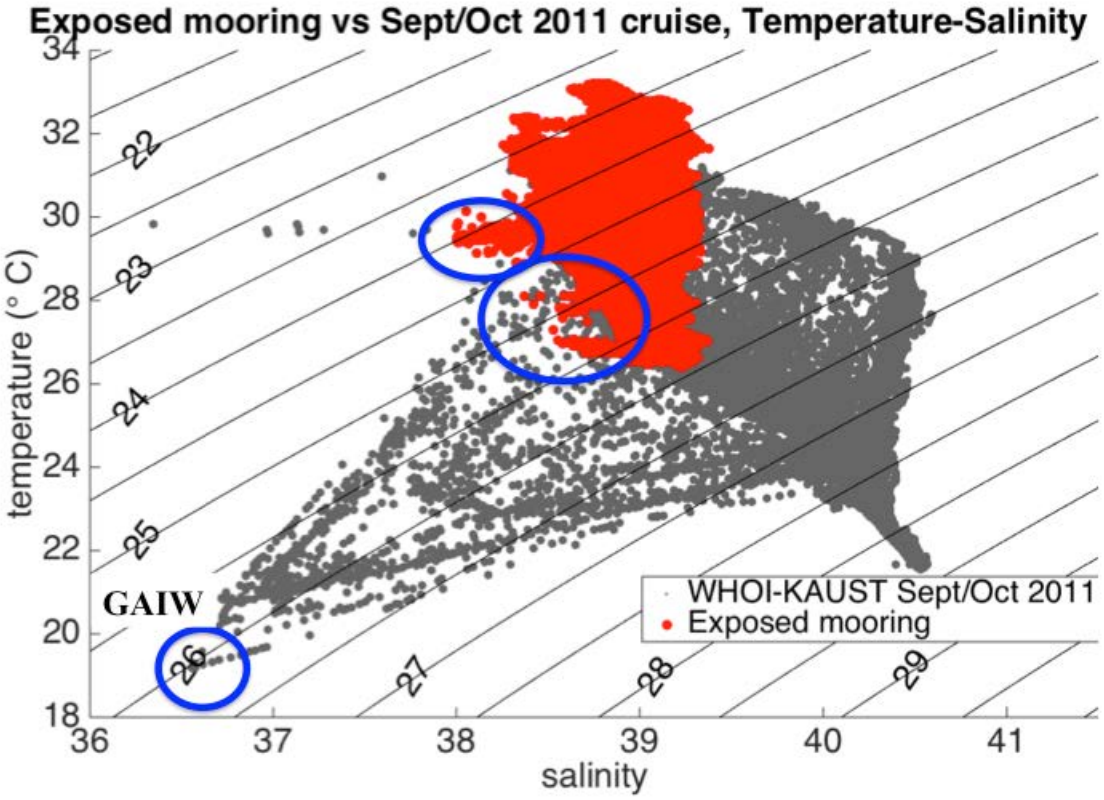

Figure 2.8. Temperature and salinity measured by the moored instruments on the exposed side of Shi'b Habil (red) is plotted with the data collected by WHOI-KAUST cruise in Fall 2011 (gray). GAIW signatures captured by the cruise data and water masses consistent with GASW characteristics are indicated with blue circles. The density contour lines are shown.

Furthermore, we observed sudden dips in temperature, which coincided with the dips in salinity (Figure 2.7). This temperature drop was observed by the

mooring observations, which provided much higher temporal resolution than the monthly surveys. These dips occurred at both mooring sites simultaneously, suggesting that instrument biofouling is not causing sudden, short periods of lower temperature and lower salinity. These drops in temperature and salinity are consistent with the occurrence of GASW intrusion at this nearshore reef that occurs as events from May to October, rather than as a continuous supply. The timing of the events varies between the years as seen in the contrast between the 2013 and 2014 temperature data (Figure 2.7). The periods of low temperature ranged from 5 to 26 days.

High salinity and high c_p, indicative of suspended particles, were observed consistently at NE and occasionally at exposed stations (N, NW, and W). Elevated salinity and c_p characterize the bottom 2 to 3 meters of all the vertical profiles obtained at NE (Figure 2.5). High salinity values were observed at N, NW, and W and were most prominent in September. At mid-water column (37, 38, and 39 m for N, NW, and W, respectively), this salinity peak (>39.4) coincided with a temperature peak (~31 ˚C) (Figure 2.5). A comparison of stations at Shi'b Habil with coastal stations closer to the aquaculture outfall from Chapter 3 showed this feature deviated from its vertically stratified water column towards the temperature-salinity signature of the discharge water (Figure 2.9). When compared to the temperature-salinity plot of June, which has a clean vertical structure, the deviation of this peak in September is clear (Figure 2.9). This mid-water column layer with high salinity and temperature is the aquaculture-associated discharge observed 8.4 km offshore from the outfall.

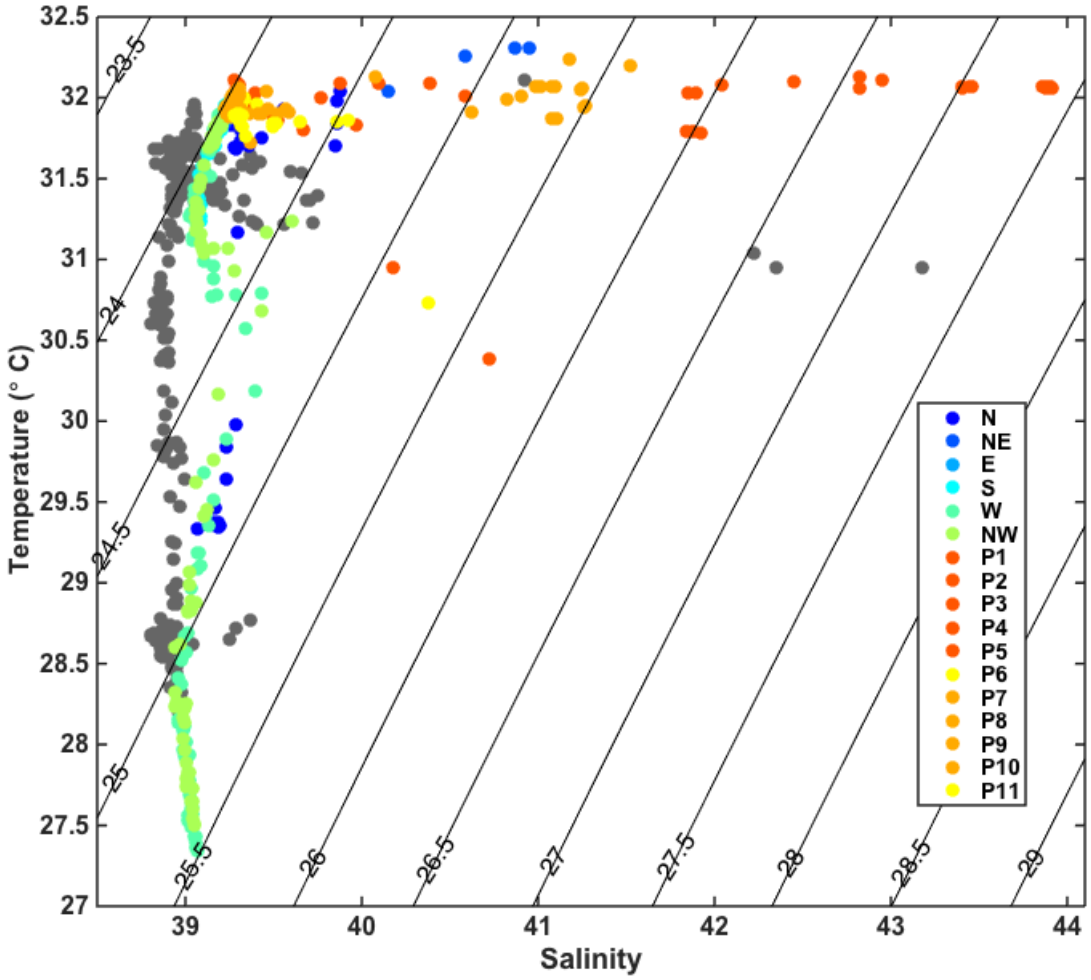

Figure 2.9. Temperature-salinity plot comparing September water mass deviation to the aquaculture-associated effluent (colored as per legend) to the June water mass (gray). Density is shown as contour lines. P1-P11 are stations nearshore to the aquaculture outfall (Chapter 3).

The most consistent and strongest periodicity signals for sea-level variability measured at the moorings were 23.9 h and 12.4 h (Figure 2.10). This is consistent with the semidiurnal tidal periodicity. Other weaker signals were at 45 d, 11.3 d, 20.2 d, 8.4 d, 3.6 d, 8.2 h, and 5.8 h. Temperature also had strong periodicity at 23.9

h and 11.6 h (Figure 2.10) that was consistent with the tidal periodicity. Salinity signals showed the weakest periodicity signals but 8.66 d and 23.48 h were common signals in three of the seven deployments.

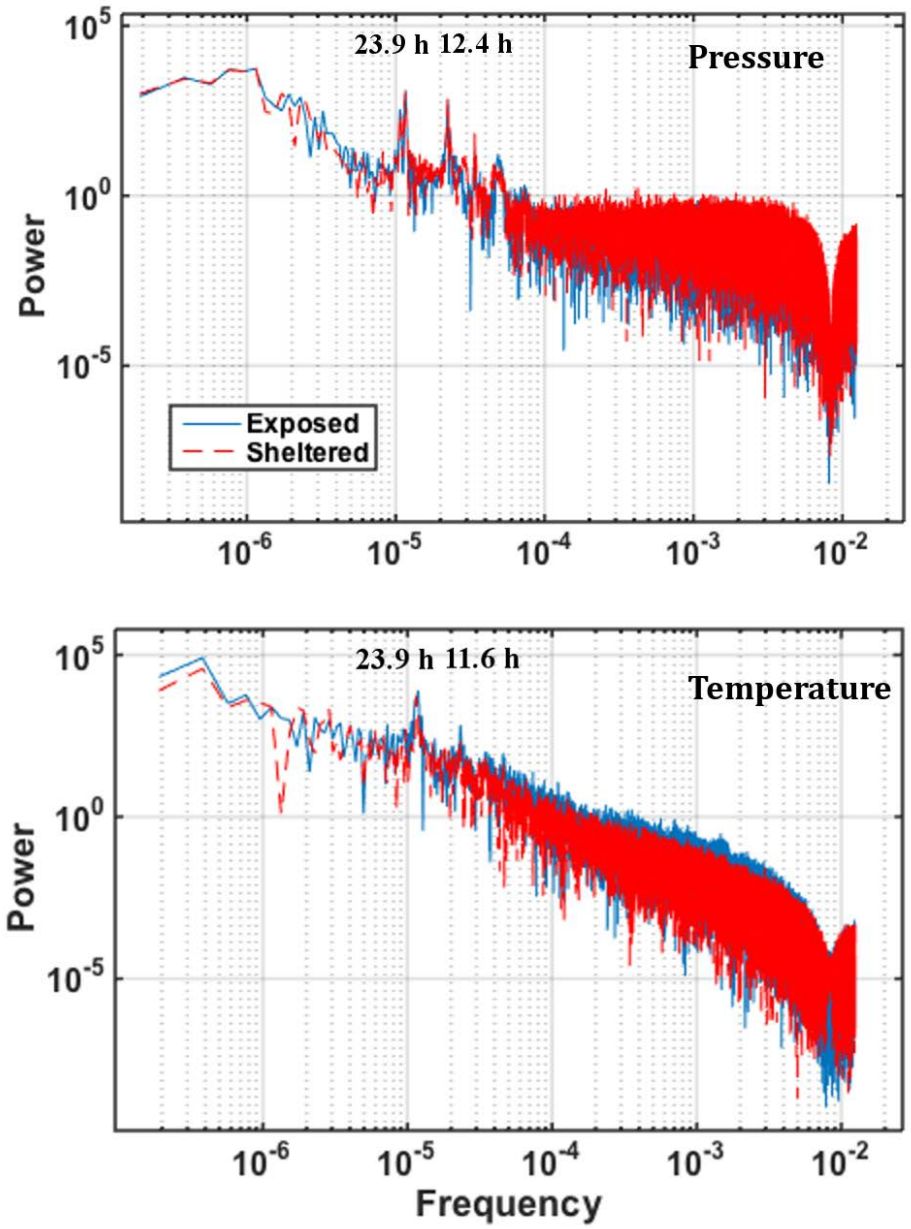

Figure 2.10. Fast Fourier Transform frequency plots for moored pressure (top) and temperature (bottom) data collected in Al-Lith. The periodicity is shown in hours

above the corresponding peaks. Both exposed (blue) and sheltered (sheltered) mooring data are plotted.

Chla and Bio-optical patterns

At Shi'b Habil, the waters on the sheltered side, where the instruments were deployed at shallower depth (6 m), was homogenous all year, had higher chla and scattering (Figure 2.11) than the exposed side of this coral reef, where the instruments were deployed at deeper depth (10 m). Due to instrument set-up failure, there is no fluorometer data from the moorings to capture the bio-optical characteristics of the bursts of GAW. Optical measurements from the monthly profiles of deeper areas (>60 m) in July showed the saltier, colder RSDW had low chla fluorescence (< 0.3 $\mu g l^{-1}$) and c_p (< 0.003 m^{-1}) (Figure 2.12). Only the discharge water with high salinity and temperature relatively close to ambient waters seen at NE (20 m depth) had high c_p and chla values.

Seasonal variability of chla fluorescence was not clear from the moored fluorometers (Figure 2.13). Frequent spikes in the data suggest phytoplankton aggregates passing by the detection zone of the fluorometer, or mechanical noise (especially for very high values). Spikes in chla data decreased after factory calibration of the FLUNTBs (after September 2014) (Figure 2.13). From February to March a slight peak in the sheltered site was seen (Figure 2.13). At the exposed site, higher values are observed in the fall. This does not parallel the observations of more whale sharks on the exposed side than the sheltered side of this reef.

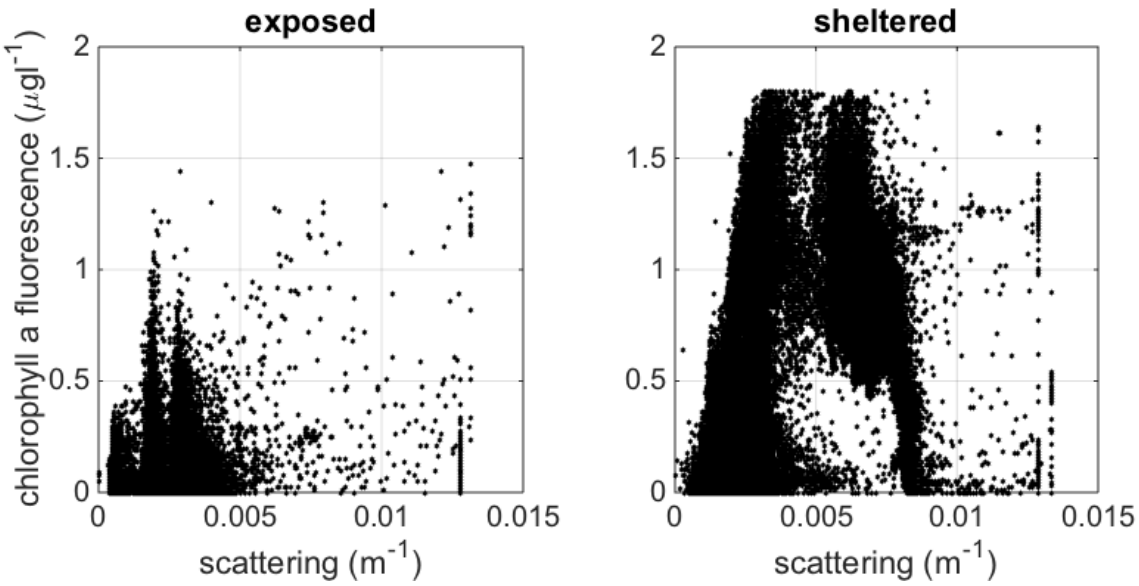

Figure 2.11. Correlation of chla and turbidity fluorescence on the mooring sites on Shi'b Habil. Data was filtered by a moving average with window of 300 for n> 172000 to reduce outliers. The sheltered (red) and the exposed (blue) side of the reef are compared.

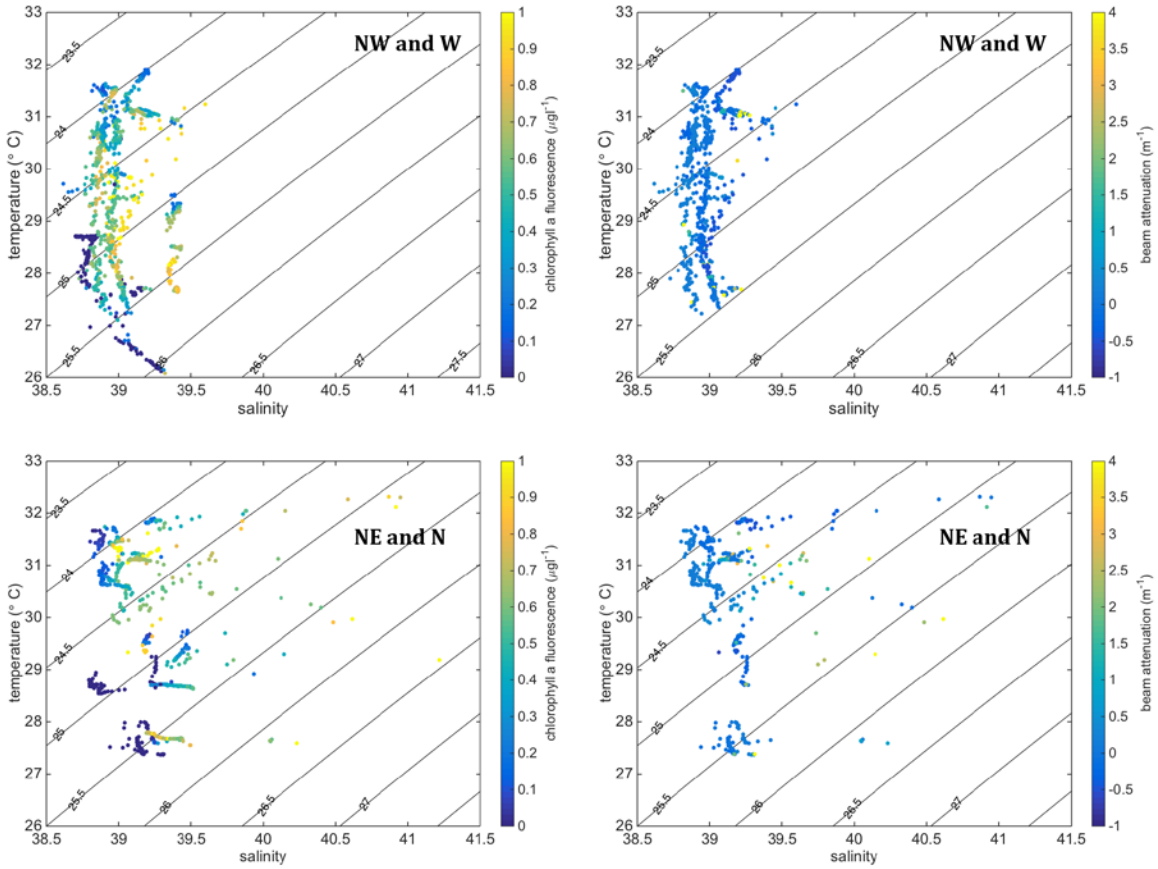

Figure 2.12. Temperature-salinity for all months plotted with chla fluorescence (left) and c_p (right) represented by a color scheme. Stations with RSDW signatures (NW and W) (top) and stations with aquaculture plume signatures (NE and N) (bottom) are presented separately. Months without chla (February) or c_p (July) measurements are excluded from the plots.

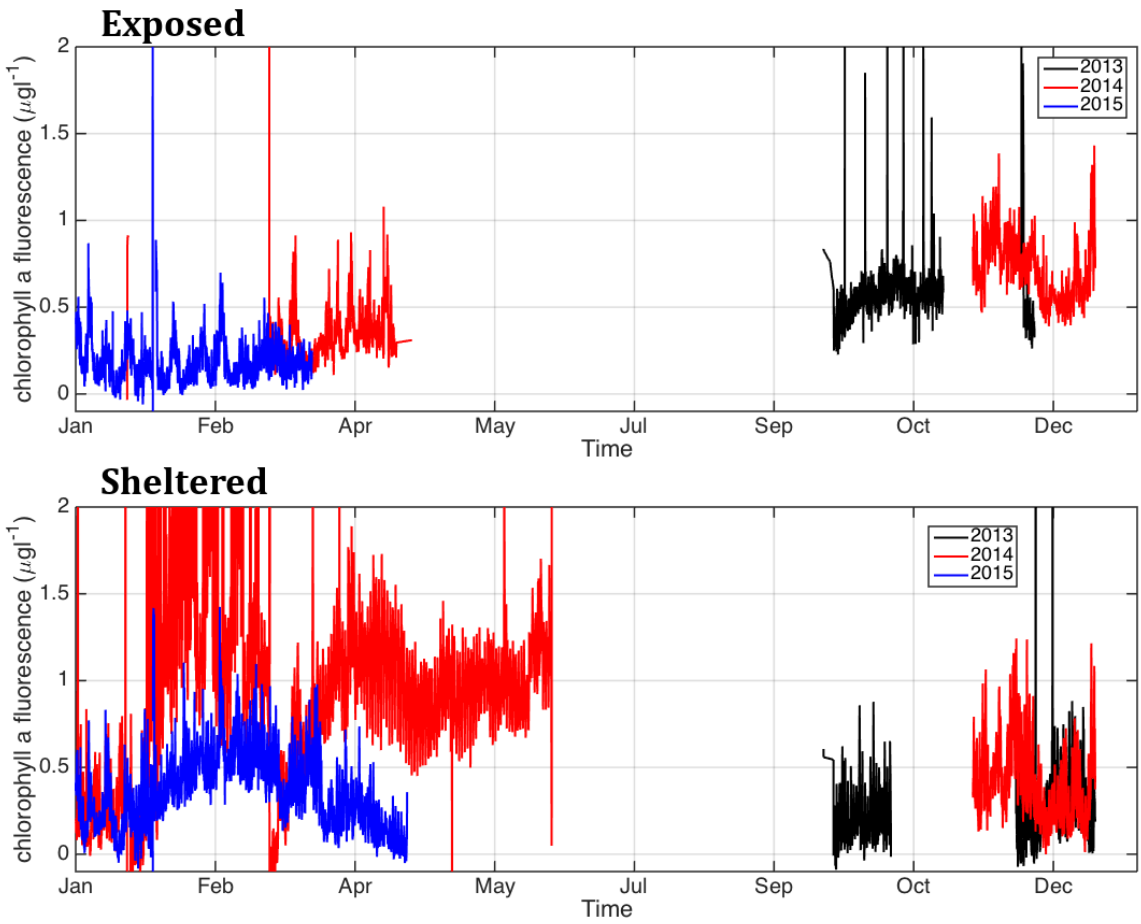

Figure 2.13. Time-series from the fluorometer deployments on the exposed (top) and sheltered (bottom) moorings. The colors represent different years (2013 = black, 2014 = red, 2015 = blue).

2.4 Discussion

Water mass variability around Shi'b Habil, a whale shark aggregation site, shows very clear seasonality of the temperature and salinity. The temperature minimum in February and associated homogenous water column is expected as a result of colder atmospheric temperature and winter mixing. On the other hand, the lower temperature in July when the atmospheric temperature reached its maximum was unexpected, based on interactions with the atmosphere. We suspect the

decrease in temperature is a consequence of the Tokar wind jets that occur in the summer.

From mid-June to mid-September, strong westerly Tokar wind jets enter the basin modulating the wind system as frequently as daily, adding a cross-basin component to the otherwise along-basin winds that dominate the region (Jiang et al., 2009). The strongest Tokar wind jets occur in July, according to monthly mean surface wind stress from Weather Research and Forecasting model in 2009, with diminishing wind jets in August (C. Chen et al., 2014). The strong wind stress curls associated with these wind jets may create dipole eddy pair with a cyclonic eddy to the north and an anticyclonic eddy to the south of the wind jet (Jiang et al., 2009; Sofianos & Johns, 2007; Zhai & Bower, 2013). This will transport waters in the coastline offshore, which will depress coastal sea level and upwell deeper waters to compensate. Sea level at Shi'b Habil was 0.8 m lower from May to October (minimum in July and August), similar to previous studies in coastal Red Sea (Patzert, 1974). Coastal upwelling ecosystems are known to be productive. Thus phytoplankton biomass and primary productivity rates, as well as the trophic cascade of carbon, of the exposed side of Shi'b Habil should be examined to compare the upwelling summer (July) with the non-upwelling seasons (Vargas et al., 2007).

The mooring data showed that the summer (May to September) period was relatively fresher and colder than the rest of the year and experienced sudden and short (5-26 days) episodes of colder, fresher water. Because there are no land-based sources of fresher water in the region (2002-2012 average rainfall 0.3-4 mm from May to September (World Weather Online, accessed November 2, 2015)), source of

the cool, fresher water is most likely GASW, consistent with GAIW inflow during the southwest monsoon season (Churchill et al., 2014; D. A. Smeed, 2004). The GAIW mixed with the Red Sea water as it travelled to Shi'b Habil resulted in the GASW (Figure 2.1). We suggest that this July temperature minimum is GASW, which appears to enter this nearshore reef in episodes.

A secondary salinity minimum from the end of December into early January could be attributed to the winter wind convergence in the SCRS. In winter months, winds in the southern half switch to southeasterlies (Jiang et al., 2009; Pedgley, 1972; Sofianos et al., 2002; Sofianos & Johns, 2003). The opposing surface winds converge at approximately 19° N and escape westward through the Tokar Gap (Jiang et al, 2009). Elevated sea levels in the central Red Sea are observed during this time and suggest that this latitude becomes a convergence zone (Sofianos & Johns, 2001). The southeasterly winter winds in the southern half of the basin transport GASW from the south, with a net eastward flow of surface waters. This would introduce GASW to the eastern coast of the SCRS and lower salinity without the temperature drop. Thus GAW reaches the nearshore reef in Al-Lith during the summer and early winter.

Our study is the first to confirm the penetration of GAW through the coastal reefs in the Red Sea and reaching a nearshore (<5km from shore) reef. The GAIW intrusion is documented offshore of this complex coastal reefs in SCRS with low salinity (37.5) and high nitrate and nitrite concentrations (14-16 $\mu mol l^{-1}$) near 19 ˚N (Churchill et al., 2014). This subsurface feature was seen as a continuous northward stream along the eastern coast enhancing productivity at euphotic depths (35-67 m;

photosynthetic available radiation (PAR) light level measured at 67 m was 1% measured at 2m) (Churchill et al., 2014). This suggests all of our stations are above the 1% light level depth (67 m in September-October 2011 cruise) and is within the euphotic zone. Instead of a continuous stream as in the open ocean, the GAIW episodically appears at this nearshore reef. This episodic pattern may relate to mixing with adjacent water masses from turbulence caused by topographic features and eddy-driven circulations that dictate the incursion of GAIW inside the topographically complex reef system. The GAIW intrusion offshore is affected by eddies generated by a combination of both thermohaline processes and wind dynamics (Churchill et al., 2014; Jiang et al., 2009; Zhai & Bower, 2013; Zhai, 2011). Because eddies in the Red Sea have an average life span of about 45 days (Zhan et al., 2014) they may not be linked directly to the periodicity of the GAIW episodes (lasting 5-26 days). These eddies evolve through time, varying in size and location (Quadfasel & Baudner, 1993; Zhan et al., 2014). Therefore, their coastal interactions may vary at shorter time scales depending on the proximity to the reef systems. Thus filaments and other circulations created by the eddy are likely to transport the GAIW in short events to reef systems. Time-series at this reef will evaluate the frequency of GAW bursts and whether it is a yearly occurrence.

This natural burst of nutrient supply to the coral reefs from May to September provides a baseline for future studies focused on the effects of nutrient patterns on coral reef ecosystems. Compared to the Farasan Islands, a complex of reefs south of Al-Lith, Al-Lith has much higher coral cover and diversity, accompanied with less macroalgal growth (M. Berumen, unpublished data.). This

could be due to the periodicity of the nutrient supply in Al-Lith that becomes an intermediate disturbance that increases species evenness and subsequently resulting in high diversity as observed with storm debris and corals (Aronson & Precht, 1995). The Farasan Islands are part of the eastern coast of the southern Red Sea that has high surface chlorophyll concentrations based on remotely sensed ocean color data (Racault et al., 2015; Raitsos et al., 2013). This is indicative of a sustained nutrient supply in this region, potentially from the Indian Ocean (as GAIW), whereas Al-Lith receives nutrient supply in episodes (Figure 2.7). Nutrification can cause localized coral degradation, although it is not thought to be the sole factor driving degradation (Szmant, 2002). Shifts from a coral to algae dominated system can be fueled by a lack of herbivores due to fishing, disease, and environmental changes (Hughes, Graham, Jackson, Mumby, & Steneck, 2010; McCook, Jompa, & Diaz-Pulido, 2001). Further work along the coastline to determine the periodicity of GAIW and GASW at nearshore reefs, its nutrient flux, and its potential role as an intermediate disturbance is necessary to test this hypothesis.

A genetic break in reef fish (anemonefish and fourline wrasse) was suggested between 19 and 20 ˚N (Froukh & Kochzius, 2007; Nanninga et al., 2014), whereas the genetic break was at 16 ˚N in a common reef sponge (*Stylissa carteri*) (Giles, Saenz-Agudelo, Hussey, Ravasi, & Berumen, 2015). These genetic differentiations seem to correlate with environmental factors (e.g., nutrients) but the fit is not perfect, suggesting multiple physico-biological factors are involved. Common reef fish (butterflyfish and angelfish) were most abundant and showed highest species

richness in the central Red Sea (20 ˚N), decreasing both northward and southward (C. M. Roberts et al., 1992). In contrast, visual surveys of reef fish and benthic categories at 40 reefs along the Saudi Arabian Red Sea coastline (18.6 to 26.8 ˚N) revealed no significant difference in latitude (ref). The surveyed reefs were seven to 81 km from shore (median=26 km) compared to the 5 km distance for Shi'b Habil. If penetration of water masses (e.g., GAIW, RSDW) into nearshore reefs is affected by how it interacts with basin-scale oceanographic features (i.e., eddies, filaments, fronts), then a cross-shelf gradient is expected with higher exposure at offshore sites than the protected nearshore regions. Thus we suspect an environmental or oceanographic feature near the latitude of Al-Lith that creates the observed boundary and gradient.

The aquaculture plume was seen at stations (NE and N) closest to the outfall (3.8 and 4.7 km away, respectively). Signatures of high salinity, accompanied by high c_p indicated the consistent presence of plume water at this whale shark aggregation site. Interestingly, effluent was observed offshore from the reef at sites NW and W that were 6.5 and 8.4 km travelling distance from the outfall, respectively. At these stations on the exposed side of the reef, the plume was a mid-water column layer. We suspect the effluent trajectory was around the northern end of the reef to reach these offshore areas since there was never evidence of discharge at E and S. Thus around August to November, this plume layer was advected offshore. A regional model with fine-scale bathymetry map would aid in our understanding of the circulation that allows or prevents the effluent to reach offshore.

For the first time, an oceanographic survey was conducted to fill in the lack of data at the coastal coral reef systems of the SCRS. Three water masses with potentially high nutrients were present at this whale shark aggregation site. GAW arrived episodically from May to September. RSDW apparently upwelled on the exposed side of the reef in July. Aquaculture discharge was always present on the northeastern side of the reef but reached the offshore stations in August to November. Although we observed distinct timing and spatial patterns from these three sources, none of them appears to vary in a manner that would directly explain the habitat selectivity of the whale sharks. But the nutrient input could indirectly affect the aggregation if animals that later on mature to spawn depend on this nutrient source, and their spawning event attracts the whale sharks.

Acknowledgements

We thank the RV Thuwal captain and crew, Francis Mallon, Ajay Sancheti, Lloyd Smith, Ioannis Georgakakis, Brian Hession, Gazi Aljehdali, the KAUST Coastal and Marine Resources Core Lab, Jesse Cochran, Isabelle Schulz, Fernando Cagua, Amr Gusti, Pedro De La Torre, Joseph DiBattista, Moustapha Harb, Ahmed Shibl, Holger Anlauf, Alex Kattan, Maha Khalil, and Dream Divers for their field and logistical support. We express our gratitude to Stein Kaartvedt for his editorial input.

CHAPTER 3. WATER QUALITY, SEASONALITY AND TRAJECTORY OF AN AQUACULTURE-ASSOCIATED PLUME IN THE RED SEA

Abstract

We examined the characteristics of the wastewater (estimated 42-48 m^3s^{-1}) from a land-based aquaculture facility, discharged near a spring whale shark aggregation reef. The effluent was suspected to influence the spatio-temporal patterns of whale sharks by chemical cues, plankton blooms from nutrification, and toxins. The area around the aquaculture outfall was surveyed using an AUV, echosounder, and profiling package to characterize the physical, chemical, optical and microbial properties of the effluent and its spatial distribution. The discharge had elevated salinity, density, and turbidity, and formed a dense layer 1-3 m thick above the seafloor. The plume travelled along paths determined by the bathymetry, potentially creating areas with higher residence times. Total nitrogen concentration at the outfall was five times higher than surface waters 1.4 km away from the outfall. Estimated daily fluxes of nutrients were 109-123 kg for nitrate-N, 72-82 kg for nitrite-N, 121-138 kg for phosphate-P, and 882-999 kg for silica-Si. Bacteria and cyanobacteria analysis revealed significantly higher cell counts and relative abundance of genus *Arcobacter*, a genus associated with opportunistic pathogenic species (e.g., *Arcobacter butzleri*), while *Prochlorococcus sp*. was significantly less abundant at the outfall. The effluent was observed near the northeastern side of the reef (3.8 km from the outfall) throughout the year, but even further away during late summer and autumn when it was observed across the northern end of the reef,

extending to the exposed side of the reef (8.2 km from the discharge). Benthic and demersal communities are most likely to be negatively affected by this dense bottom-hugging plume. Since this plume was observed at the whale shark aggregation site during their season, it is possible they influence the shark's behavior via chemosensory cues, a hypothesis warranting further chemical analysis (e.g., dimethyl sufide).

3.1 Introduction

A large aquaculture facility in Al-Lith (20.15˚N, 40.25˚E), on the eastern coast of the South Central Red Sea (SCRS), spans over 40 km of coastline and occupies 4000 ha of land for pond farms and hatcheries. In 2014, 13,000 t of prawn were produced, accounting for 70-80% of the total produced biomass. Other products included sea cucumber, algae, and beta-carotene. Before stocking, the ponds are enriched with molasses, wheat bran, di-ammonium phosphate, and urea to create a zooplankton bloom (N. Ayaril & M. Villarreal Ricord, pers. comm.). Feed pellets composed of 34-40% crude protein and 9-11% fat are produced at the facility and are fed to the shrimp. Wastewater from the ponds merges to form one main outflow and should approximately equal the intake flow, which has an estimated volume flux of 42-48 m^3s^{-1} (N. Ayaril, pers. comm.). This intake supposedly does not stop, thus this suggests continuous flow at the outflow at varying rates that depend on environmental factors (e.g., evaporation rate) and aquaculture operations (e.g., water kept for hatcheries and beta carotene farms). The wastewater goes through a settling basin to minimize suspended particles; otherwise there is no treatment of

the effluent. No other comparable anthropogenic discharge is known in the area (e.g., Al-Lith's (population of 72,000 in 2010) municipal wastewater) and terrestrial runoff is minimal due to low precipitation rates. We speculate there is an outflow from the lagoon west of the aquaculture outfall (20.161 ˚N, 40.229 ˚E), which will provide a "natural" flux of unknown water quality, potentially with higher salinity. Thus in the oligotrophic Red Sea, the aquaculture discharge is potentially a major anthropogenic nutrient input.

Al-Lith's coastal ecosystem is shallow (2-40m) and complex with steep coral reef structures dispersed on sandy bottom and seagrass beds. Coastal mangrove patches have been replaced by the construction of the aquaculture facility (Gladstone et al., 1999) but some line the interior side of the barrier island that forms the lagoon along the aquaculture facility. To our knowledge, no studies have evaluated the impact of the aquaculture plume on the mangrove community (Kotb et al., 2004). Reef fish, invertebrates, and mammals associated with these habitats attract local fishermen and tourism, and are a source of income. Additionally, an annual spring whale shark aggregation at a nearshore reef (Berumen et al. 2014) and frequent visits by manta rays (Braun et al., 2014; Braun, 2013) boost tourism. Reefs near the outfall have less coral cover, the community composition shifts toward bigger and stress-tolerant species, and the fraction of non-living substrate is greater than in offshore reefs in Al-Lith (Sawall et al., 2014). The plume is suspected to promote algal blooms that may include chain-forming diatoms, filamentous *Trichodesmium sp*., toxin-producing phytoplankton, and other pathogenic organisms (Kürten, Khomayis, et al., 2014).

Despite the proximity (<5 km) of the outfall to Shi'b Habil, where the sharks aggregate, the aquaculture discharge's effects on the whale sharks are not known. One hypothesis is that the plume could provide a chemical cue, such as dimethyl-sulphide (DMS), that either entices or deters whale sharks (Dove, 2015; Hay, 2009; Martin, 2007; Savoca & Nevitt, 2014). A recent aquarium study showed whale sharks displayed foraging behavior when encountering DMS and homogenized krill solution (Dove, 2015). Thus whale sharks react to chemosensory cues and could be influenced by the plume's chemical and biological constituents. Alternatively, plankton blooms triggered by nutrification and altered plankton species composition could affect their seasonal distribution. The motivation for this seasonal whale shark aggregation is uncertain. If the motivation is a "bottom up" driven availability of prey for the whale sharks, then the basic understanding of the water masses that might contribute to this productivity is of interest. Consequently, it is important to examine the largest aquaculture effluent's trajectory, nutrient, suspended particulate matter (SPM), and organic matter concentrations, and the microbial community to evaluate its overall effect on the coastal environment and to predict its potential implications on the whale sharks and other marine life.

Untreated aquaculture wastewater has diverse ecological implications that could directly or indirectly influence the whale sharks. Previous studies have shown that aquaculture wastewater can contain high concentrations of nutrients, organic matter, SPM, chemical substances, pathogens, and non-native animals (Burford et al., 2003; Jackson, Preston, & Thompson, 2004; PÁez-Osuna, 2001). Burford et al. (2003) observed nutrient concentrations of 65.5 μM nitrogen and 4.1 μM

phosphorus downstream of one such outfall. In addition, the discharge plume exhibited enhanced phytoplankton and bacterial production, increased microzooplankton grazing rates, decreased mesozooplankton grazing, and altered zooplankton community structure and abundance. This will have ripple effects in the food web dependent on these primary producers. Smothering by a specific genus of algae (*Ulva*) as a result of high nutrient input causes mangrove diebacks and retards growth in seedlings (Schaffelke, Mellors, & Duke, 2005). Furthermore, SPM and microalgae abundance increase, causing greater light attenuation. Macroalgae overgrowth, resulting from decreased herbivorous fish abundance could shade and prevent coral recruitment and growth (Hughes et al., 2010). This limits photosynthetic available radiation (PAR) for primary production and degrade habitat-forming seagrass beds and coral reefs (Abal & Dennison, 1996). This could devastate nursery grounds and decrease reef fish populations (Nagelkerken et al., 2002). Organic matter from the plume could settle to form enriched sediments, degrading benthic and demersal communities; however, Smith (1996) found organic carbon was less than 2% of sediments accumulating in the center of the prawn ponds. Nonetheless, no studies reveal the extent of ecological impact on these communities. Previously no significant relation of lesioned Fungiidae corals with distance to the outfall was revealed (Furby et al., 2014) but these corals are known to have high thermal and saline tolerance (Baria, Kurihara and Harii 2015; van der Merwe et al., 2014) and further assessment of other families is necessary. The plume had higher dissolved and particulate organic matter (POC and PN), bacteria, phaeopigment, calanoid copepodite, and Chaetognatha abundance (Kürten,

Khomayis, et al., 2014) and studies should continue to examine other unique characteristics of the plume to understand its environmental impacts to Al-Lith's coastal region.

This study aims to characterize and track the aquaculture-associated plume to understand its subsequent effects on the region's biogeochemistry. We focus on 1) describing the physical, chemical, optical, and microbial water qualities of the effluent, 2) its seasonality, and 3) its trajectory.

3.2 Methods

Study site

Our study site, Al-Lith, is on the eastern coast of SCRS. It hosts a seasonal whale shark aggregation from mid-February to May centered at Shi'b Habil (Figure 3.1) (Berumen et al., 2014). Manta rays, dugongs, mangrove patches, seagrass beds, coral reefs, and reef-associated fauna also occur in this region.

Spatial surveys

The coastal area offshore from the outfall was surveyed with an autonomous underwater vehicle (AUV) (REMUS 100, Kongsberg, Norway) on December 4, 2013. The platform was programmed to survey a 5.5 km zigzag line (Figure 3.1) measuring temperature, salinity, chlorophyll *a* (chla) fluorescence, turbidity, and water current velocity while traveling at a constant 1 m depth beneath the surface at a speed of 4 knots.

The plume was mapped acoustically using a 200 kHz echosounder (SIMRAD EK 60, Norway) on January 15, 2014. Car batteries powered the echosounder, and the transducer was fixed to a pole on a boat while a GPS logged the position and time of the survey. The GPS turned off near the end of the survey, but this affected only a small part of the data. The path of the survey was chosen based on the real-time data of acoustic backscatter. Our operational assumption for tracking the plume was that high backscatter would characterize the turbid plume layer providing an indication of its horizontal track and its depth.

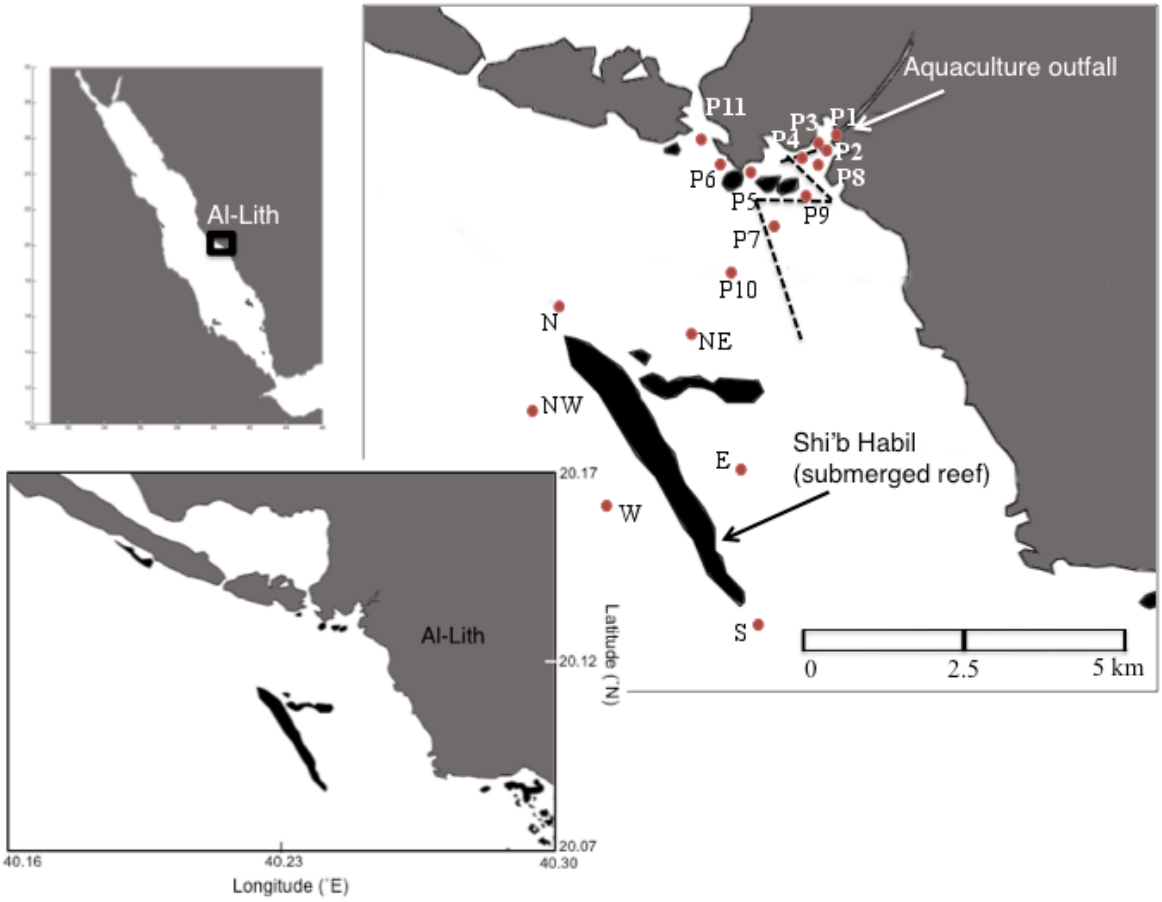

Figure 3.1. Map of the Red Sea and insets with Al-Lith's coast and outfall for the coastal aquaculture. The REMUS survey line (dashed line) and monthly survey stations (circles) are labeled.

Monthly surveys

Following these findings from the spatial surveys, monthly surveys were conducted from January 2014 to January 2015, except for the month of October for logistical reasons. Vertical profiles were obtained at 13 stations (P1-P7, N, NE, E, S, W, NW) around the outfall from January to June 2014, and an additional four stations (P8-P11) were added from July 2014 as part of a complementary field effort (Figure 3.1). The profiling package included a CTD (Microcat 37SM, Seabird, USA or Ocean Seven 304, Idronaut, USA), fluorometer (FLNTUB, WETLABS, USA), and laser diffractometer (Laser in-situ Scattering and Transmissometry (LISST), Sequoia Scientific Inc., USA). The measured variables include temperature, conductivity, pressure, chla fluorescence, (excitation 470 nm/ emission 685 nm), turbidity (700 nm), particle size distribution (PSD), and particulate beam attenuation coefficient (c_p, 670 nm with 5cm path length). The optical measurements were proxies for phytoplankton biomass and suspended particulate matter (SPM). Measurements were aligned by time stamps and averaged into 0.5 meter bins.

Optical sensors were referenced with clean filtered Milli-Q® water for correcting the field data. For the LISST, after the conversion from ring data to PSD data, the first two and last two size ranges were dismissed following the example of previous studies (Boss et al., 2015; Kheireddine & Antoine, 2014). Thus particle size distribution between 1.9 and 165 μm was calculated using a laser diffraction method and Mie theory under the assumption that the particles are spherical.

Water samples were collected for chla filtrations (0.5-2 L depending on the proximity to the outfall) and were filtered with GF/F Whatman® filters for acetone extraction (Arar and Collins, 1997). For SPM measurements, 0.5 L of water was filtered on pre-weighed GF/F Whatman® filters and dried in the oven at 50 ˚C for 24 h. Following a desiccation period, they were re-weighed (Brügmann & Kremling, 2007). At P1 and P7 stations, water samples (100 mL) were frozen and later analyzed for nitrate, nitrite, phosphate, and silica using US EPA Methods 353.1, 354.1, 365.1, and 370.1. The detection limits were 2, 1, 1, and 5 $\mu g l^{-1}$ for nitrate, nitrite, phosphate, and silica, respectively. The former three were measured using AAA3 Segmented Flow Analyzer (Seal, Germany). Silica was measured using Aquakem 250 Auto Photo Analyzer (Thermo Scientific, USA). Ammonium was not measured because analysis was not completed on the day collected. Nutrient analyzer for urea was unavailable and could not be done. Nutrient concentrations at P1 station representing the aquaculture plume was compared to surface waters at P7 station.

The R/V Thuwal was used pending availability. Otherwise a local recreational boat was used. The R/V Thuwal is equipped with a winch and CTD rosette, enabling water sampling at multiple depths for the offshore stations (W, NW, N, S). The months when the R/V Thuwal was used were January, March, and April. In other months, subsurface water sampling was limited and the inshore stations were inaccessible by the R/V Thuwal. In these cases, it was only possible to collect using hand-triggered single line Niskin.

Data analysis

For comparison, we assigned station P1 as the "plume" water because it is in the outfall, and station E as the "ambient" coastal water. Plume signatures were never seen during our sampling period at E, probably because the branching reef blocks the discharge from reaching this station (Figure 3.1). Also east of Shi'b Habil is shallower than north of Shi'b Habil so the dense plume most likely follows the deeper bathymetry and does not travel to the east of Shi'b Habil. Stations P6 and P11 are located nearshore and could be control stations, but they are close to P5 (0.5-1.3 km) that regularly receives plume water. In addition, they are at the mouth of a lagoon with an unknown flow of potentially high salinity waters. No evidence for cross-shelf salinity gradient was observed from our yearlong observations. Thus it is possible to track the plume by its salinity gradient (P1 values vs E values). The physical and optical characteristics of the plume were derived by comparison of the water at P1 with the ambient water, which was assumed to be unaffected by the plume. We evaluated whether these water masses have distinct seasonal variability by using a paired t-test.

To examine the spatial distribution, the salinity from the plume was used to calculate the dilution factors (DF) at different stations for each monthly survey.

$$DF = \frac{(S_p - S_a)}{(S_x - S_a)}$$

where S_p is maximum salinity at P1, S_a is the mean salinity at E for ambient, and S_x is the maximum salinity at station of interest. In the same way, we analyzed its vertical distribution in the water column where S_x is the salinity at depths of interest.

The effluent velocity was estimated from ADCP (upward and downward-facing ADCP, Teledyne RD Instruments, USA) equipped on the REMUS. Data was extracted in WinADCP (Teledyne RD Instruments, USA) and analyzed on MATLAB (The MathWorks, USA). The water velocity at the outfall was not measurable because the depth at the outfall did not surpass the blanking bin (1.15 m) and the parking depth of the REMUS (1 m). Water velocity was only obtained at areas deeper than 2.65 m. Every 100 ensembles were binned for a horizontal resolution of approximately 130 m and temporal resolution of one minute.

Microbial analysis

Water samples were collected three times for microbial (bacteria and cyanobacteria) analysis and measured for total nitrogen (high-temperature catalytic oxidation method using TOC-V_{CPH} analyzer (Shimadzu)) (Ansari et al., 2015). The first batch was collected at 0.5 m depths at four stations (P1, P2, P4, P7) on April 14, 2014 (Figure 3.1). Collection was at 0.5 m depths and 0.5 m above bottom at the same four stations on December 15, 2014 and January 29, 2015. Samples were stored at 4 ˚C after collection. Cell counts were measured using Accuri C6 flow cytometer (BD Biosciences). The water samples were stained with SYBR Green I (Invitrogen) and incubated for 10 minutes at 35 ˚C in darkness (Ansari et al., 2015). They were tested for differences between samples using the t-test.

Genomic DNA was extracted from the 0.45 μm polycarbonate membrane (Millipore) and were stored at -20 ˚C. The total DNA was extracted from the membranes using the UltraClean® Soil DNA Isolation Kit (MoBio) and amplified for

the 16s rRNA genes with universal forward 515F and reverse 909R primers, and submitted for high-throughput sequencing on an Ion Torrent PGM platform (Ansari et al., 2015). We used the methods described in detail by Ansari et al. (2015). Sequences that passed the quality check were checked for chimera, and chimera-free sequences were classified to their taxa using RDP Classifier and distinguished to their operational taxonomic units (OTU) (Ansari et al., 2015). Multidimensional scaling (MDS) plots were made using Bray-Curtis similarity values of the abundance matrix after square-root transformation. ANOSIM was used to calculate significant differences between stations and seasons. Best-matched identities (82-97 % similarity) of OTUs were obtained by BLASTN against the NCBI 16S rRNA gene database.

3.3 Results

Preliminary survey

The REMUS survey in December 2013 showed that water leaving the outfall was characterized by significantly higher salinity (40.2 outfall vs 38.7 ambient), lower temperature (29.2 outfall vs 30.3˚C ambient), higher density (1025.9 outfall vs 1024.4 kgm^{-3} ambient), higher chla (0.8 outfall vs 0.6 μgl^{-1} ambient), and higher turbidity (2.3 outfall vs 0.15 NTU ambient) where the ambient water was surface water >1 km away from the outfall (Table 3.1). The dense plume sank below the surface approximately 250 m offshore from the outfall and was not detected past that distance at a depth of one meter where the REMUS was operating.

Table 3.1. Results of the two sample t-test testing the null hypothesis that the water at the outfall and water 1.4 km away from the outfall are physically and optically the same. Temperature, salinity, density, chla, and c_p were significantly different.

	temperature	**salinity**	**density**	**chla**	**c_p**
tstat	-626	936	842	26.3	241
df	899	899	899	169	169
p-value	0	0	0	1.1×10^{-61}	1.9×10^{-216}

The spatial survey using the echosounder showed that the turbid effluent sank approximately 250 m offshore from outfall, similar to the REMUS survey results obtained ~6 weeks prior. Following the effluent proved difficult due to the complex topography and lack of bathymetric charts. Consequently, our survey track was complex with loops and overlaps and therefore excluded from Figure 3.1 (included as Appendix E). The turbid effluent sank from the surface and traveled following the bathymetry, occupying a 1-3 m thick layer above the bottom (Figure 3.2a). The density discontinuity formed between the interface of the coastal water and the saline effluent was acoustically visible (Figure 3.2a and b). Observations in Figure 3.2b were taken along the survey line illustrated in Figure 3.2d, where the colorbar along the time-axis (Figure 3.2b) corresponds to the colors in the map (Figure 3.2d). The sharp salinity gradient (39.3 above water vs 41.2 effluent) was established by the CTD casts (Figure 3.2c) at the depths of the acoustic signal. Cast 3 and 4 were at stations P6 and P5, respectively, which were separated by a sill (Figure 3.2b and 3.2d).

The acoustic survey revealed steep topographic features, ranging from 5 m to 12 m height that obstructed the plume's trajectory. This causes the effluent to

disperse in a complicated pattern and likely forms “pools” with high residence time of the plume. We could not identify where the plume water left the inner basin of our study, which for this dense water mass will be determined by the fine scale bottom topography.

Trajectory

The spatial distribution of dilution is consistent with the aquaculture plume following a near-bottom trajectory toward the southeast during our surveys. The near-bottom, 1-3 meters thick layer had lower dilution (higher plume water concentration) than surface waters above it (not shown). By comparison, the plume dilutions at station P2, P3 and P4 were lowest, while dilutions at P6 and P11 were the highest observed (Figure 3.3). The map of dilution factors showed that the effluent layer is physically blocked by topography from reaching P6 and P11, consistent with the echosounder survey observations. The effluent reaches stations N and NE on Shi’b Habil that are 4.7 and 3.8 km away from the outfall and have bottom depths of 40 and 20 m, respectively. During the early autumn 2014 survey, the plume was observed at the offshore stations (NW, W) in the mid-water column. The mid-water column position is consistent with the dynamic from both dense and buoyant plumes coming into density equilibrium following an initial buoyancy-driven mixing phase (Snider & Andrews, 1994).

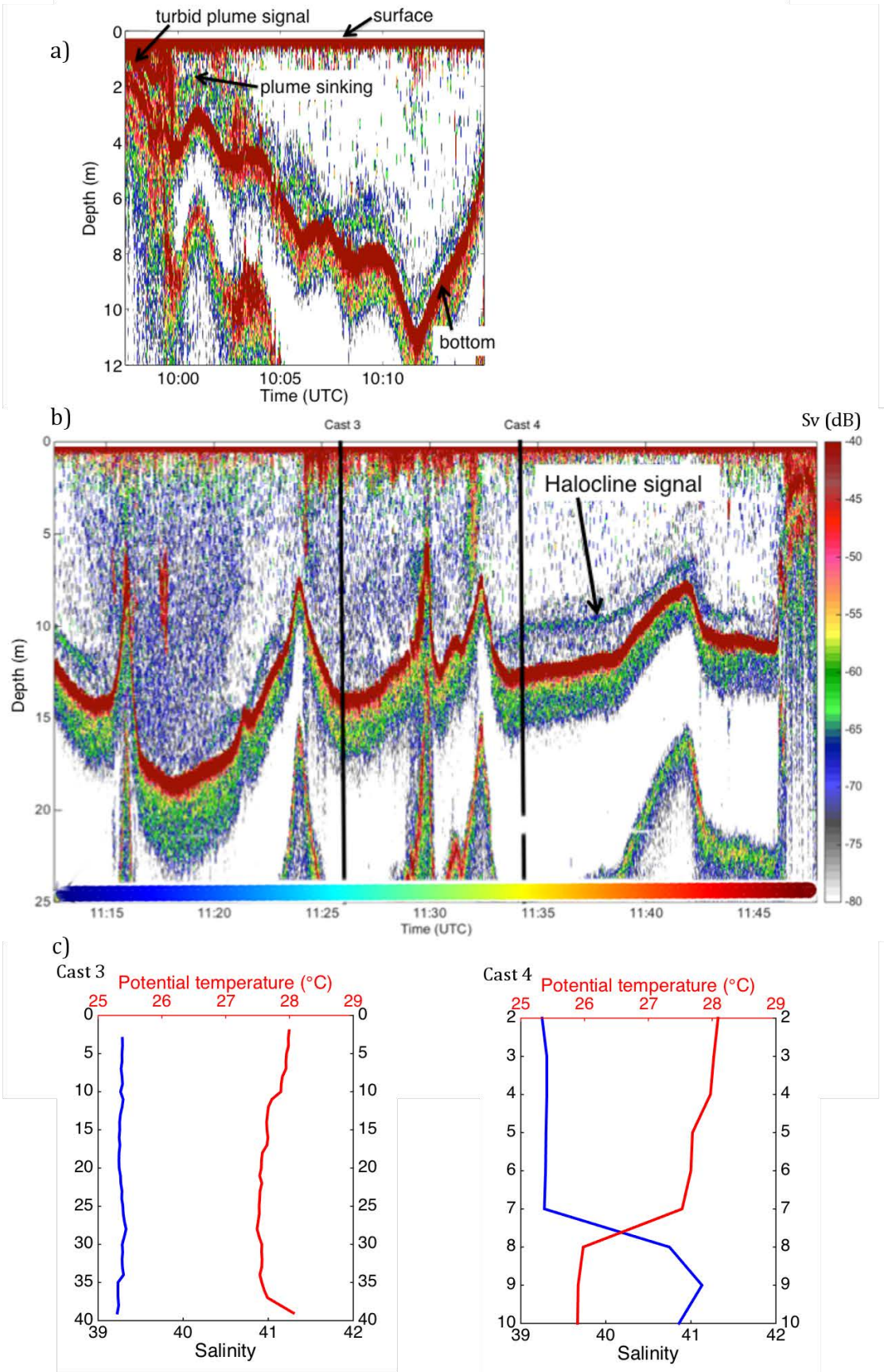
a)
turbid plume signal
surface
plume sinking
bottom
Depth (m)
Time (UTC)
b)
Cast 3
Cast 4
Sv (dB)
Halocline signal
Depth (m)
Time (UTC)
c)
Cast 3
Potential temperature (°C)
Salinity
Cast 4
Potential temperature (°C)
Salinity

d) 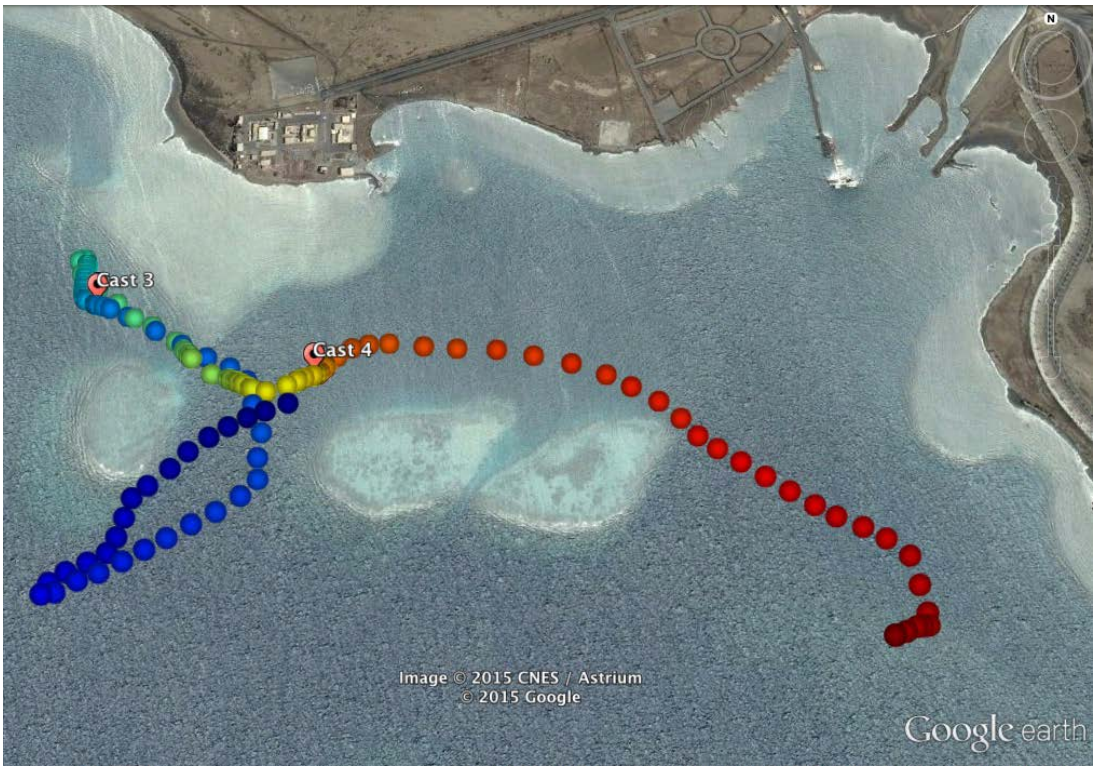

Figure 3.2. High resolution echograms of a) the plume's turbid signal leaving the surface to form a layer above the bottom. A part of the survey b) with and without the plume and its c) salinity and temperature profiles showing the signal 1-3 m above the seafloor is a result of the sharp salinity gradient (halocline). The b) color scheme above the x-axis (time) of the echogram corresponds to the spatial position of the colored path in the d) map of a close up near the outfall. The locations of cast 3 and 4 are shown here as well.

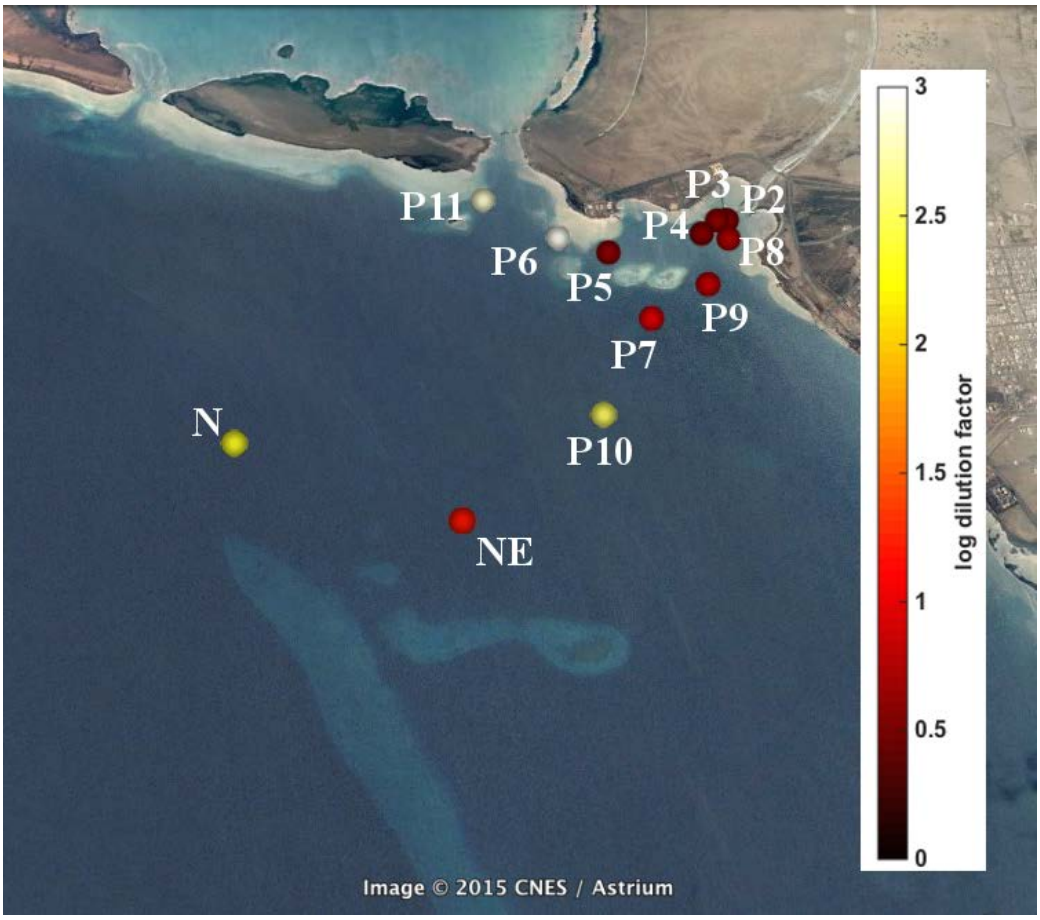

Figure 3.3. A map with the median of all monthly log dilution factors to illustrate the distribution of the effluent. The lower log dilution factors (dark red) represent waters with higher plume concentrations. The dilution factor increases with distance from the outfall as expected, but is still present at its farthest station 4.7 km away, suggesting its effect on Shi'b Habil.

The current patterns outside the outfall are complex. The depth-averaged water velocity became a southwestward current south of 20.145 ˚N (Figure 3.4). The bottom depth was between 3-19 m in this area. We did not see significant vertical patterns in the water velocity that suggested the 1-3 thick plume layer traveling at the bottom had a different water velocity. The mean depth-averaged velocity of the surveyed area was (± standard deviation) 2.8 cms^{-1} (±5.5). Maximum water velocity

was observed at the outfall (Figure 3.4) at 38.5 cms^{-1}. The mean (± st. dev.) water velocity without this maximum at the aquaculture outfall was 1.9 cms^{-1} (±1.0). The range was from 0.3—5 cms^{-1}.

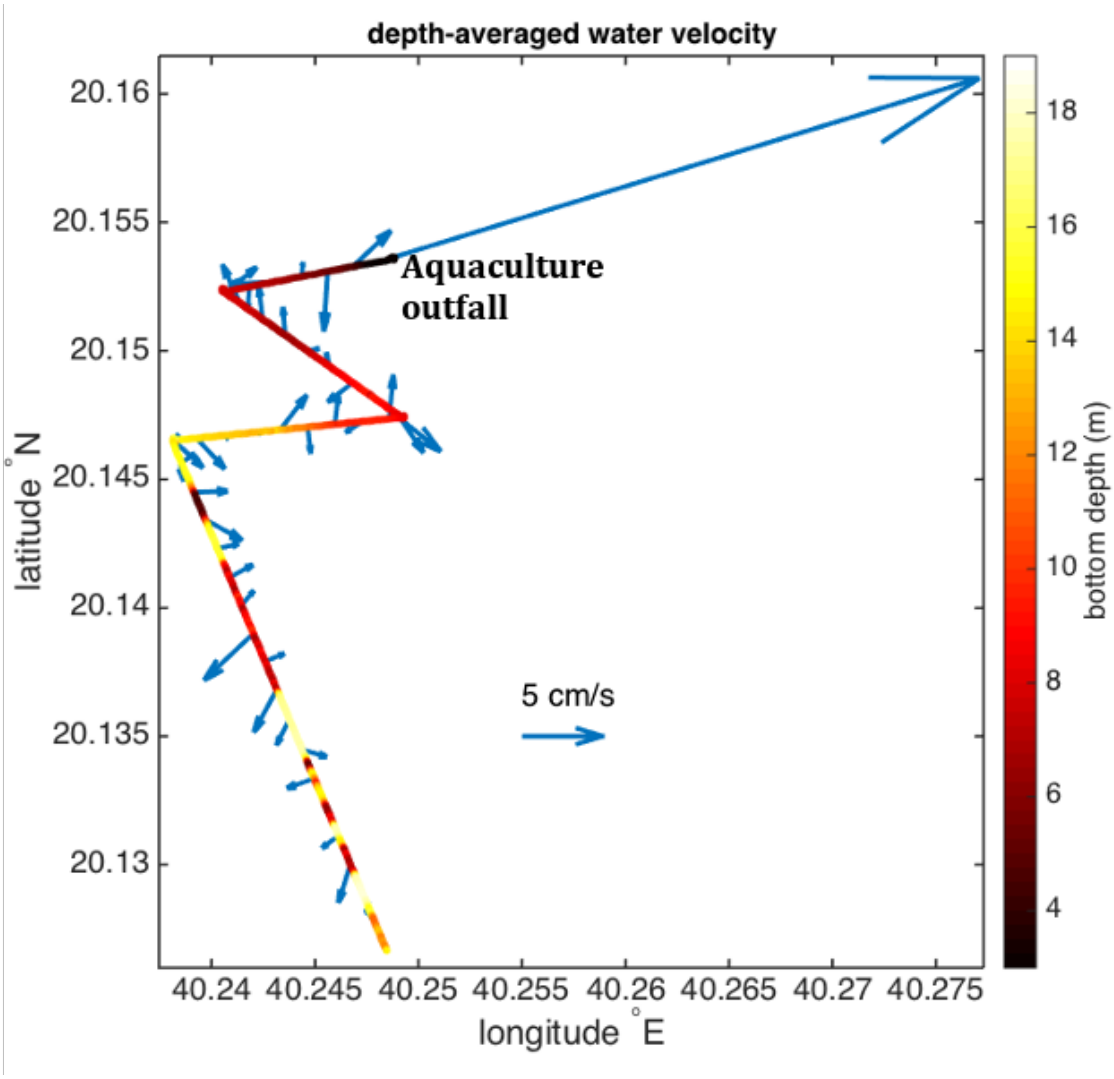

Figure 3.4. Depth-averaged water velocity from the REMUS survey is illustrated as vectors. Mean (±st. dev.) of the depth-averaged water velocity was 2.8 cms^{-1} (±5.5). The maximum measured near the outfall was 38.5 cms^{-1}. The survey line is shown in the map (Figure 3.1) to give perspective of its relation to the stations and outfall. The bottom depth is shown as the color of the line. The scale vector represents 5cm/s.

Physical properties

The temperature of the plume paralleled the ambient water, which followed the monthly mean atmospheric temperature (not shown), except in February. Both water masses increased in temperature from March to October, and then decreased with a minimum in February. Paired t-test showed that temperature did not significantly differ between the plume and the coastal water (Table 3.2; p-value=0.08, tstat=-50.5); although the plume temperature was almost 5 ˚C lower than the ambient in February (Figure 3.5a). On the other hand, the plume's salinity was significantly higher than the ambient and was exceptionally high in June, reaching 48, 10 salinity units higher than the ambient (Figure 3.5b) (Table 3.2; p-value<0.001, tstat=103). The ambient salinity never exceeded 39.3, while the plume's salinity never dropped below 40.5. Density of the plume was also significantly higher than ambient density during our sampling period (Table 3.2; p-value<0.001, tstat=40.2).

Table 3.2. Results (±st. dev.) for the two sample t-test for testing the null hypothesis that the discharge water at the outfall (P1) and station E are physically and optically the same. The salinity and chla of the discharge water is significantly different from the coastal reef water found at station E.

mean	**temperature**	**salinity**	**density**	**chla**	**c_p**
tstat	-50.5 (± 165)	103 (± 104)	40.2 (± 20)	10.2 (± 7.4)	9.19 (±12)
df	40.7 (± 17)	36.5 (± 19)	38.6 (± 18)	27 (± 24)	29 (±22)
p-value	0.081 (±0.19)	4.16×10^{-4} ($\pm1.4\times10^{-4}$)	1.75×10^{-6} ($\pm5.5\times10^{-6}$)	1.24×10^{-4} ($\pm2.2\times10^{-4}$)	0.10 (±0.17)

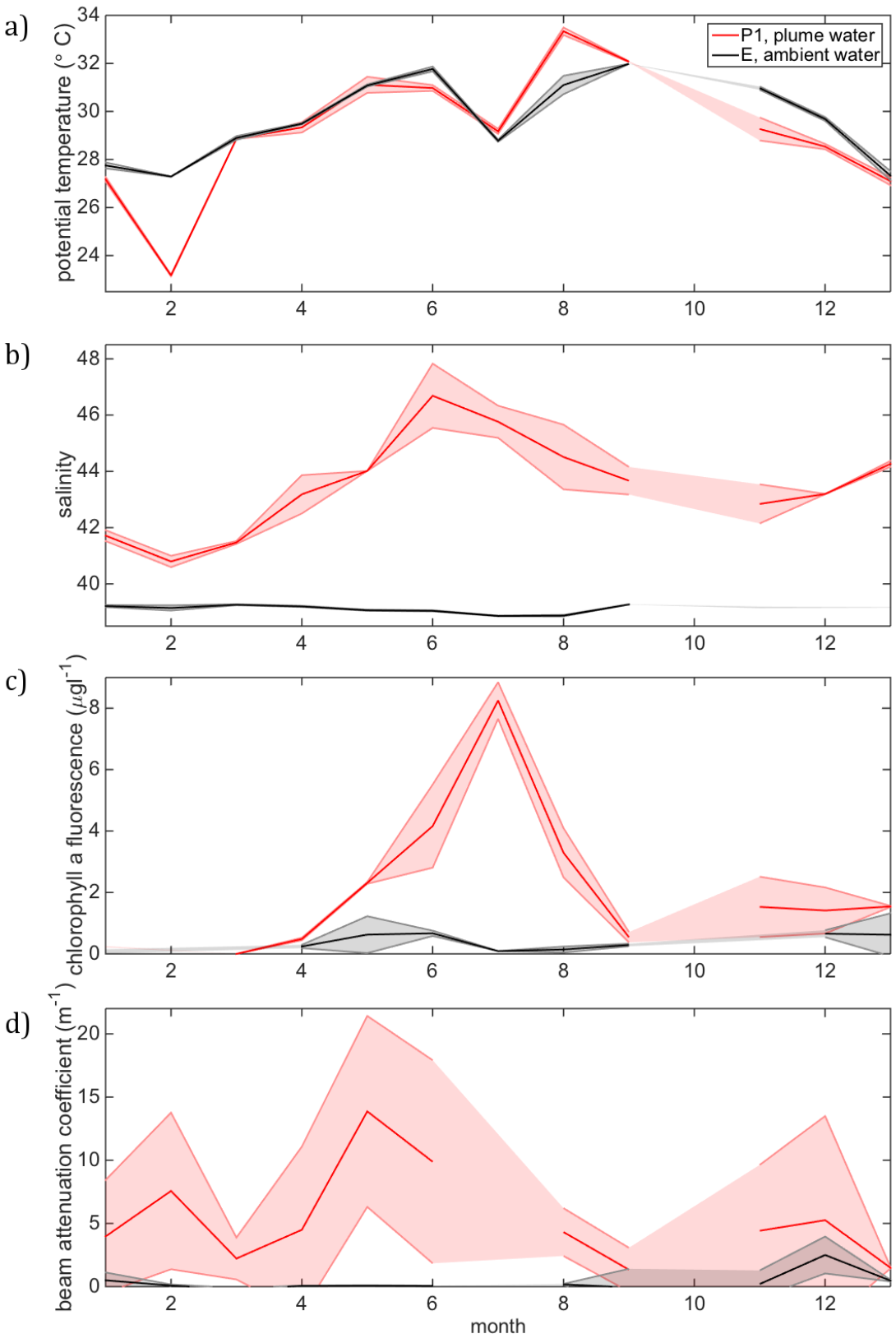
a)
potential temperature (° C)
P1, plume water
E, ambient water
b)
salinity
c)
chlorophyll a fluorescence (μgl-1)
d)
beam attenuation coefficient (m-1)
month

Figure 3.5. Comparison of a) potential temperature, b) practical salinity, c) chlorophyll *a* fluorescence, and d) particulate beam attenuation coefficient time-series between P1 (red) and E (black) stations. The mean (solid line) and standard deviation (shaded area) are plotted.

Optical properties

The plume water contained higher chla and c_p values than the coastal ambient water and exhibited greater seasonal variability. In fact, the chla fluorescence values were over an order of magnitude higher in the plume in July. The spring chla peak in the ambient water dropped to background levels by mid-summer; however, in the plume, it peaked in July and dropped to background values in September (Figure 3.5c). A smaller secondary peak in the plume's chla occurred during winter from November to January, which was similar in amplitude to the ambient water's secondary fall peak. The plume water's c_p peaked in May, earlier than the chla peak in July, with secondary peaks in winter (December and February). A slight elevation in the ambient c_p was observed in December (Figure 3.5d). The correlations between c_p and chla suggest the January peak in c_p is due to non-algal particles. Unfortunately the fluorometer data is not available in February to confirm if the c_p peak in February is also from non-algal particles.

The filtered SPM measurements (Appendix F) showed no correlation with c_p data measured with the LISST. The waters beyond the outfall were unexpectedly clear where particle concentrations were below the limit of detection for the 5 cm path length of the LISST. The instrument may not have been appropriate for measuring these low values. The SPM was lowest at stations close to the reef.

Surprisingly, the highest values were seen at intermediate stations (P5, P7) and not the waters by the outfall (P1, P2, P3, P4, P8). SPM at station NE was a magnitude lower than P7 (not shown). Insufficient samples were analyzed to evaluate the SPM seasonality.

The PSD revealed a seasonal pattern that differed between the surface and bottom waters. Data from January, April, August and November were chosen to represent the seasonal patterns in PSD at P1 (Figure 3.6). P1 had varied depths (Jan = 4 m, Apr = 3 m, Aug = 9.5 m, and Nov = 4.5 m) depending on the exact location of sampling: this was affected by our ability to stay in a location, fighting against the flow of the discharge. In the winter, the PSD of the surface (top half of the water column) and the bottom (bottom half of the water column) waters were similar in magnitude and shape (Figure 3.6). In the spring, the surface waters had low volume concentrations of the pico- and nano-particles (1.9 to 20 μm diameter) but with a peak in micro-particles (Figure 3.6). The bottom waters had a similar pattern in PSD but with a higher magnitude. In the summer, this reversed and the surface waters had a higher volume concentration (>70-fold) than the bottom waters (Figure 3.6). Both waters had low pico- and nano-particles but peaks in micro-particles. This pattern continued into autumn, where similar magnitude and PSD were seen as the summer except the bottom waters decreased in volume concentrations.

The surface waters (top half of the water column) peaked in the summer and had its minimum in the winter (Figure 3.6a) and the bottom water (bottom half of the water column) peaked in the spring with its minimum in autumn (Figure 3.6b). The plume water's volume concentrations were significantly higher than station E

(up to 80-fold in August) during our sampling period. Waters in station E had low volume concentrations, close to zero, and were in the lower detection limit of the LISST. Depth at P1 is shallow (<9.5 m) so we expect sediment resuspension by the discharge flow could create a vertical particle gradient; however, the bottom water had higher volume concentrations in the spring and was actually lower than the surface waters in the summer and autumn. Alternative hypotheses for our observed peak in surface waters vs the bottom waters is that positively buoyant particles are present, or bubbles caused by the turbulence at the outfall (personal observations) are detected by the LISST at the surface. This will suggest there is more positively buoyant particles or turbulence at the outfall in the summer and autumn.

a)

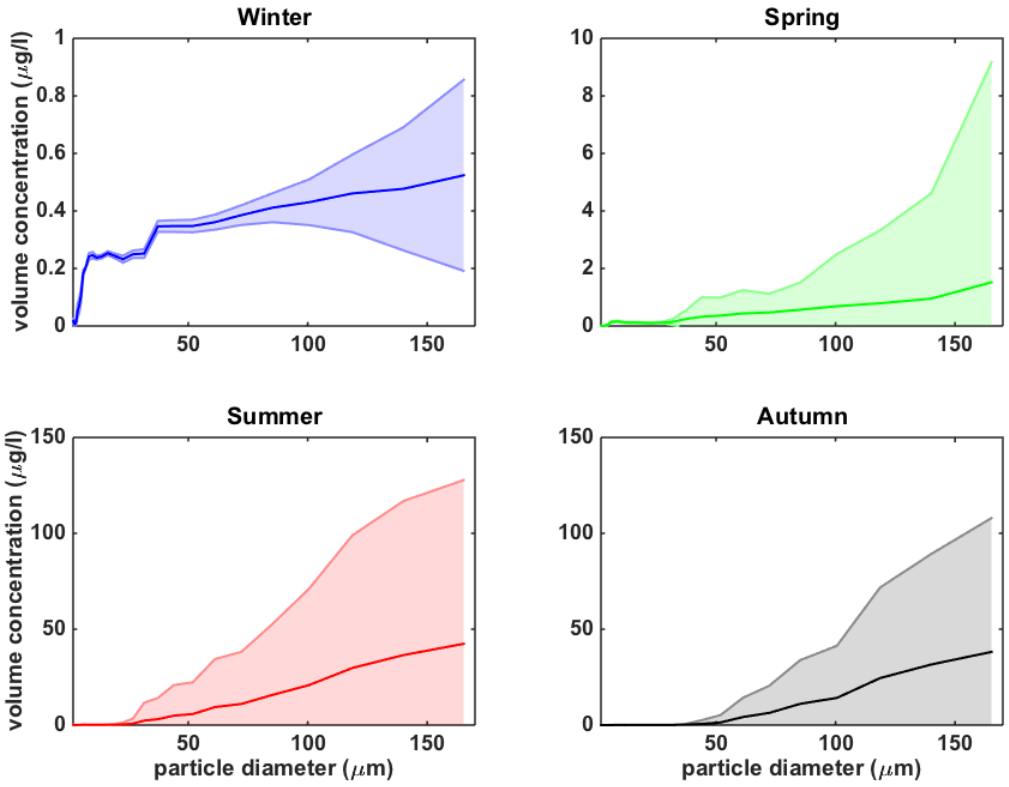
Winter
Spring
Summer
Autumn
volume concentration (μg/l)
particle diameter (μm)

b)

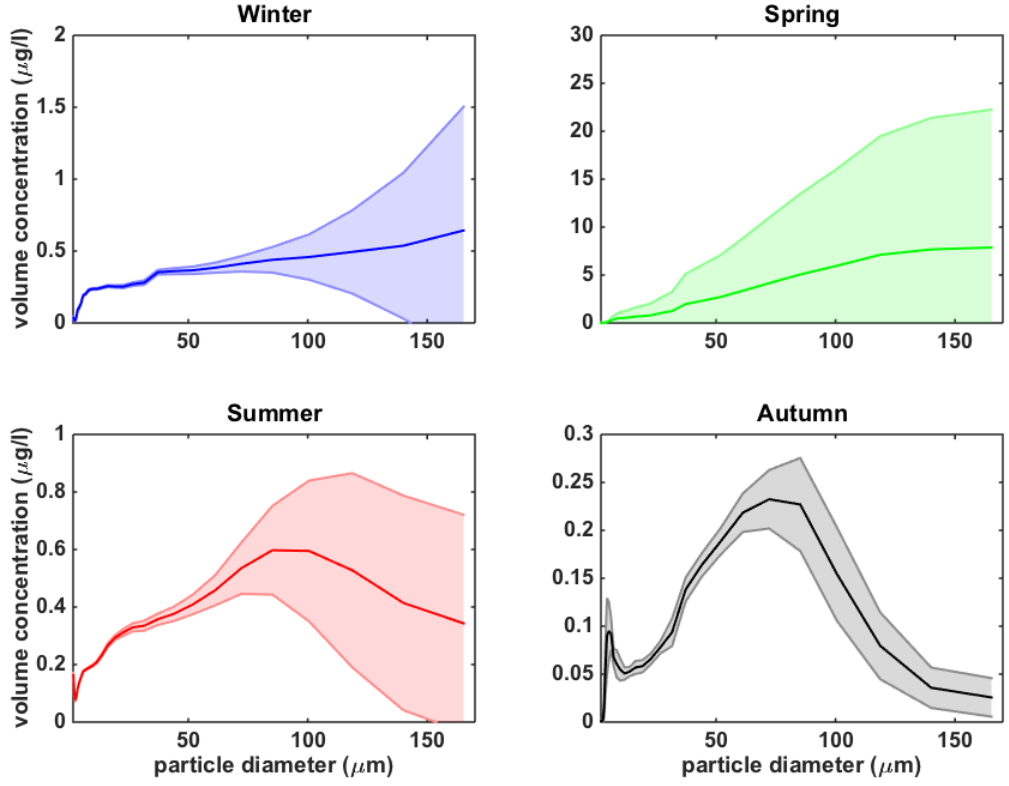
Winter
Spring
Summer
Autumn
volume concentration (μg/l)
particle diameter (μm)

Figure 3.6. Volume concentration against particle diameter is shown for a) surface and b) bottom waters at station P1 to illustrate the difference between depths. January, April, August and November data are shown to represent winter, spring, summer and autumn.

Nutrient concentrations

Nitrate, nitrite, phosphate, and silica concentrations were significantly higher in P1 than P7 (Table 3.3). Nutrient concentrations were highest in August for silica, December for nitrate and nitrite, and January for phosphate (Figure 3.7). Total nitrogen concentrations at the surface and bottom of P1 were nearly five-fold higher than total nitrogen levels at P2, P4 and P7. The nutrient levels at NE were not significantly different from P1 and was higher than other stations at Shi'b Habil (p-value=0.48-0.75, df=6, tstat=0.34-0.75). This is presumed to be result of the continuous presence of the plume at this station, as delineated by its physical properties. If the volume flux of the plume is indeed 42-48 m^3s^{-1}, then the estimated daily flux of nutrients from the discharge are 109-123 k g for nitrate-N, 72-82 kg for nitrite-N, 121-138 kg for phosphate-P, and 882-999 kg for silica-Si.

Table 3.3. Two-sample t-test results comparing nutrient concentrations between P1 and P7.

	silica	**nitrate**	**nitrite**	**phosphate**
tstat	4.68	2.20	2.22	4.18
df	11	11	11	11
p-value	6.71×10^{-4}	0.0497	0.0483	0.0015

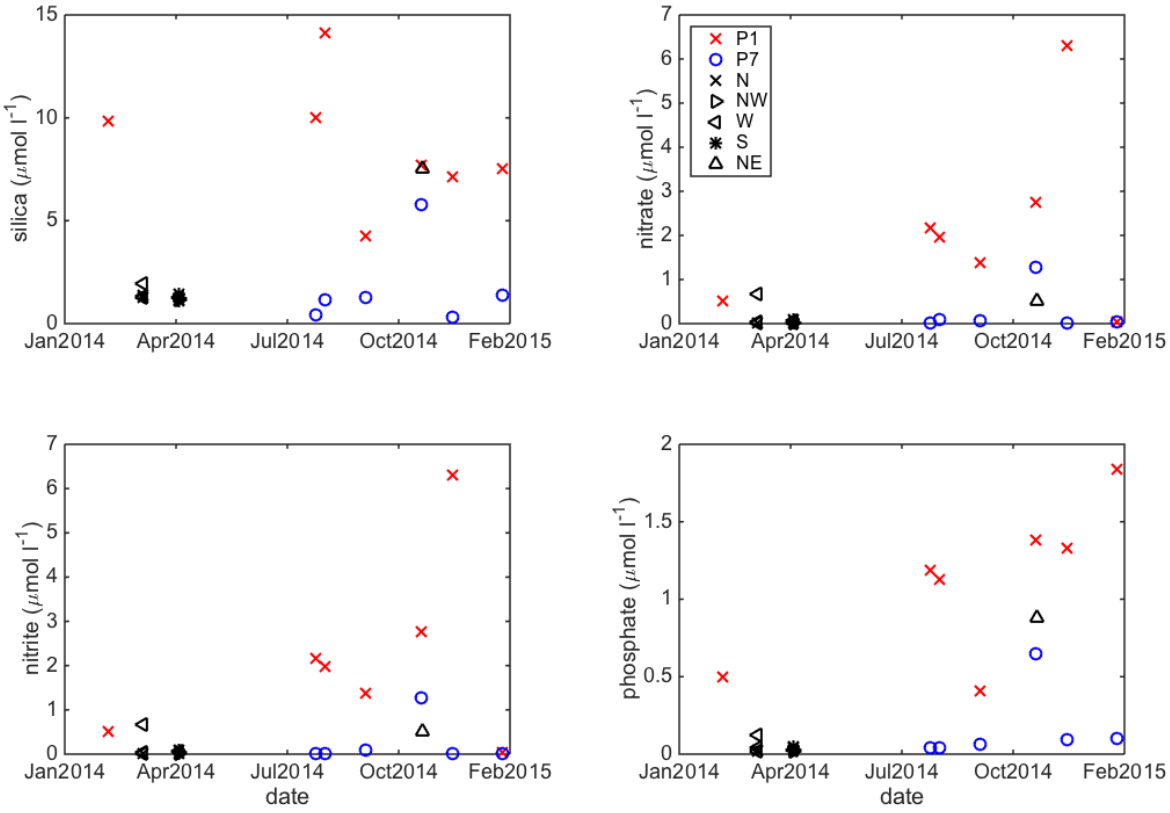

Figure 3.7. Nutrient concentration measured from P1 (red), P7 (blue), and other stations (black) are shown for silica, nitrate, nitrite, and phosphate over the sampled months.

Microbial communities

Microbial communities were distinct between P1 and the other three stations (P2, P4, P7). Cell counts were significantly higher in surface water at P1 than at other sites (p-value <0.05), and in the bottom water at P1 was significantly higher than P2 and P7 (p-value <0.001) and P4 (p-value= 0.01) (Appendix G). We found no significant difference in cell counts using flow cytometry between P2, P4 and P7 (p-value >0.05), except that P4 was lower than P7 (p-value= 0.01). Species richness (number of OTUs) was not significantly different among the stations; however,

certain OTUs are significantly more abundant in P1 (inside the outfall) (Appendix G). P1 also had significantly higher (>four-fold higher) total nitrogen concentrations than the other stations (Appendix G).

Relative abundance of microbial groups varied with distance from the outfall (Figure 3.8a), where P7 is 1.4 km away from P1 (Figure 3.1). Relative abundance refers to the number of sequences of a particular microbial group in a sample over the total number of sequences obtained for that sample after amplification of the bacterial 16S rRNA genes. A complete list of OTUs present at P1 at higher abundance than P2, P4, and P7 is provided in Appendix G. *Bacteroidetes* and *Actinobacteria* were relatively most abundant in P1, and decreased in relative abundance from P1 to P7. In contrast, *Cyanobacteria* (*Prochlorococcus*) increased in abundance from P1 and had highest relative abundance in P7. ANOSIM analysis revealed the microbial community at P1 was significantly different (Figure 3.8b) from the other three stations (P2: R= 0.306, p-value= 0.04; P4: R= 0.356, p-value= 0.024; P7: R= 0.552, p-value= 0.008) and microbial communities were significantly different between the sampling periods (R= 0.681, p-value= 0.001). There was no significant difference between surface and bottom (R= 0.015, p-value= 0.361). Unclassified *Actinomycetales*, unclassified *Microbacteriaceae*, and unclassified *Micrococcineae* were major microbial populations that were responsible for the distance between P1 and the other stations in the MDS plot. We found highly significant clustering among the three months (R = 0.681, p-value= 0.001), implying sampled months exhibited different species composition. Table 3.4 lists genera associated with opportunistic pathogenic species that are significantly more abundant in P1 than

other stations. Twelve genera associated with opportunistic pathogenic species were present at P1. *Arcobacter sp*. was the one genus with significantly higher abundance in P1 than other stations (Table 3.4).

Table 3.4. Tables listing OTUs present in the different stations (P1, P2, P4, P7) and the p-values for testing its relative abundance in the outfall (P1) compared to the other stations. Relative abundances of genera associated with opportunistic pathogens are listed. *Arcobacter* genus is significantly higher in P1 than the other sampled stations.

genera	P1	P2	P4	P7	t-test, *p*-value
Acinetobacter	0.038	0.177	0.193	0.023	0.234
Arcobacter	0.023	0.012	0.013	0.002	0.022
Aeromonas	0.001	0.026	0.068	0.001	0.239
Bacteroides	0.002	0.009	0.018	0.001	0.241
Bacillus	0.001	0.004	0.003	0.001	0.223
Enterococcus	0.003	0.006	0.010	0.000	0.572
Legionella	0.000	0.000	0.000	0.000	0.374
Escherichia/Shigella	0.000	0.006	0.008	0.000	0.181
Mycobacterium	0.005	0.012	0.009	0.001	0.576
Pseudomonas	0.103	0.453	0.387	0.055	0.271
Staphylococcus	0.001	0.000	0.000	0.001	0.629
Streptococcus	0.033	0.134	0.125	0.006	0.433

a)

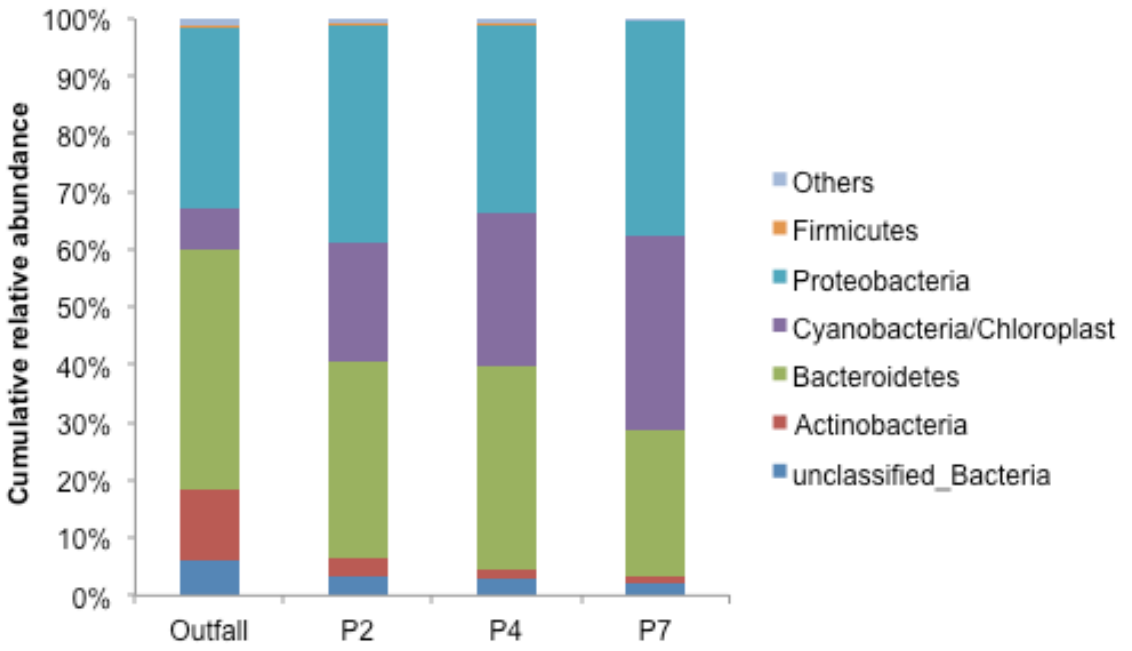

b)

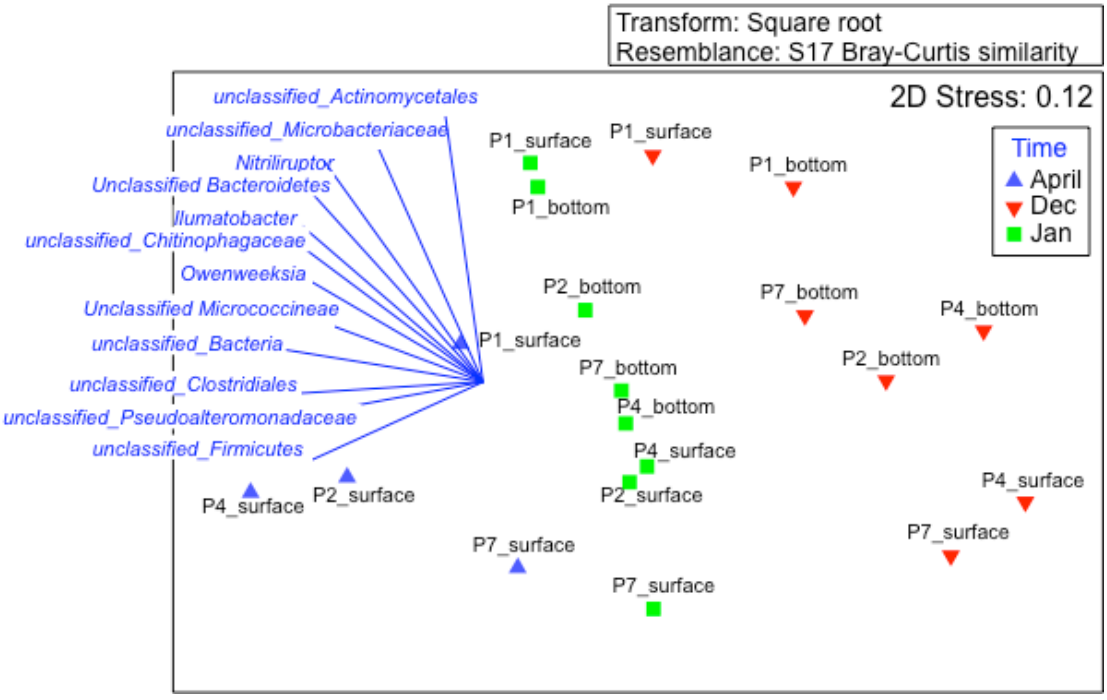

Figure 3.8. Relative abundance of phylum is shown as a) bar graph. *Bacteroidetes* and *Actinobacteria* are significantly relatively more abundant than at P7. A b) MDS plot showed bacteria community was different between sampling efforts (symbols). Within these sampled months, stations (labeled) showed patterns where P1

(surface and bottom) are different from other stations. The bottom waters at P2, P4, and P7 were closer to P1 samples than its corresponding surface waters. A list of microbial populations that accounted for the spatial distribution of P1 samples away from the other samples is included.

3.4 Discussion

Our study was the first to estimate how the water was modified during the process of passing through the integrated aquaculture farm in Al-Lith, under the assumption that the intake water is similar to that off Al-Lith. This study was the first to characterize its water quality and trajectory, vital information for the region and country, and provided a baseline to assist future ecological surveys and conservation efforts to protect the ecological and economical value for local fishermen and recreational facilities. Observations confirmed that the plume has significantly different physical, chemical, optical, and microbial properties than the ambient coastal waters. The plume had high phytoplankton biomass, based on chla fluorescence, and high SPM, which could be organic material (i.e., feed, animal parts). This could provide a chemosensory cue for whale sharks to detect. We could not conclude this from our data; however, we can speculate that ecological impacts are substantial on the benthic fauna due to the plume's trajectory near the seafloor.

The shallow aquaculture ponds are exposed to high summer solar radiation, increasing evaporation rate and will result in extremely high salinity during the summer. The maximum salinity of the plume was on the higher extreme limits of coral tolerances. Such high-tolerant corals are found in the Red Sea and the Arabian Gulf, where they survived 50 ppt (Coles, 1988, 2003). It is likely that Al-Lith has

some coral species adapted to hypersalinity; however, Sheppard (1988) estimated a loss of one coral species per increase of ppt from 41-50 ppt on the coast of Bahrain. The regions affected by effluent therefore could have reduced coral species compared to the nearby areas not affected by the discharge plume. Changes in coral diversity would most likely modify the associated fauna inhabiting the reefs. This could be tested by coral surveys at Shi'b Habil and adjacent reefs.

Brine discharges from desalination plants also discharge water with higher salinities than ambient conditions (Winters, Isquith, & Bakish, 1979). Altered community structures in corals, seagrass, and soft-sediment ecosystems have been documented in areas with high residence times of plumes (D. a. Roberts, Johnston, & Knott, 2010). In these cases the discharge returned to background levels within 10-4000 m from the outfall, and most discharges returned to background levels within 100s of meters. This limits the impact zone to be 10s of meters around these outfalls. Salinities at stations N and NE were routinely 0.5 and 2 units, respectively, over the ambient salinities. There stations were more than 4.7 and 3.8 km from the outfall discharge, respectively. At times the effluent has a much larger spatial extent as observed in September 2014, when the plume was observed at station W, nearly 9 km from the outfall discharge. Because the entire region was not sampled routinely, it is possible that the discharge plume extended over larger spatial areas along the coast and outside of the sampled region.

The measured nutrient concentrations, nitrate, nitrite, phosphate, and silica, were much higher within the discharge plume than in the ambient waters. Estimated daily fluxes are 109-123 k g for nitrate-N, 72-82 kg for nitrite-N, 121-138

kg for phosphate-P, and 882-999 kg for silica-Si, assuming the volume flux of the plume is 42-48 m^3s^{-1} (N. Ayaril, pers. comm.). The nitrogen and phosphorus components are suspected of deriving from the decomposing organic matter and residual feed. The increased nutrients from the plume likely contribute to phytoplankton productivity in the otherwise oligotrophic sea. We highly recommend that both urea and ammonium be measured in future studies of the aquaculture discharge. Urea is added to fertilize the ponds, and ammonium is the common nitrogenous excretion of shrimp. Urea enrichment may lead to harmful algal blooms because it is the preferred nitrogen form for some dinoflagellates species over nitrate and nitrite (Glibert, Trice, Michael, & Lane, 2005). The high nutrient load will increase plankton abundance. This bloom may be evident in the extended spring bloom seen in chla fluorescence that was an order of magnitude higher than the ambient chla peak and lasted two months longer.

Silica is likely to come from the sediments flushed from the ponds as found in Australian prawn farms (Smith, 1996). An average sedimentation accumulation rate from three farms (2-60 ha of pond area) was estimated as 288 kg ha^{-1} day^{-1} of which 5% was silica by weight (14.4 kg ha^{-1} day^{-1}) (Smith, 1996). With these values, the largest pond Smith (1996) measured (60 ha) gives similar values to our estimated daily silica-Si flux (864 vs 882-999 kg). We suspect sedimentation to accumulate in areas with reduced momentum (e.g., pockets with high residence times).

Increased silicate may facilitate diatom growth due to higher silicate availability to form their external shells and shift to a diatom dominated phytoplankton community. It may also increase the vertical transport of material

since diatom-rich material sink faster, particularly following nutrient depletion, providing more biomass for decomposition in the sediments (Turner et al., 1998). Due to regulations set by Saudi Arabian government after the white spot disease closed down all shrimp farms along the Red Sea coast from 2011 to 2013, the ponds must be dry for at least one month every year. To the best of our knowledge, the last harvest is aimed to occur by February, when the ponds are drained and sediments are oxidized before the new harvest season in April and May (N. Ayaril, pers. comm.). This suggests the highest discharge of silica will follow the flushing of the ponds in early summer, end of summer, and mid winter if the operation is achieving its goal of three harvests per year. Silica concentrations at P1 was highest in summer but was two-fold higher than in mid-autumn (Figure 3.7) but otherwise showed no seasonality. Higher temporal resolution of nutrients at the outfall along with production rates in aquaculture ponds are necessary to resolve the seasonal impact of the plume in relation to the aquaculture harvests.

The SPM was highest at sites P5 and P7, which could be attributed to the bathymetry creating areas with high residence time and trapping the turbid plume. High turbidity and c_p will attenuate PAR in the waters, negatively affecting light-dependent species such as zooxanthellae in corals, seagrass, and phytoplankton in the coastal region. The complex bathymetry of the area, which is not a simple gradual slope from coast to open water, creates topographic depressions where the dense effluent may become trapped. These pockets will have low flushing rates and expose the fauna to high salinity, high nutrient, and high turbidity waters for longer periods. Since these pockets are within the euphotic zone, the entrapment of the

nutrient-rich plume could cause an increase in primary productivity. In fact, the high c_p signal was accompanied by relatively higher chla fluorescence at P5 and P7 (not shown). Nutrient, sediment load, and toxins of low flushing sewage wastewater have been shown to detrimentally affect corals (Pastorok & Bilyard, 1985). Corals were outcompeted by benthic algae, their recruitment repressed, and oxygen levels decreased in these observations. We suspect similar ecological changes occur within these pockets, or depressions, but no studies have addressed this. We suggest conducting a high-resolution bathymetric survey to map out these areas of depressions and assess its environmental health.

Microbial dynamics at P1 and P2 showed strong impacts from the aquaculture plume, while P4 and P7 did not show significant influence from the discharge. The relative abundance of the plume's microbial groups is characteristic of coastal runoff water. Specifically, microbial groups isolated from hypertrophic lake (*Rhodoluna lacicola*), marine sediments (*Loktanella agnita*, *Sediminocola luteus*), contaminated water (*Alkaliphilus sp.*), and *Synechococcus* (*Gracilimonas rosea*) (Cho et al., 2013; Hahn, Schmidt, Taipale, Doolittle, & Koll, 2014; Ivanova et al., 2005; Takai et al., 2001) were significantly more abundant in P1 (p-value <0.05) than other stations. In addition, OTUs identified in previous studies to be isolated from seawater (*Aquiluna rubra*, *Pontimonas salivibrio*, *Alteromonas sp.*) and freshwater sediment (*Solitalea koreensis*) (Christen & Ivanova, 2004; Hahn, 2009; Jang, Cho, & Cho, 2013; Van Trappen, Tan, Yang, Mergaert, & Swings, 2004; Weon et al., 2009) were more than five-fold more abundant in P1 with >0.5 % relative abundance. Species isolated from water plants, algae from marine littorals (*Calothrix desertica*),

estuary sediment (*Illumatobacter fluminis*), marine sediment and sea snails (*Lewinella persica*), and seawater (*Crocinitomix catalasitica*) were only present in P1 with relative abundance >0.01 % (Berrendero, Perona, & Mateo, 2011; Bowman, Nichols, & Gibson, 2003; Khan, Fukunaga, Nakagawa, & Harayama, 2007).

One genera associated with an opportunistic pathogenic species (*Arcobacter*) was significantly more abundant (p-value <0.05) in P1 than the other stations. Species associated with this genus, e.g., *Arcobacter butzleri*, could be pathogenic to animals including humans, and future studies should test samples for the presence of such species. The microbial community at P7 was typical of oligotrophic waters, with higher abundance of *Prochlorococcus sp*. This is expected due to their high rate of organic nitrogen uptake, which was observed in oligotrophic regions of the Arabian Sea (Zubkov, Fuchs, Tarran, Burkill, & Amann, 2003). A previous study on this aquaculture discharge and fungiidae coral health saw higher incidences of lesioned corals when *Prochlorococcus sp*. was less abundant, ammonium was higher and silicate was lower (Furby et al., 2014). They suspected nutrient concentrations were not a major cause of coral deterioration in this region.

We cannot conclude if other plumes (e.g., lagoon, Al-Lith's municipal wastewater) exist that contribute to Al-Lith's ecosystem; however, we have measured the seasonal variability of the aquaculture wastewater, which has never been done before. The plume was observed at exposed sides of Shi'b Habil, where the whale sharks detections are higher, but its timing was not during the aggregation season. Thus it is unlikely that this plume is the sole motivation for their aggregation; however, chemosensory cues (e.g., DMS) and toxic substances (e.g.,

harmful algal blooms) should be measured to test whether the plume will affect their distribution during their aggregation. The aquaculture outfall had distinct characteristics and seasonality deviating from ambient waters. It was observed to reach 8.4 km offshore from the outfall in September 2014. The plume was a bottom-hugging layer so we advise future ecological surveys to focus on benthic and demersal communities. A multibeam bathymetric survey of the area followed by an echosounder survey will benefit the efforts by pinpointing topographic basins contributing to extended residence times of the effluent and mapping where the effluent is with respect to these basins. Further analysis to resolve horizontal and vertical distributions of nutrients, and microbial and plankton groups will be valuable. We also recommend to map coral, seagrass, and mangrove cover, monitor their change through time, and to study the abundance and diversity of their associated fauna in different gradients of plume exposure.

Acknowledgements

We thank Mohd Ikram Ansari and KAUST Analytical CoreLab for the nutrient analysis, and Anders Røstad and Stein Kaartvedt for help in the echosounder work and analysis. We are grateful for the field and logistical support from the RV Thuwal captain and crew, Francis Mallon, Lloyd Smith, Ioannis Georgakakis, Ajay Sancheti, Brian Hession, Gazi Aljehdali, the KAUST Coastal and Marine Resources Core Lab, Jesse Cochran, Isabelle Schulz, Fernando Cagua, Amr Gusti, Pedro De La Torre, Joseph DiBattista, Moustapha Harb, Ahmed Shibl, Maha Khalil, and Dream Divers.

CHAPTER 4. SPATIO-TEMPORAL VARIABILITY OF ACOUSTIC BACKSCATTER AT A RED SEA WHALE SHARK AGGREGATION SITE

Abstract

A spring whale shark aggregation occurs at a nearshore submerged reef near Al-Lith on the Saudi Arabian coast of the Red Sea. It is hypothesized that the region becomes a foraging hotspot for sexually immature megaplanktivores attracted to a prey biomass peak that coincide their aggregation. We tested this hypothesis by continuously measuring acoustic backscatter of the water column at 120 kHz and 333 kHz - a proxy for prey biomass - spanning the period prior to, during, and subsequent to the seasonal whale shark aggregations. No peak in acoustic backscatter was observed at the time of the aggregation. However, a decrease in acoustic backscatter in the last ten days of deployment was seen, which coincided with the trailing end of whale shark season. The water column was homogenous in temperature, salinity, and chlorophyll *a* fluorescence during the season until it began to stratify near the end of whale shark season in May. Salinity and beam attenuation signatures indicated that run-off from an adjacent aquaculture facility reached this site as a 1-2 meter bottom layer. The main scattering layer performed inverse diel vertical migration (IDVM), with backscatter peaking at mid-depths during the day and in the deeper half of the water column at night. Target strength analyses suggested the backscatter was most likely composed of fish larvae. This main scattering layer could be prey for whale sharks and they could be interacting

with the local prey's IDVM. However, the subsurface foraging behavior of the whale sharks remains to be established.

4.1 Introduction

From February to May each spring, whale sharks (*Rhincodon typus*) aggregate at Shi'b Habil, a nearshore fringing reef (20.11˚N, 40.22˚E) offshore from Al-Lith, Saudi Arabia, on the eastern coast of the south central Red Sea (SCRS) (Berumen et al., 2014). One suggested explanation for such seasonal and localized aggregations is that the whale sharks seek out "foraging hotspots" where they encounter high aggregations of prey. Individuals spotted in Al-Lith actively feed at the surface, supporting this hypothesis. Whale sharks are megaplanktivores with zooplankton and micronekton as their major source of prey (Colman, 1997; Martin, 2007; Rowat & Brooks, 2012; Stevens, 2007).

The oceanographic processes that make Al-Lith a potential whale shark foraging hotspot every spring is unknown. However, several oceanographic processes in the SCRS could create favorable conditions for zooplankton and micronekton aggregations. First, winter winds converge at this latitude and escape westward through the Tokar mountain gap in Sudan. Sea surface height (SSH) is elevated by the surface winds, evidence of the wind stress convergence zone (Zhan, 2013). Convergence zones and fronts can accumulate positively buoyant biomass and animals that swim near the surface (Dandonneau, Menkes, Duteil, & Gorgues, 2008) and provide a foraging hotspot for predators (Godø et al., 2012; Scales et al., 2014). At Ningaloo reef, Australia, frontal zones had repeated whale shark sightings

(Wilson, Pauly, & Meekan, 2002). Second, winter mixing of Red Sea Deep Water (RSDW) or Gulf of Aden Intermediate Water (GAIW) brings nutrients into the upper water column (Chapter 2) and enhances biological productivity of the region. Coastal upwelling from basin-scale anticyclonic eddies introduces RSDW (Zhai, 2011). GAIW enters the Red Sea at mid-water column propelled by monsoonal forces from July to late fall as an eastern boundary current (Churchill et al., 2014; Sofianos & Johns, 2007; Yao, Hoteit, Pratt, Bower, Zhai, et al., 2014). GAIW mixes with Red Sea water as it travels northward and forms the Gulf of Aden Surface Water. Additionally, anthropogenic input of nutrients and organic matter from a coastal aquaculture facility could increase productivity or create an odor-plume, such as dimethyl sulfide, that attracts marine top predators (Dove, 2015; Hay, 2009; Martin, 2007; Savoca & Nevitt, 2014). If we observe a prey biomass peak co-occurring with whale shark season, it will support the hypothesis that Al-Lith provides a high prey density area for effective foraging.

The nutrients in the aquaculture plume could fuel primary productivity in the region contributing to the attraction of whale shark prey populations. Alternatively, the plume could provide a chemical odor impacting whale shark distribution (Dove, 2015; Martin, 2007). According to N. Ayaril and M. Villarreal Ricord, pers. comm., the aquaculture ponds are flushed after the last harvest in January or February and are dried to aerate the sediments until they start the restocking process in April and May. Thus detailed analysis of the effluent's nutrient flux before and during the whale shark aggregation season is necessary to investigate whether it impacts prey abundance. It may be unlikely that the

aquaculture discharge is the sole reason for the aggregation because the plume's seasonal variability does not correspond to the aggregation season. Records of ship strikes in the Red Sea are suggested to indicate substantial numbers of whale sharks in the region long before the aquaculture was established (Gudger, 1940); however, an aggregation was not formally observed until 2008 and the plume could influence whale shark distribution and health.

It is difficult to achieve sufficient temporal scales and spatial resolution of plankton biomass with net sampling or video plankton recording methods. However, battery equipped echosounders can provide long temporal scales and high vertical resolution. High frequency echosounding is a non-intrusive sampling method that has the ability to observe zooplankton and micronekton (Axenrot, Didrikas, Danielsson, & Hansson, 2004). By deploying autonomous echosounder systems, such investigations can be carried out over long periods of time. For this study, we deployed bottom-mounted upward-looking echosounders to detect temporal patterns of zooplankton and micronekton prior to, during, and following the whale shark aggregation season in Al-Lith. This method was supplemented with vertical net tows to identify the biotic scatterers responsible for the acoustic signals recorded by the echosounders. In this way we provide insight into the abundance and seasonality of acoustic backscatter, a proxy for prey populations, at this whale shark aggregation site.

This study assumes that the observed acoustic scatterers are biomass that are potential prey for whale sharks, and therefore motivating factors for their aggregation (Rowat & Brooks, 2012). Goals of this chapter are to 1) compare

progression of acoustic backscatter abundance throughout whale shark season, 2) describe the diel vertical variability of acoustic backscatter, 3) differentiate scatterers by target strength, 4) identify zooplankton vertical distribution by net tows, and 5) investigate correlations between scatterers and environmental factors.

4.2 Methods

Site selection

The annual whale shark aggregation in Al-Lith occurs mainly on Shi'b Habil (20.11˚N, 40.22˚E) approximately 4 km offshore (Figure 4.1) (Berumen et al., 2014). This submerged reef is 5 km long and averages 600 m wide with an eastward branching reef 1.8 km long on its northeast side. The inshore side of the reef is shallow and complex with steep coral structures dispersed on sandy bottom. Offshore of the reef the topography drops steeply from a plateau of a few meters depth to over 60 m depth. The echosounder was deployed at the northern end of this reef, where the highest whale shark detections occurred from a five-year acoustic tag effort (Cochran, 2014). The average depth in this region the echosounder was deployed is about 40 meters.

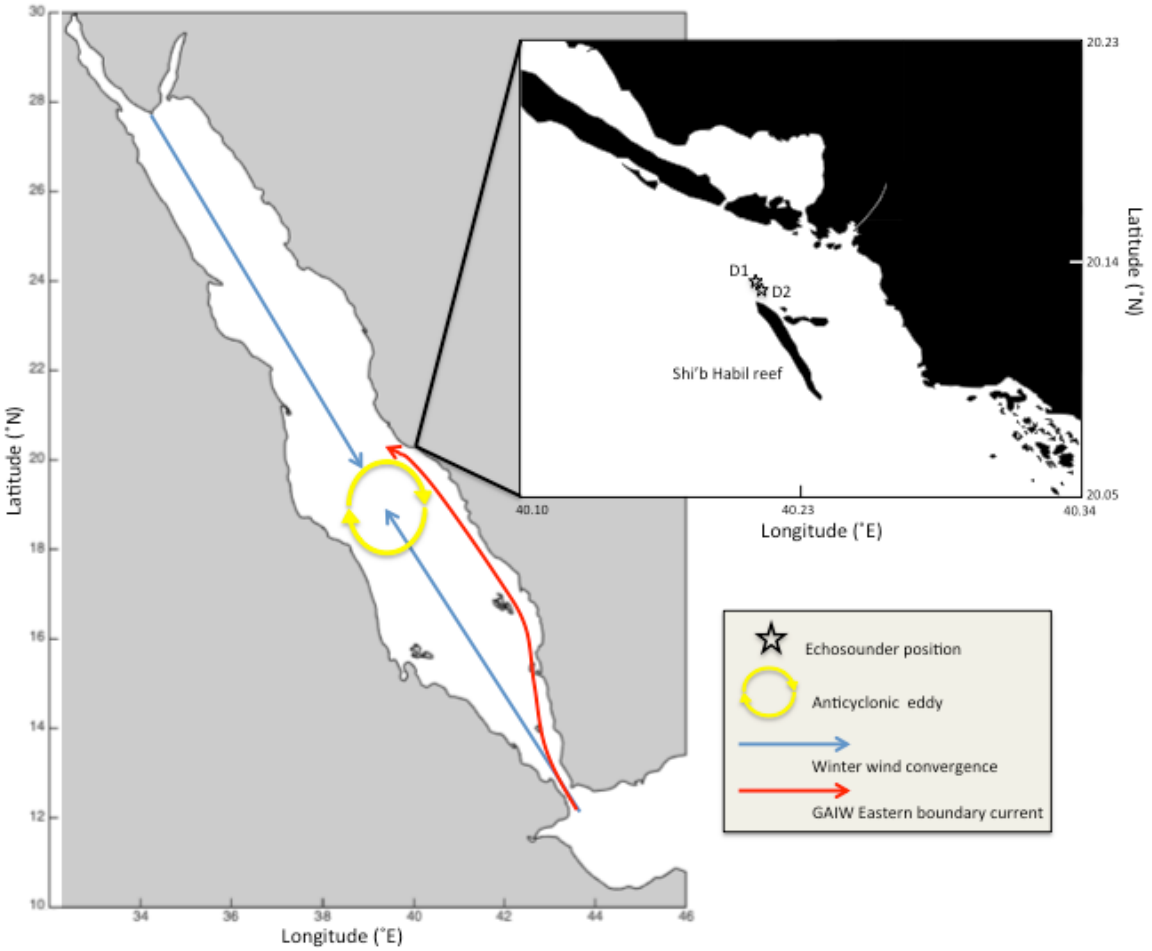

Figure 4.1. A map of the Red Sea highlighting wind and oceanographic features relevant to Al-Lith is shown. The anticyclonic eddy may upwell Red Sea Deep Water, particles (e.g., prey) may accumulate at the winter winds convergence zone, and GAIW intrusion can supply nutrient-rich water along the coast. The locations of Shi'b Habil in Al-Lith with the echosounder mooring sites are illustrated in the inset.

Environmental data

Each month during the period of the echosounder deployment, an instrument package for environmental data was used to profile the waters at the northern end of Shi'b Habil. The package descended one meter per 12 seconds to obtain one-meter resolution data. The instrument package consisted of an Onset

HOBO Water Level Data Logger for pressure (depth) and temperature, Seabird Microcat CTD 37SMP for temperature and conductivity (salinity), Sequoia Scientific Laser In-Situ Scattering and Transmissometry 100-X (LISST) for pressure (depth), particle size distribution and particulate beam attenuation coefficient (c_p) (670 nm) with 5 cm pathlength, and WETlabs fluorometer/turbidity sensor (FLNTUB) for chlorophyll *a* fluorescence (chla) (ex 470/em 695 nm) and turbidity (700 nm). The chla and turbidity measurements were based on factory calibration and dark counts measured in the lab. Measurements and sampling frequencies are summarized in Table 4.1. Data were merged according to their time stamps. Mixed layer depths (MLD) were calculated with density gradient criterion of 0.125 kg m^{-3} (Kheireddine & Antoine, 2014) and stratification (N^2) were calculated using the equation for buoyancy frequency. The environmental data was correlated with the corresponding acoustic data.

Table 4.1. Measured variables and sampling frequencies of each instrument used for monthly hand casts at position D1.

Instrument	Variables measured	Sampling Frequency
Onset HOBO Water Level Data Logger	absolute pressure (kPa); temperature (˚C)	1 Hz
Seabird Microcat CTD	temperature (˚C); conductivity (s/m)	1/6 Hz
Sequoia LISST	particle size distribution; beam attenuation (m^{-1});	1 Hz

WETlabs FLNTUB	chlorophyll *a* fluorescence (µg/l); turbidity (NTU)	1 Hz

Fixed moorings

Two moorings were fixed at ~10 m and ~6 m depth directly on the reef for the exposed and sheltered sites, respectively. CTDs were deployed to measure temperature, conductivity, and pressure every 40 seconds. FLNTUBs were deployed to measure chla at excitation 470 nm/emission 695 nm, and turbidity at 700 nm for particulate backscatter every hour for 20 seconds at 1Hz. Continuous measurements from January to May were taken in 2015, although data collection failed in 2014 due to battery deaths and instrument setup error.

Echosounder deployment

A mooring rig with two SIMRAD EK 60 echosounders operating at 333 kHz and 120 kHz was deployed at the northern end of Shi'b Habil. The transceivers were mounted in a pressure proof casing together with a PC, with batteries mounted in a separate container. The echosounders were operated at a pre-programmed duty cycle with one hour of sampling every three hours to save battery but still resolve the daily pattern of the vertical distribution. However, due to instrument computer failure, the sampling did not strictly follow the pre-programed duty cycle and sampled at random intervals, yet with an appropriate resolution to achieve the objective. The mooring was deployed for deployment 1 (D1) on 15 January 2014,

retrieved 10 March 2014 for battery charging, and re-deployed the next day. Recording continued until the instrument package ran out of power on 30 April 2014, ending deployment 2 (D2). Time was recorded in UTC (local time is UTC+3). Sampling rate was set to 1 ping s^{-1}, bin size 4.9 cm, and pulse length 0.256 ms. For deployment and retrieval purposes, the mooring was tied to an anchor and subsurface buoy. Mooring sites for D1 and D2 were located within 180 m of each other (Figure 4.1, 20.1337˚N, 40.2089˚E and 20.1326˚N, 40.2102˚E respectively), where D2 was (unintentionally) 100 m closer to the reef than D1. The instrument depths were at 44 and 38 m respectively. The echosounder was calibrated following SIMRAD protocol (Foote et al., 1987).

Data processing

The acoustic data was processed using the Sonar 5 Pro processing software (Balk and Lindem, 2002) and MATLAB (2012b). To compensate for periods without echoes as a consequence of the intermittent duty cycle, two weeks of data were averaged into bins of 30 seconds into one “daily” echogram. These averages were separated for the two deployments due to differences in deployment depths, giving four averages for each deployment period. In the same way, a “daily” average echogram of each deployment was created to compare between D1 and D2.

Temporal variability of acoustic backscatter was analyzed. Data from the top 10 m were especially affected by wave-induced turbulence, therefore excluded from further analysis to minimize noise. The data from 10 m to bottom (the surface of the transducer) was back transformed into linear values to calculate the mean and

median for night and daytime, then log-transformed for comparison. Data collected during 6:00-17:59 and 18:00-05:59 (local time) were treated as daytime and nighttime, respectively. A t-test and one-way ANOVA were used to check for differences between day and night acoustic backscatter and between deployments.

To obtain preliminary information on acoustic targets that formed the main, diel migrating scattering layer (SL), the target strength (TS) was measured when the layer resided near-bottom. The close proximity to the echosounder then enabled resolution of the acoustic data into individual targets. For this analysis we used Sonar5 Pro (Balk and Lindem, 2002) and non-averaged 120 kHz data. Isolated pings were captured using auto-mode with four to ten continuous pings and maximum one skipped ping. The compiled isolated pings (n=12718) were linear transformed and calculated for mean, median, and standard deviation, and then log-transformed for comparison. The TS analysis was done separately for the two deployments. Ascent and descent pings were analyzed separately. A t-test and one-way ANOVA were used to test for differences in TS between the two deployments and between ascent and descent.

Multinet tow and visual inspection

Zooplankton was sampled from 10:00-11:30 UTC on April 14, 2014 using a multinet with 200-μm mesh size. Three replicate series with three depth resolutions [bottom-25 m; 25-15 m; 15 m-surface] were taken at position D2. The nine samples were preserved with 90% ethanol in 50 mL individual tubes with screw-on caps. In the laboratory, all samples were analyzed and enumerated to genera, and to species

when possible. Enumeration was performed using a dissecting microscope, tally counters, and a glass counting chamber. The abundance data (Appendix H) was log-transformed and analyzed using Primer6 (Clarke & Gorley, 2006). ANOSIM was used to test for significant pairwise relations between the three depths, and PERMANOVA to test whether depth factor or replicate factor was significant in species abundance. We created multidimensional scaling (MDS) plots to illustrate vertical patterns in species abundance.

In an attempt to visually inspect the main SL, divers dove to 25 m depth near position D2 during the daytime to coincide with the main SL occupying the mid-water column. We hoped to identify organisms in the main SL but this effort did not help to identify the acoustic targets as no scatters (e.g., small fish) could be observed.

4.3 Results

Environmental data

Mooring data with high temporal resolution showed that temperature steadily increased from February to May (Figure 4.2a), following the trends in monthly atmospheric temperature (not shown). Salinity started to decrease from late March until it stabilized in May. The water column was well mixed from January to April until stratification became evident in May (Figure 4.2b). During our sampling period, the absolute values of chla were relatively low (<0.9 $\mu g l^{-1}$). They were highest prior to and subsequent to the whale shark aggregation season. In January and May, chla fluorescence was homogenously distributed by depth. But from February to April, chla was higher near the bottom (Figure 4.2b). Similarly c_p, a

proxy for suspended particles, was homogenous except just above the seafloor. This layer near the bottom with mass of high-suspended particles had markedly higher salinity than waters above. This is clearly seen in the vertical profiles except March as a peak in salinity and c_p or scattering (Figure 4.2b).

a)

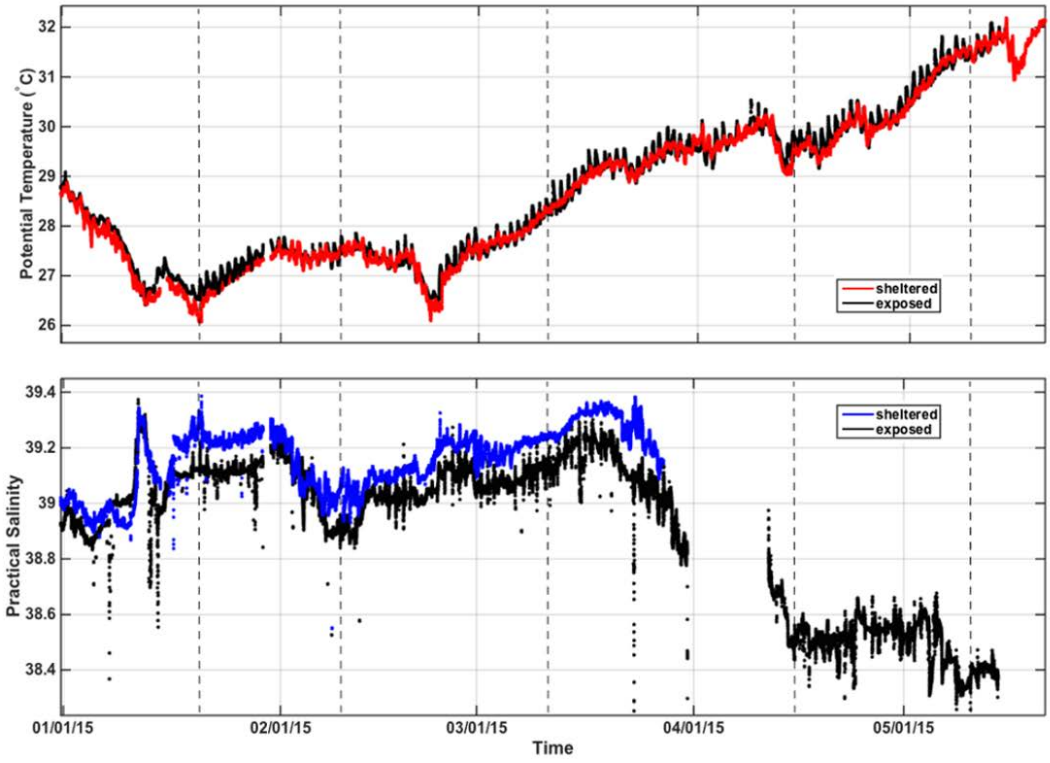

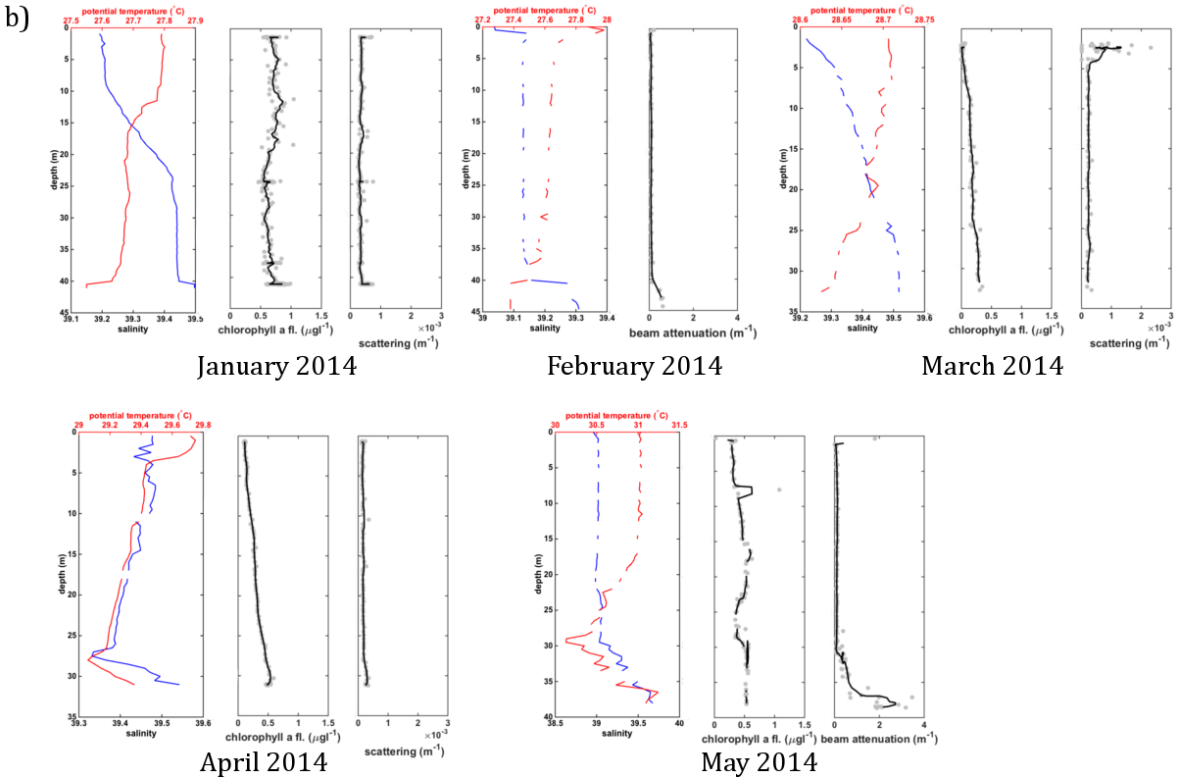

Figure 4.2. Environmental data over the four monthly surveys while the echosounder was on and the following month in May at position D1 are presented. The (a) temperature and salinity time-series from fixed moorings show the seasonal variability at higher temporal resolution and b) the profiles of temperature, salinity, and optical measurements show homogenous water column until the stratification in May and optical measurements reflect this homogeneity except near the bottom where higher suspended particles are measured.

Acoustic data

The acoustic data was characterized by high backscatter in the deeper half of the water column at night while backscatter peaked in mid-depth during the day (Figure 4.3-4). This inverse diel vertical migration (IDVM) of the prevailing acoustic targets was found throughout the registration period and at both frequencies, although backscatter was stronger at 120 kHz than at 333 kHz (Figure 4.5). The

main SL ascended to mid-water around dawn and stayed approximately 14 to 20 m above the bottom during the daytime (Figure 4.3). Around dusk, this SL descended to near-bottom waters and occupied the deeper half of the water column throughout the night. Apart from the surface noise that occasionally penetrated deep (20 m depth), the acoustic backscatter was lower near the surface compared to the main SL.

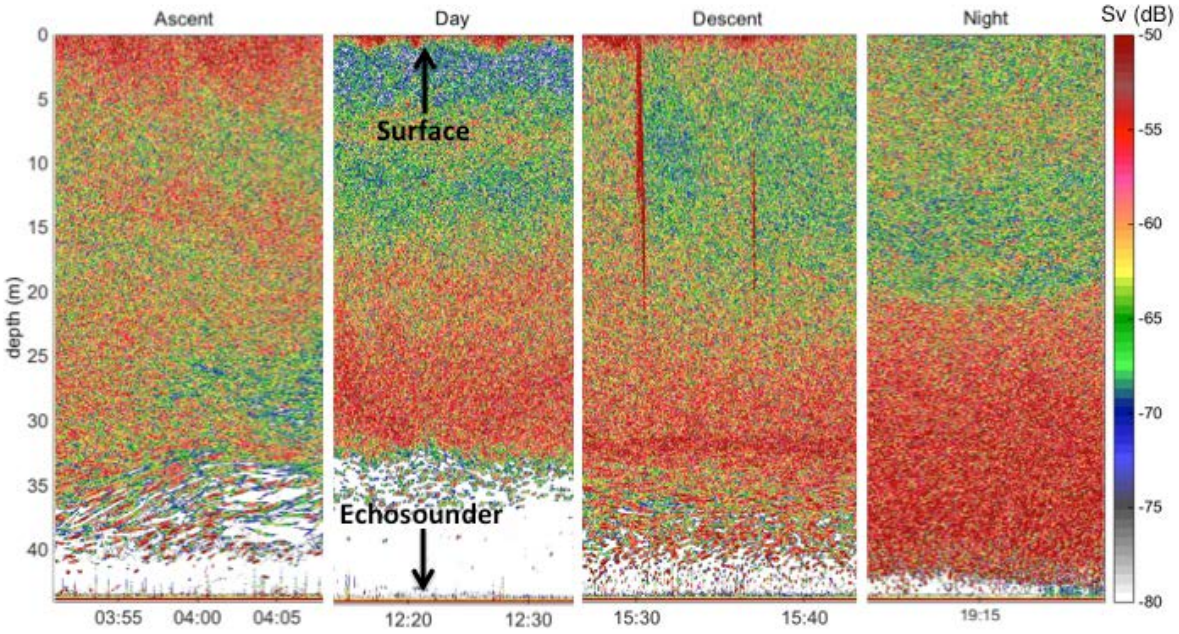

Figure 4.3. Echograms of ascent, vertical distribution during daytime, descent at dusk, and vertical distribution at night are shown in high resolution from the 120 kHz frequency data from D1. The time on the horizontal axis is in UTC and local time is UTC+3.

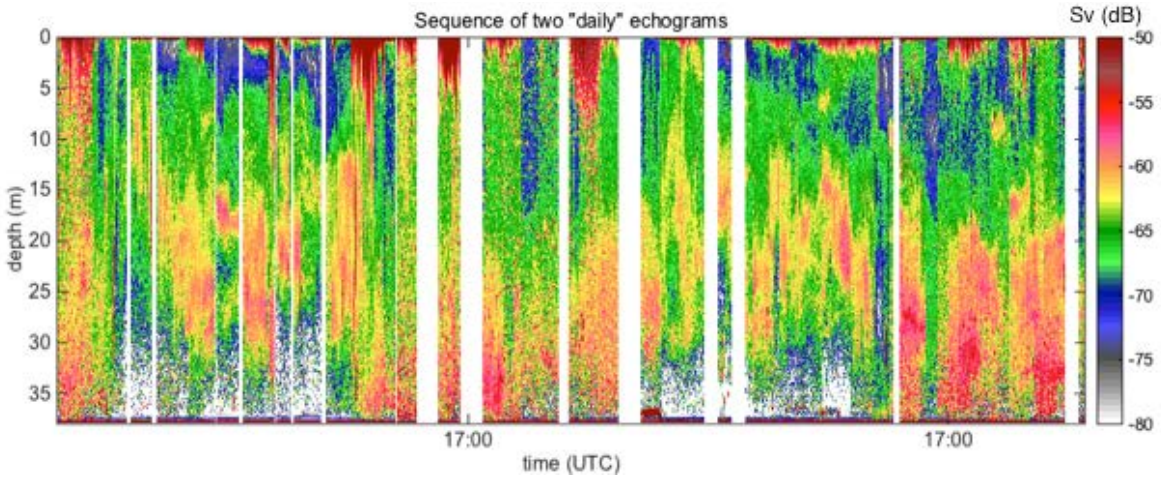

Figure 4.4. A sequence of two “daily” averages from D2 binned to every 30 seconds is shown for 120 kHz frequency. The echogram shows the diel pattern of reverse diel vertical migration with the x-axis as UTC where local time is UTC +3.

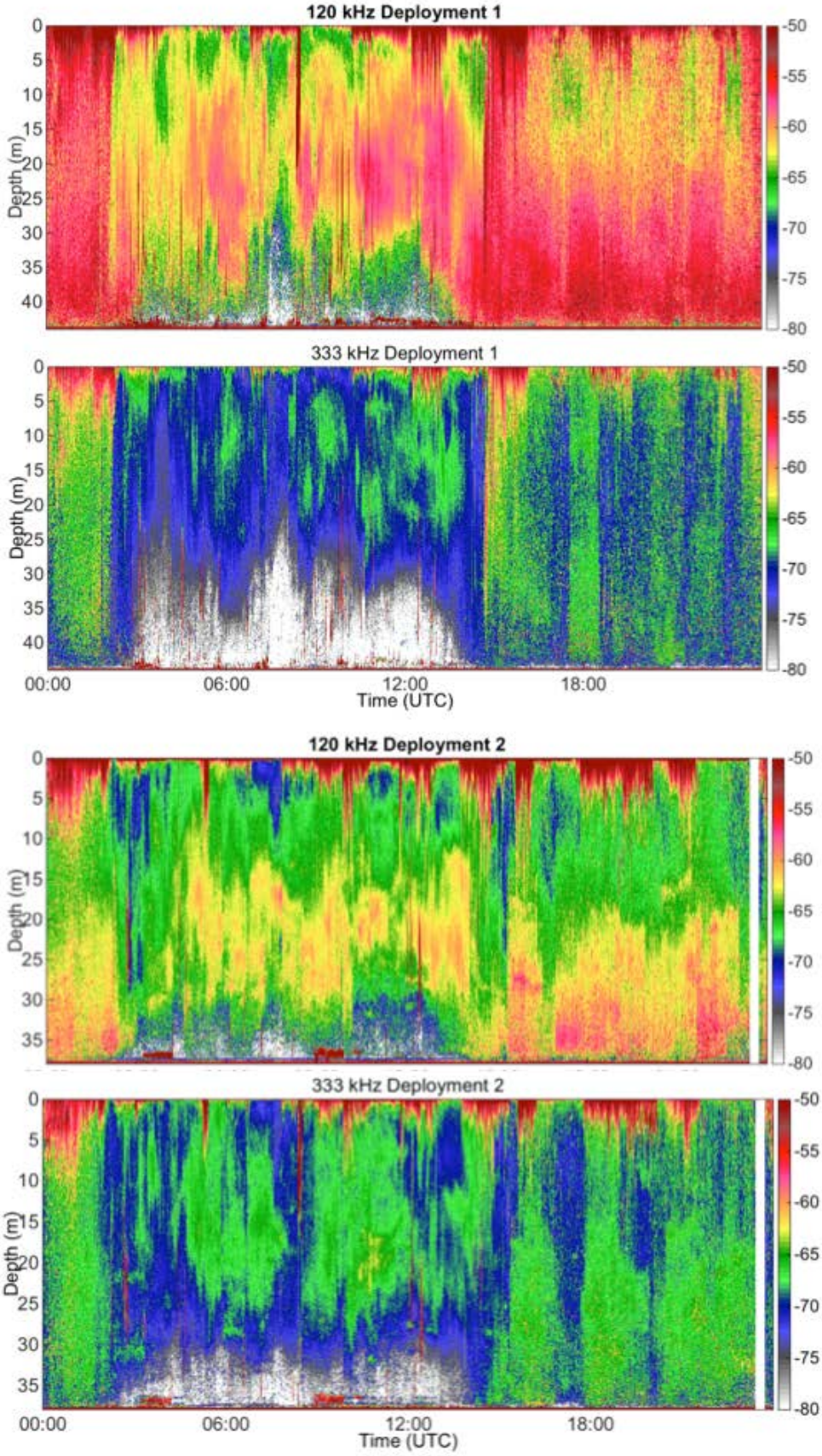
120 kHz Deployment 1
333 kHz Deployment 1
120 kHz Deployment 2
333 kHz Deployment 2
Depth (m)
0
5
10
15
20
25
30
35
40
-50
-55
-60
-65
-70
-75
-80
00:00
06:00
12:00
18:00
Time (UTC)

Figure 4.5. Average daily echograms of the deployments, D1 (top) and D2 (bottom), for 120 and 333 kHz echosounder data are shown. Strength of acoustic backscatter (dB9 is shown as color-scheme. Data are recorded in UTC time (local time is UTC +3) and binned every 30 seconds. The two deployments have different depths, 44m and 38m for D1 and D2, respectively.

The TS of individuals ascending into the main SL around dawn suggest they are small acoustic targets. The median TS of these individuals at 120 kHz were -64.8 and -66.5 dB for ascent and descent respectively during the first deployment (D1) and -72.3, and -73.7 dB for ascent and descent, respectively during the second deployment (D2) period. The mode TS were -64.1, -69.5, -72.4, and -73.9, for D1 ascent, D1 descent, D2 ascent, and D2 descent respectively, which represents the most produced backscatter during ascent and descent (Figure 4.6). The TS from the two deployments were significantly different (p-value=<0.0001, t-stat=122.7) according to the t-test. The one-way ANOVA also showed significant differences between D1 and D2 TS values (one-way ANOVA p-value= <0.05, F-stat 173.8).

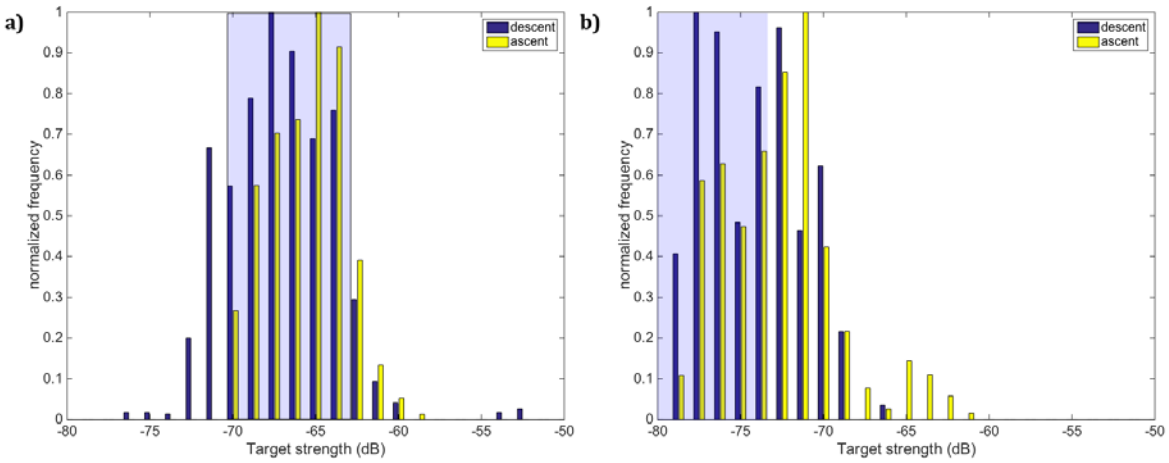

Figure 4.6. A histogram of target strengths of individuals ascending and descending into the main scattering layer near dawn and sunset is represented for a) D1 and b) D2 for the 120 kHz dataset. The median TS were -64.8, -66.5, -72.3, and -73.7 dB, and the mode TS were -64.1, -69.5, -72.4, and -73.9 dB, for D1 ascent, D1 descent, D2 ascent, and D2 descent respectively. The target strengths for a) 1 cm perch larvae (-70 to -63 dB; Frouzova & Kubecka, 2004) and for b) 3-4 cm krill (-81 to -74 dB; Foote, Everson, Watkins, & Bone, 1990) are shaded for comparison.

We saw no increase in acoustic backscatter or diel fluctuations during the registration period. However, acoustic backscatter decreased by 13 dB for the 120 kHz frequency in the last ten days of D2 (Figure 4.7). This drop was not observed in the 333 kHz data during the same registration period.

Another contradiction between 120 and 333 kHz observations was the decrease in baseline from D1 to D2. The 120 kHz data showed a noticeable drop in its baseline from -60 to -65 dB (Figure 4.7) after the second deployment in a position 180 m away from the first. This decrease is not reflected in the 333 kHz data, where the baseline remains the same between D1 and D2.

Unidentified aggregations with approximately -30 to -20 dB were observed through our deployment. These were separate from the main SL and appeared mostly below the main SL (Figure 4.8). There was no apparent pattern for their timing. Whale shark detections at the acoustic tag receiver 380-480 m away (within detection range) did not correlate to this unknown fauna's appearance. The main SL was seen to react to this unidentified scatterer where the main SL bent away from it to avoid contact (Figure 4.8).

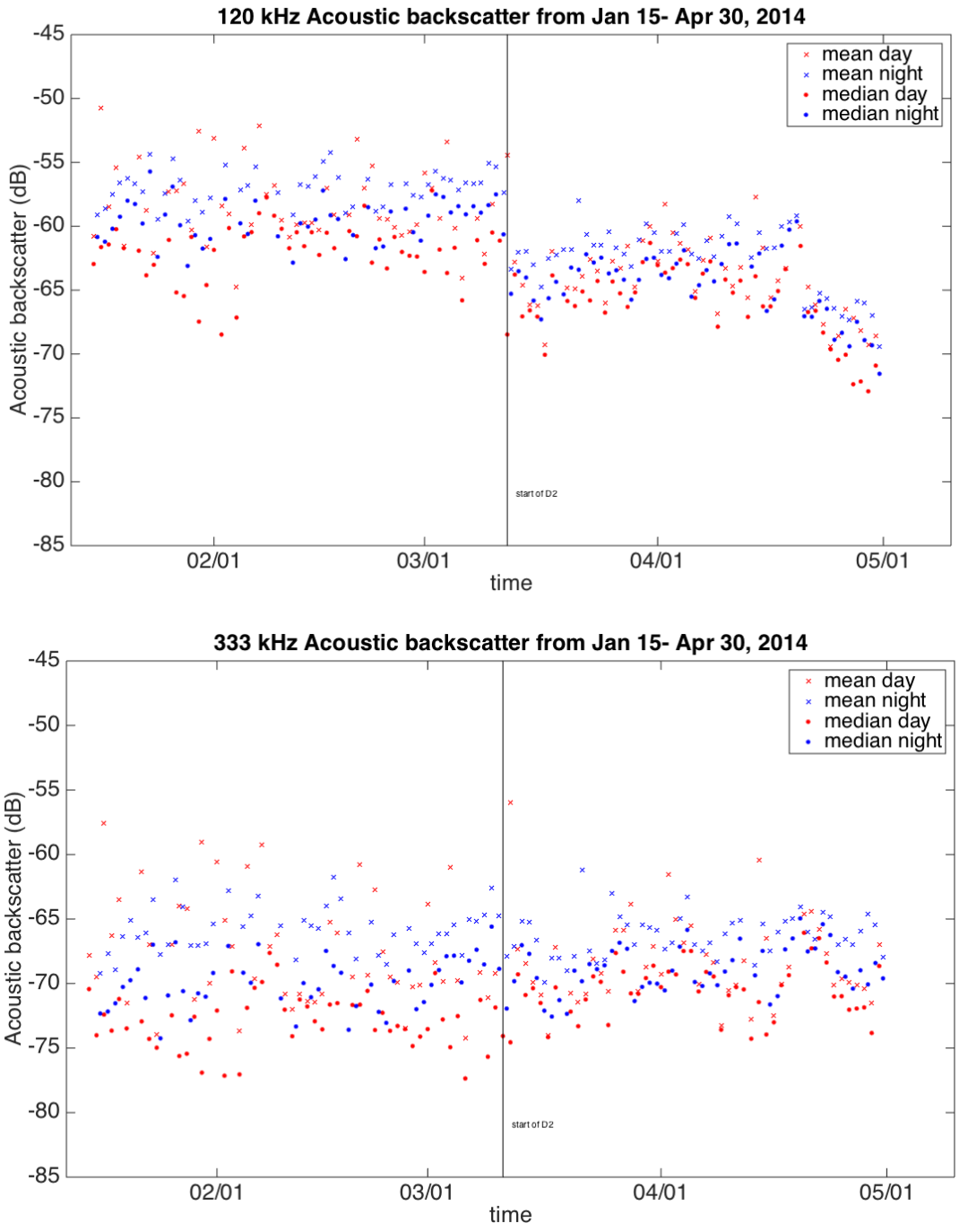

Figure 4.7. A time-series of the mean and median of acoustic backscatter of 120 kHz (top) and 333 kHz (bottom) frequency are shown. Day and nights were 03:00-14:59 and 15:00-02:59 UTC, respectively. The acoustic backscatter between 10 m to bottom was included in the analysis. The two deployments are graphed continuously with a vertical line separating the two.

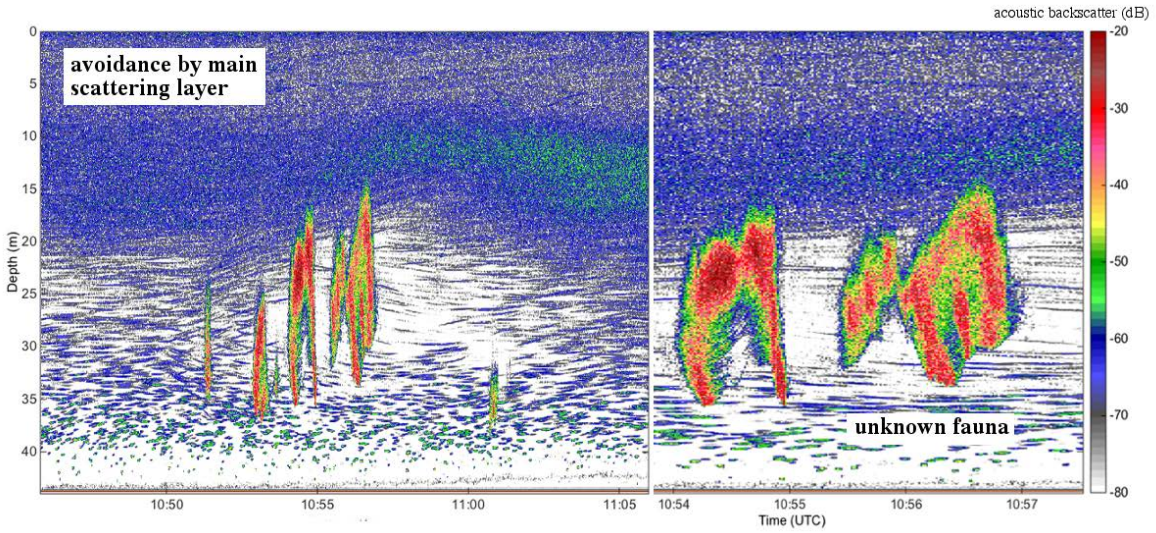

Figure 4.8. Echograms of the 120 kHz data on January 17, 2014 that was one of the few observations made of the unidentified fauna not part of the main SL. It usually appeared below the main SL with approximately -30 to -20 dB acoustic backscatter (right). The main SL is seen avoiding this unknown target (left).

Zooplankton samples

Zooplankton abundance data from multinet samples revealed no vertical patterns among the three depth cells. Complete abundance data from our effort is summarized in Appendix H. MDS plots showed that replicates formed no clusters, illustrating there were no significant difference in zooplankton abundance among depth cells (not shown). ANOSIM and PERMANOVA results agreed (ANOSIM p-value=0.79, Global R=-0.15, PERMANOVA p-value=0.40, Pseudo-F=1.1). Copepod-only and separately for hard-shelled-genera-only abundance data also had non-significant differences between casts or depth cells (ANOSIM p-value=0.10, Global R=0.22, PERMANOVA p-value=0.22, Pseudo-F=1.5 and ANOSIM p-value=0.24, Global R=0.14, PERMANOVA p-value=0.18, Pseudo-F=2.0 respectively). Copepods, sergestids, euphausiids, chaetognaths, and fish eggs, as well as fish and crustacean

larvae were present (Figure 4.9) with no distinct vertical distribution. To compare with the vertical distribution of the acoustic backscatter at the time of the net tow, we used echosounder data collected on April 14, 2014 11am UTC (not shown). This data showed the main SL was distributed from 10-35 m depths, which spans over all depth cells. The 15-25 m depth cell best matches the main SL.

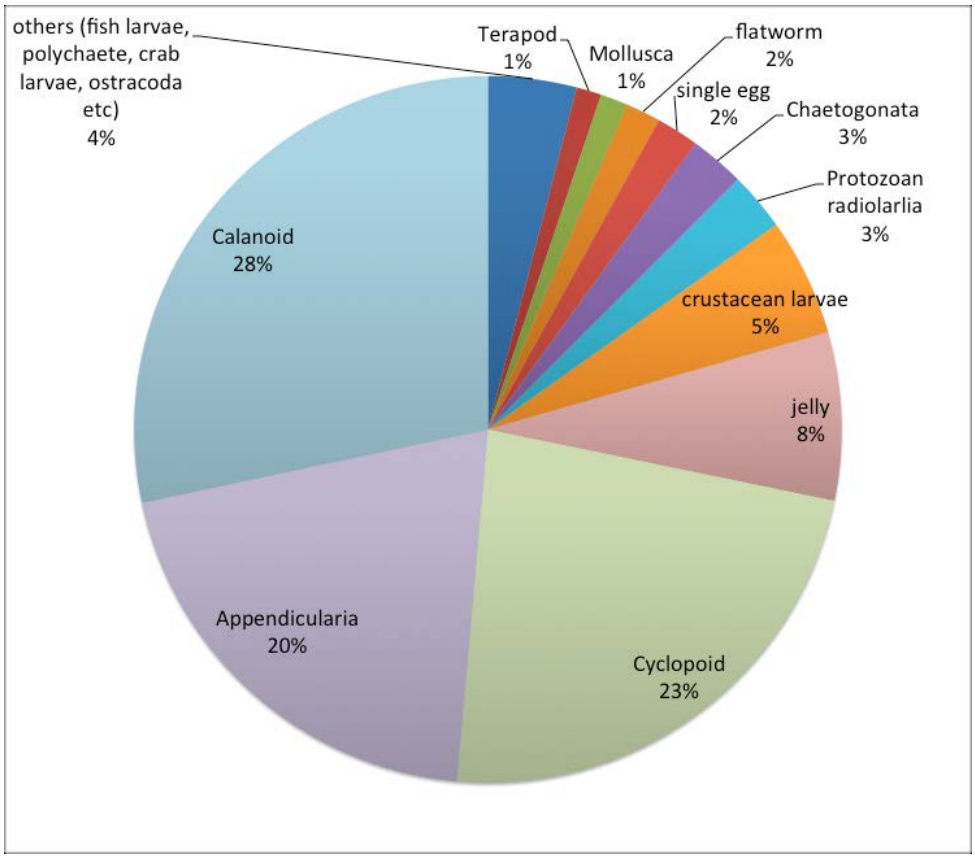

Figure 4.9. Relative abundance in counts of genera and species identified in the multinet samples. Copepod *sp*. (e.g., Calanoid and Cyclopoid) were most abundant in number.

4.4 Discussion

The use of bottom-mounted upward-looking echosounders allowed for observations (mid-January to end of April) over most of whale shark aggregation season (late-February to mid-May). This sampling period provides a time-series of acoustic backscatter, a proxy for biomass, during their aggregation. Tagged whale shark detections increase up to 16-fold by its peak in mid-April (Figure 4.10). Thus we expected a peak in prey populations (acoustic backscatter) coinciding with their detection peak. However, acoustic backscatter was consistent during D1 (mid-January to mid-March) and similarly, during D2 (mid-March to May). This suggests biomass did not increase significantly during the whale shark aggregation. Note, however, that data are missing from the upper 10 m from the analysis and therefore do not cover the neuston layer, where the active feeding behavior of whale sharks was observed. But a study in Tanzania revealed whale sharks stayed subsurface, possibly following prey, during "off-season" periods of their visual sightings at the neuston (E Fernando Cagua et al., 2015). This suggests the importance of foraging also at subsurface depths.

The acoustic data revealed that the main SL performs IDVM at subsurface and demersal depths and likely does not reach the neuston layers (Figure 4.3). Plankton performing IDVM are hypothesized to do so for predator avoidance from animals performing normal DVM (Ohman, Frost, & Cohen, 1983). Visual predators, like fish larvae, will ascend to forage in mid-waters at day and descend to safer deeper waters at night when they are not foraging, thus performing IDVM. Other whale shark aggregation sites have found prey associations with plankton blooms

dominated by sergestids, copepods, euphausiids, and chaetognaths (Cárdenas-Palomo et al., 2014; Motta et al., 2010; Rohner, Armstrong, Pierce, Prebble, & Cagua, 2015; Taylor, 2007), as well as spawning events (Cárdenas-Palomo et al., 2014; Graham et al., 2006; Heyman et al., 2001; Hoffmayer & Franks, 2007; Robinson et al., 2013). These animals are capable of performing diel vertical migration and were captured by the vertical net tow during the peak of whale shark detections (mid-April).

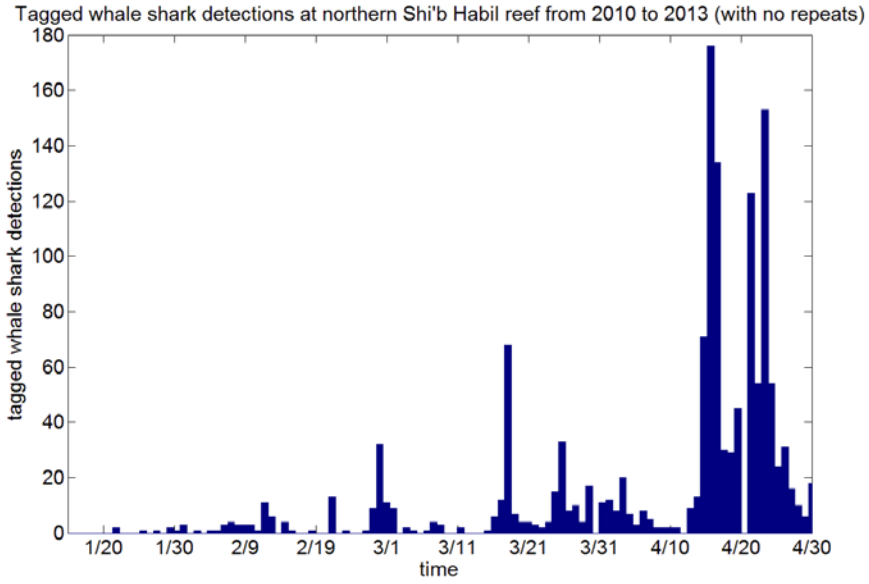

a)

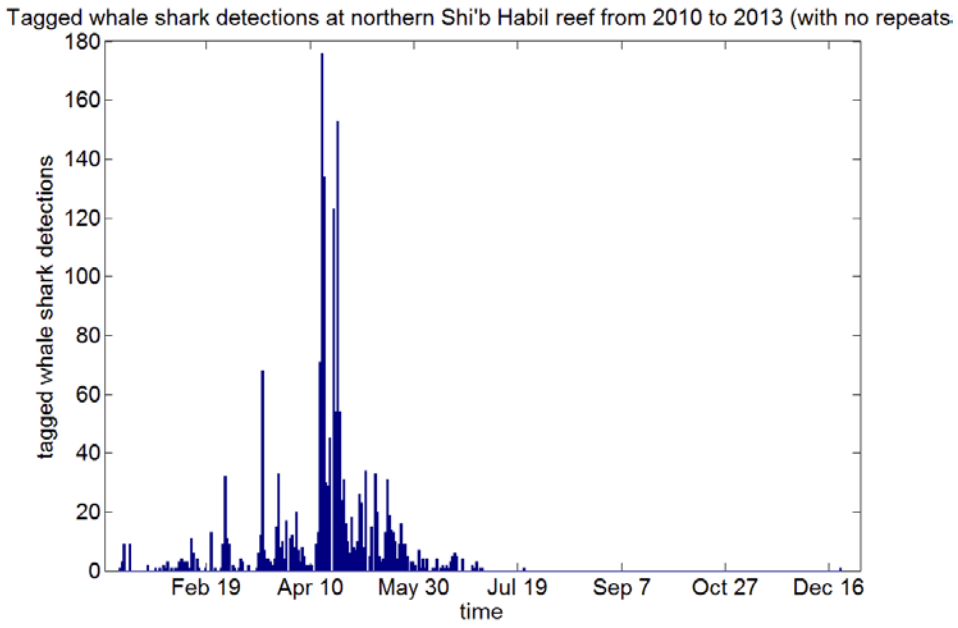

b)

Figure 4.10. Frequency of tagged whale shark detections from 2010 to 2013 by an acoustic receiver at the northern end of Shi'b Habil (<500m from echosounder positions) are shown. Data during a) our sampling period and for b) the entire year is shown to illustrate the peak of detections at this site around mid April. Data are binned by day and repetitive detections of the same whale shark within the same hour are not plotted.

The TS analysis of individuals during D1 are similar to 1 cm length perch larvae which ranges from -70 to -63 dB (Frouzova & Kubecka, 2004), and higher than 3-4 cm length krill which has -81 to -74 dB at 120 kHz (Figure 4.6) (Foote et al., 1990). The TS in D2 were a little higher than those of krill. The TS is dependent on target size, composition, presence of swimbladder, and orientation (Foote, 1980; McClatchie, Alsop, & Coombs, 1996). Our results suggest these individuals in the main SL could be small fish larvae with swimbladders, large plankton, or hard-shelled organisms (*e.g.* mollusks). These organisms can avoid nets, which explains

the lack of coherence with the acoustic backscatter and the vertical distribution of plankton as established from depth resolved sampling with the multinet tows.

Visually foraging fish larvae might benefit from mid-water foraging during daylight. Alternatively, organisms that are able to predate under minimal light conditions may descend to forage on nocturnal demersal zooplankton that emerge at night (Kringel, Jumars, & Holliday, 2003). IDVM was also observed by acoustic registrations at a coastal station north of Al-Lith, near 22˚N (unpublished results). Both study areas are in close proximity to coral reefs and reef face zones that have higher densities of emergent nocturnal demersal zooplankton (Alldredge and King 1977), supporting this hypothesis for IDVM motivation.

Prey populations performing IDVM have been reported to be paralleled by IDVM of basking sharks, *Cetorhinus maximus*, (Sims, Southall, Tarling, & Metcalfe, 2005) and porbeagle sharks, *Lamna nasus* (Pade et al., 2009). Tagged sharks followed the local IDVM of biomass to maximize their foraging in well-mixed coastal waters. These sharks demonstrated plasticity and switched to normal DVM when foraging in deeper stratified open water where the local SL performed normal DVM. Tagged whale sharks in Al-Lith were subsurface (25-50 m) ~22% of their time (Berumen et al., 2014), but it is unknown if they are foraging at these depths. Feeding of whale sharks in the neuston layer (0-2 m depth) accounted for ~17% of their time (Berumen et al., 2014). This is lower than the 31% average spent at the surface (0-1 m depths) by tagged whale sharks off the Yucatan Peninsula, which dove to deeper depths at nighttime (Motta et al., 2010). Motta et al. (2010) recommended investigating the relationship of their diel vertical movements and

food sources. In Western Australia, tagged whale sharks dove to forage on species seeking refuge at depths (Wilson, Polovina, Stewart, & Meekan, 2006). In Mozambique, these deeper dives were made 79% during the nighttime (Brunnschweiler & Sims, 2011). Thus to better understand the ecology and foraging behavior of megaplanktivores, we encourage sub-surface behavioral studies for whale sharks in Al-Lith using advanced satellite tags with accelerometer (Shepard et al., 2008).

The backscatter at 120 kHz became markedly reduced after recharge and redeployment for D2. Also the TS of migrating individuals decreased from D1 to D2 (Figure 4.6). Corresponding changes did not occur at 333 kHz. This suggests that a methodological problem between the deployments could have affected the measurements. However, the two transducers were connected to the same batteries and computer. Alternatively, small scale patchiness is very pronounced at reef habitats, and different responses at different frequencies could be explained biologically if more animals with swimbladder resonance (which at given sizes give strongly enhanced backscatter at given frequencies) at 120 kHz but not 333 kHz are present at the first deployment site than the second. Small scale patchiness of prey would be in accordance with the spatial variability in tagged whale shark detections along this 5 km long reef (Cochran, 2014).

Acoustic backscatter at 120 kHz decreased the last ten days of April (Figure 4.7). This suggests a decrease in biomass that coincides with the trailing end of whale shark season when a 4-fold decrease in tagged detections is observed. The 13 dB decrease is on a log-scale unit so this change is considerable. This decrease was

only seen in the 120 kHz data and not in the 333 kHz data. Again, this could be explained biologically if animals with specific resonance at 120 kHz but not at 333 kHz left the site in the last ten days. This will result in a much more pronounced drop at 120 but not in 333 kHz. Resonance echoes are associated with fish with swimbladders and change with their depth occupancy and how adjusted they are to the depths (Levik & Hovem, 1979).

Monthly profiles of temperature, salinity, and chlorophyll suggest that the water column at this site was physically well-mixed during our deployments. There was no peak in chla during our observation period, which could explain why the acoustic backscatter did not peak (assuming that the acoustic targets feed on phytoplankton). The halocline that correlates with high-suspended particles near the bottom is suspected to be the plume water from the large coastal aquaculture facility discharged from an outfall approximately 4.7 km away. We observed no GAIW or RSDW temperature and salinity signatures at this station during our deployment. Thus we were not able to associate these two water masses as nutrient sources for primary productivity, contributing to increased secondary producer populations, which could motivate whale shark aggregation.

In conclusion, the autonomous acoustic echosounders successfully monitored the temporal and vertical variability of biomass at a whale shark aggregation site in Al-Lith. The prevailing acoustic targets performed IDVM throughout the registration period and were most likely composed of larval fish, large zooplankton, or hard-shelled organisms. We observed evidence for small-scale patchiness of biomass at this aggregation site in the 120 kHz data. We also observed

a decrease in backscatter at 120 kHz coinciding with the trailing end of tagged whale shark detections. Yet, by and large the acoustic backscatter (proxy for their prey biomass) showed little temporal variability and no increase in abundance associated with the arrival of whale sharks. Thus it is not possible to identify any possible indication of an increase in prey biomass during the peak of the whale shark detection period. However, given the very limited sampling area covered by a single echosounder and given the potential patchiness of the prey, it is also not possible to rule out a correlation between prey biomass and the occurrence of whale sharks in this area. .

Acknowledgements

We thank the RV Thuwal captain and crew, Francis Mallon, Lloyd Smith, Ioannis Georgakakis, Brian Hession, the KAUST Coastal and Marine Resources Core Lab, Ingrid Solberg, Joseph DiBattista, and Dream Divers for field and logistical support, Riata Amundsen for help in zooplankton identification, and Darren Coker for analysis help.

SUMMARY OF EACH CHAPTER

This work contributes to assessing the environmental conditions which may be responsible for the whale shark aggregation observed in the Red Sea by characterizing the physical and biological (e.g. microbial, phytoplankton, zooplankton, micronekton) conditions and the variability of nutrients inputs at the aggregation site (Figure S.1). Our observations corrected our speculations of how the Gulf of Aden Intermediate Water (GAIW) flows into the nearshore coral reef systems in the South Central Red Sea as episodes rather than as a continuous supply. The aquaculture facility's discharge was described for the first time with estimates of nutrient flux and evidence for a seasonally variable microbial community. The gradient effect of this point source from the outfall is expected from our observations of its spatial variability, which may change as they switch to cage farming and become non-point sources. Although whale sharks are speculated to aggregate in Al-Lith for foraging, we observed no evidence for increase in their prey abundance (e.g., acoustic backscatter). Other reasons may be motivating the aggregation (e.g., nursery ground biologically imprinted on whale sharks, chemical cues we did not measure).

The main findings, perspectives, and limitations of each study and some reflections on the way forward are presented in this section. To reiterate, the objectives of my dissertation are:

1) To identify what bio-physical processes could play a role in a bottom-up process at Shi'b Habil

2) To determine if the aquaculture plume affect and modify the coastal waters of Al-Lith

3) To determine the seasonal variability of plankton biomass at this whale shark aggregation site

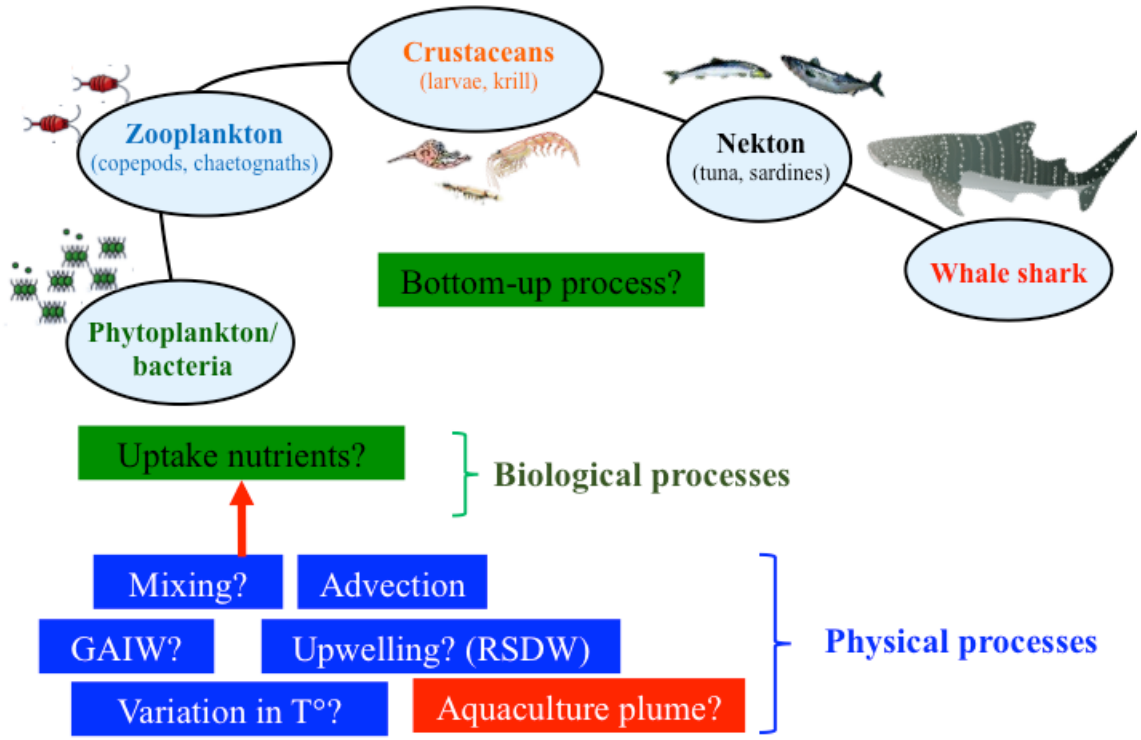

Figure S.1. The physico-biological processes that were examined at Shi'b Habil in attempt to explain the motivation behind the whale shark aggregation. The findings resolved the spatio-temporal variability of these physical processes (natural = blue; anthropogenic = red) and of different levels of this food chain that we hypothesized were contributing to the whale shark aggregation.

Chapter 2: Spatio-temporal variability of water masses in the whale shark aggregation site

We examined the residence time and seasonality of nutrient sources at Shi'b Habil to investigate whether there is a bottom-up process that is responsible for the annual spring whale shark aggregation. Whale shark aggregations elsewhere are known to be motivated by high prey density from fish and coral spawning and zooplankton blooms (Duffy, 2002; Heyman et al., 2001; Robinson et al., 2013; Rohner et al., 2015; Taylor, 2007)*. A time-series effort unveiled the seasonality of water masses that are suspected to carry high nutrient concentrations. These nutrient inputs could potentially trigger a phytoplankton bloom and subsequent food chain responses that attracts the whale sharks to this reef. However, this hypothesis was not supported by the data.*

Summary and Limitations: Although seasonal water mass intrusions at Shi'b Habil were observed, their timings suggest they are not responsible for a bottom-up process that may explain the whale shark aggregations. Winter mixing, warming of the water temperature, and stratification of the water column revealed potential phytoplankton and zooplankton abundance responses that could lead to a bottom-up process. Two naturally sourced water masses, Red Sea Deep Water (RSDW) and GAIW, reached this reef in the summer. The colder, saltier RSDW was seen at the exposed side of the reef in July, coinciding the timing of highest surface wind stress from the Tokar wind jets. Salinity was reduced at all sites from May to September, indicating the arrival of the Gulf of Aden Intermediate Water (GAIW). During this period, colder, fresher GAIW arrived in bursts lasting 5-26 days.

Without oxygen measurements, we were not able to distinguish the low-oxygen GAIW from the higher-oxygen GASW. The nitrate and nitrite concentrations are most correlated to oxygen levels (Churchill et al., 2014), so we could have used it as a good estimate of the nutrient load. The lack of nutrient measurements and low quality of available ones (due to long storage time of the samples) fail to characterize the actual nutrient concentration of these water masses at the arrival to Shi'b Habil.

The salty anthropogenic nutrient input from the aquaculture outfall was documented at the northeastern and northern side of the reef all year; seen as a layer above the seafloor at sites 3.8 and 4.7 km from the outfall, respectively. The effluent was furthermore seen at the exposed side of the reef, 8.4 km from the outfall in August and September, as a mid-water column layer, identified by its high salinity but warmer temperature that is consistent with the plume's characteristics.

A bathymetry chart of the region would have helped us understand the observations made at each station. It would have also allowed for a regional model based on the bathymetry and modeled wind stress curls. This would help unveil how the local circulation interacts with the bathymetry and explain the spatio-temporal patterns in our observations.

Chapter 3: Water quality, seasonality and trajectory of an aquaculture-associated plume

One of the largest integrated aquaculture in the world is located on the coast of a whale shark aggregation site in the Red Sea. This anthropogenic point source is the main outfall for wastewater from approximately 540 ponds that produced 13,000 t of shrimp in 2014. Ponds are enriched with fertilizers to trigger phytoplankton blooms before stocking the ponds with juvenile shrimp. These shrimp are then fed pellets made of crude protein and fat. The discharge goes through a settling basin but gets no other treatment before exiting to the coastal waters. The effluent will impact the local ecosystem and potentially affect the spring whale shark aggregation that occurs less than 5 km from this outfall. Monthly cruises measured physical (temperature, salinity), biological (bio-optical, microbial), and chemical (nutrients) parameters around this outfall to resolve its water quality, seasonality and trajectory.

Summary and Limitations: The plume could represent high stress to the marine recipient in that the plume had wider range of temperature, significantly higher salinity, nutrient and suspended particulate matter load, and microbial abundance and opportunistic pathogenic species than ambient coastal waters. The aquaculture plume had a clear seasonal variability, being coldest in February, following atmospheric temperature, and saltiest in June, reaching 48, approaching the extreme limits of coral tolerances. Nutrient (nitrate, nitrite, phosphate, silica) concentrations were significantly higher than the ambient coastal water and had

higher suspended particulate matter and phytoplankton biomass. *Prochlorococcus sp.* abundance was significantly lower in the plume's microbial community, whereas opportunistic pathogen abundance was significantly higher in the plume than in the unaffected water. This significantly different water mass reached the northeastern side (3.8 km from the outfall) of the reef all year round but also travelled around the northern end of the reef, reaching the exposed side of the reef (travelling a distance of 8.4 km) from late summer to autumn. We suspect the aquaculture plume present at this reef may impact the whale shark aggregation.

Our study was limited by the lack of a high-resolution bathymetry map. This would have better directed our survey efforts to track the dense plume that travels along the bottom. A bathymetry map would have enabled predicting the path of the plume, which could be confirmed with *in-situ* observations. If the local seasonal circulation interacts with the topography, giving seasonal variability to the trajectory of the plume, then the mechanism behind the late summer/autumn trajectory of the effluent reaching the exposed side of the reef may be revealed. A fine-scale bathymetry map will also enable us to fly the REMUS 100 more efficiently, measuring closer to the bottom while avoiding reef structures.

Chapter 4: Spatio-temporal variability of acoustic backscatter in the whale shark aggregation site

Whale sharks are seen foraging at Al-Lith where they are suspected to encounter high prey density during the spring when they aggregate. Whale shark detections are the highest at the northern end of Shi'b Habil, thus we monitored the temporal variability of potential prey populations at this site. If the high prey density attracted whale sharks, then we would expect the prey population to peak during their aggregation. To test this hypothesis, we measured acoustic backscatter of the water column at 120 kHz and 333 kHz – as a proxy for prey biomass – over the seasonal whale shark aggregations.

Summary and Limitations: No seasonal variability of acoustic backscatter was observed and acoustic backscatter had no peak during our sampling period (mid-January to end of April) during whale shark aggregation. But in the last ten days of deployment, acoustic backscatter decreased which coincided with the trailing end of whale shark detections. The main scattering layer performed inverse diel vertical migration (IDVM). Target strength analyses suggested the backscatter was most likely composed of fish larvae, large zooplankton, or hard-shelled organisms (e.g. mollusks), but net sampling did not capture the target and observations by divers failed to identify the targets. The main scattering layer could be prey for whale sharks.

This study could have benefitted from a longer registration period, i.e., until July, when whale shark detections are lowest in the year to have a comparison between months with and without whale shark detections. Additionally, this study was the

inability to identify species of the main scattering layer. Our approach captured high temporal variability at one site: this effort will benefit if it is accompanied with spatial surveys using the echosounder as in the aquaculture effluent tracking effort. This will allow us to capture the small-scale patchiness in acoustic backscatter that was suggested from our observations.

Unknown fauna with an acoustic signal of -50 dB was observed subsurface throughout our registration period, which was similar to observations during an acoustic study at an aggregation at Ningaloo reef, Western Australia (Wilson et al., 2002). In Al-Lith, the water column was homogenous until stratification near the end of whale shark season in May. Salinity signatures indicated an aquaculture-associated plume reached this site as a 1-2 meter bottom layer and as a mid-water column layer in September.

OVERALL CONCLUSIONS

Conclusion

Clear seasonal and spatial variability in water masses and biophysical processes were observed in Al-Lith's coastal waters. Basin-scale processes of the Red Sea influenced water mass variability at this nearshore region. The Tokar wind jets are highest in July and cause dipole eddies in the South Central Red Sea. An anticyclonic eddy will upwell the Red Sea Deep Water (RSDW) at its periphery and this was observed in our July observation when RSDW characteristics were present on the exposed side of Shi'b Habil. Winter winds that begin to converge near Al-Lith's latitude advected Gulf of Aden Surface Waters to the region in December. Sub-mesoscale circulation in the complex shallow reef systems of the southern Red Sea appears to cause intermittent intrusion of the Gulf of Aden Surface Water (GASW) at Shi'b Habil instead of a continuous supply.

The anthropogenic input from the aquaculture facility resulted in a plume that was significantly different in physical, biological (phytoplankton, microbial), chemical, and seasonal characteristics from the ambient non-affected coastal water. For the first time, the nutrient budget estimate with error was presented for the daily discharge as 109-123 k g for nitrate-N, 72-82 kg for nitrite-N, 121-138 kg for phosphate-P, and 882-999 kg for silica-Si. The wastewater's density and observed trajectory suggests they stay subsurface, near the seafloor, and were detected 4.7 km and 8.3 km offshore from the outfall, depending on the season. This plume is observed in the whale shark aggregation site during their aggregation season and could be influencing their behaviors by providing chemosensory cues.

Seasonal variability in plankton could be attributed to natural biophysical processes. Winter mixing decouples phytoplankton grazing from phytoplankton growth by diluting grazer densities. This has been proposed to cause phytoplankton peaks in mid-winter, which parallels our phytoplankton peak observed in February. The plankton peak in May and June could be a response to stratification from May that will increase light exposure for phytoplankton and promote primary productivity. The episodes of GAIW intrusions from May also deliver nutrients to the region to contribute to this primary production. The water temperature increase from February to June may reach optimal temperature for spawning (e.g., by fish or corals) and be a food source potentially attracting whale sharks. Our plankton measurements (1.2-250 μm and > 0.7cm) did not cover the size range expected for fish eggs (0.7-1 mm) that were seen targeted by whale sharks at other aggregation sites. Thus it is possible that spawning events occurred during this period but was not detectable through our methods.

The timing of the water mass intrusions and acoustic backscatter seasonal variability did not explain the seasonal whale shark aggregation at Shi'b Habil. Observations that will suggest a bottom-up control on the whale shark abundance were not identified. The phytoplankton and zooplankton peak in February supposedly from winter mixing decoupling grazers and phytoplankton could supply energy to higher trophic levels and increase whale shark prey density. However, the acoustic backscatter seasonal variability does not reflect this. Our methods did not measure seasonal variability of particle sizes of picophytoplankton and animals between 250 μm and 0.7 cm. It is possible that prey targeted by the whale sharks

were not represented by the particle sizes we captured or that the sampling methodology was insufficient to capture the spatial heterogeneity of the prey fields.

Perspectives

For improvement, I suggest to deploy moorings with multiple instrument packages at different depths to capture the vertical structure of the water column at higher temporal resolutions. This will provide higher temporal resolution of the vertical structure of the water column that we did not capture in our effort due to shortage of instruments at the beginning of the study. This could reveal the depth occupancy of the GAIW as it arrives in episodes to Shi'b Habil. Each instrument package should include a CTD, a fluorometer (proxy of phytoplankton biomass), an ECO-VSF (backscattering coefficient, proxy of suspended particulate matter), an oxygen optode, and an optical nitrate sensor. At the fixed part of the mooring (the anchored end), the instrument package should also include an upward looking ADCP to measure the water velocity and echo intensity. I recommend for moorings with three depths (5 m, mid-water column, and bottom) at stations N, NW, and W and two depths (mid-water column and bottom) at stations NE, E, and S to be deployed because the offshore stations had higher heterogeneity of the water column than the relatively homogenous inshore stations.

Monthly water samples should be conducted to characterize the plankton community in detail since our results showed plankton seasonal variability and succession. We recommend taking water samples at an inshore and offshore station (e.g., NW and NE) and conduct similar methods as Al-Hashmi et al. (2012) to capture

the seasonal variability of abundance and community structure of phytoplankton and zooplankton, including a control site dissociated from the aquaculture plume. 100 mL should be frozen for nutrient analysis (nitrate, nitrite, silicate, phosphate, and urea), 100 mL should be chilled in ice water for high-performance liquid chromatography (HPLC) analysis to obtain community composition by using pigments as taxonomic markers (Claustre et al., 2004), and 500 mL should be preserved with 1% Lugol's iodine solution for cell counts and identifications using microscopy or an genomic approach to identify species composition.

A series of field efforts coupled with models would improve our understanding of the aquaculture plume. We intended to have the following fieldwork and analysis during this PhD project and are realistic goals as a next step in understanding Al-Lith. This should start with a full bathymetry effort with the Coastal and Marine Resources Core Lab (CMRCL) support (especially from Francis Mallon) and deployment of an ADCP mooring at the mouth of the outfall (available in CMRCL). A regional circulation model based on a high-resolution bathymetry map and climatological surface wind stress models should be done with help from a modeling group at KAUST (I. Hoteit lab). In addition, gliders should be deployed at the South Central Red Sea (SCRS) to observe the offshore seasonal variability of the RSDW and GAIW. This glider deployment will provide a time-series of the basin-scale water mass movements and other oceanographic processes affecting the coastal regions. Time-series by a glider has been maintained in waters between KAUST and Yanbu (north of KAUST) and has been attempted in the SCRS. Coastal

observations that could be a result of the basin-scale processes could be better understood if we have simultaneous basin-scale and nearshore observations.

Surveys should be conducted using an echosounder following a whale shark spotted from the surface during visible surveys from February to May. This will require mounting the echosounder at the end of a rod (as done for Chapter 3) and securing it on the side of the boat that will be used during whale shark trips organized during the aggregation season. Comparison with echosounder survey outside the aggregation season (e.g., October, November) could reveal any seasonal biomass variability, or any frontal features that form only during aggregation season. This will capture horizontal spatial patchiness in biomass that our findings suggested. Efforts to identify the whale shark's target prey will be necessary as well to narrow down which food web is responsible for their seasonal aggregation.

Future studies should compare the ecological health of areas of heavy aquaculture discharge influence with areas without discharge influence. We would recommend the stations for these different discharge exposures (Table C.1 and Figure C.1). Benthic and demersal animals should be the focus of the ecological assessments because the plume layer is always seen near the bottom. A geostationary satellite (e.g., GEO-OCAPI) can achieve the high spatio-temporal (250 m and 8 day^{-1}) resolution of data products from ocean color (e.g., particulate backscatter, chlorophyll, total suspended matter, photosynthetic available radiation (PAR) above water surface, CDOM, POC, DOC, and PIC) to resolve rapidly evolving phenomena such as an aquaculture discharge (Ryu, Choi, Eom, Ahn, & Samples, 2011). In addition, future studies should measure the water at the intake of the

aquaculture facility and compare changes in water qualities with the effluent at the outfall. Differences between the intake water and the discharge will reveal the biogeochemical processes that the water is subjected to as it travels and is used inside the facility.

Table C.1. Recommended stations to study the discharge's environmental impact at various exposures. Based on our monthly surveys in 2014 of the aquaculture plume dilutions, we separated the stations (labeled in Figure C.1) with different exposures of the plume.

Discharge exposure	**Recommended stations**
Heavy	P1, P2, P3, P4
Medium	P5, P7, P9, P10, NE
Light	N, NW, W
None	P6, P11, E, S

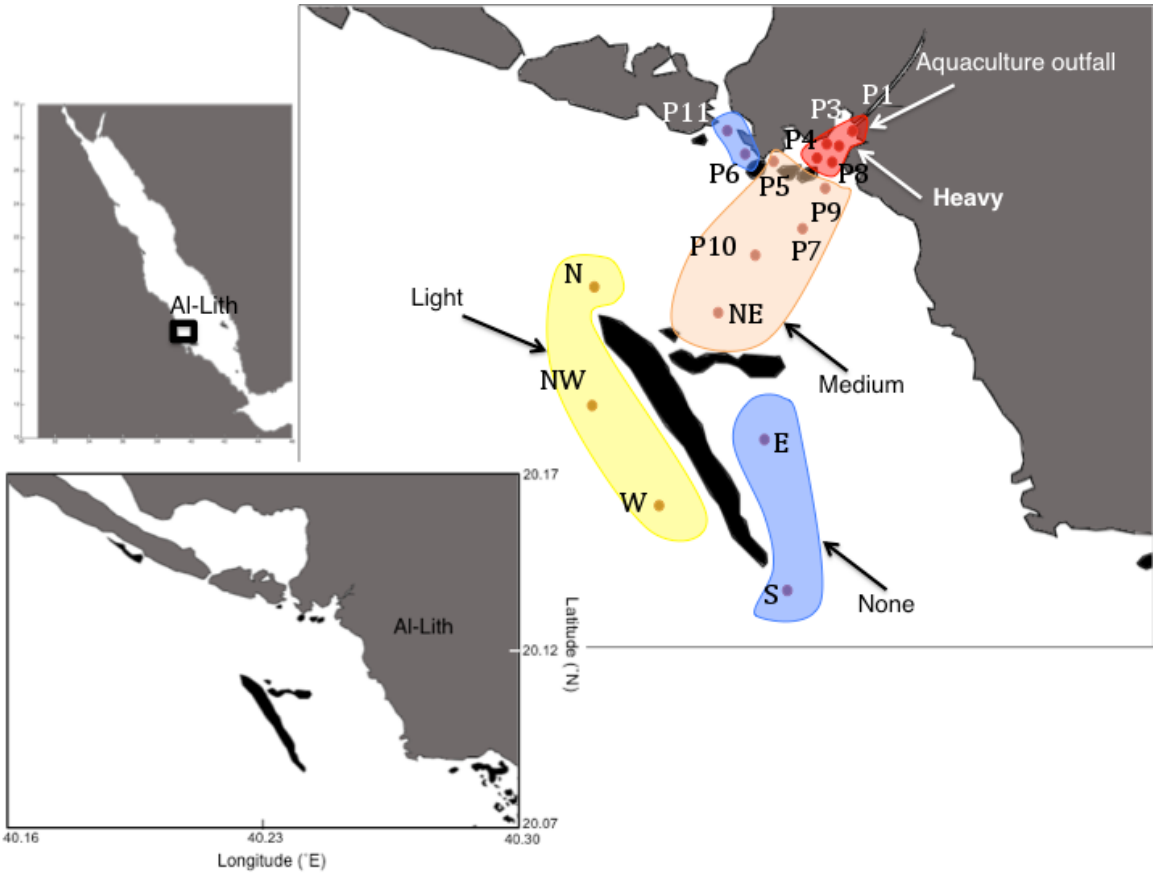

Figure C.1. The recommended stations listed in Table C.1 are color coded in the inset map of Shi'b Habil and Al-Lith's coastline.

Mesoscale current circulations

The mesoscale oceanographic processes (i.e., small-scale circulatory patterns around Shi'b Habil) potentially responsible for the whale shark aggregation should be investigated. Local current patterns may be accumulating plankton in high-density patches and should be studied. A majority of the known whale shark aggregation sites have been identifed as a feeding ground for juveniles. Whale sharks are known to feed on various planktonic and nektonic species, which range from copepods, fish and crustacean larvae and eggs to small fish, squid, and jellyfish

(Clark & Nelson, 1997; Compagno, 1984; Heyman et al., 2001; Robinson et al., 2013; Stevens, 2007). Environmental cues to signal ample prey densities to whale sharks are not well understood (Duffy, 2002; Wilson et al., 2001). Upwelling events are associated with productive biological hotspots and were associated with whale sharks in some cases (Burks & Mullin, 2006; Hoffmayer & Franks, 2007), but this was not the case in other aggregation sites (Duffy, 2002; Heyman et al., 2001). Fronts and similar horizontal gradients have enhanced biomass, especially for mobile and positively buoyant species (Franks, 1992; Genin, Jaffe, Reef, Richter, & Franks, 2005). These areas become a foraging ground for marine vertebrates such as seabirds, turtles, and whale sharks (Godø et al., 2012; Iwasaki, 1970; Scales et al., 2014; Wilson et al., 2002). Similarly, a whale shark aggregation site near an oil platform off Qatar was observed to be actively feeding on zooplankton aggregations, mainly of mackerel tuna eggs (Robinson et al., 2013), which are positively buoyant. Other sites have observed them actively feeding on reef snapper eggs (Heyman et al., 2001), crustacean *Portuniid* and *Stomatopoda* larvae (Taylor, 2007), and mobile copepods *Acartia clause* (Clark & Nelson, 1997). Vertical currents (downwelling or upwelling) are the primary mechanism to create patchy aggregations of positively buoyant and mobile zooplankton (Genin et al., 2005), and thus biomass patchiness suggests the presence of oceanographic features such as fronts, shelf breaks, and micro-scale eddies.

To investigate, a REMUS 100 equipped with upward and downward looking current profiler (RDI ADCP) could be deployed at the northern end of Shi'b Habil reef multiple times during the whale shark aggregation (Figure C.2). This effort

should be repeated when there are no whale sharks (July-November). A moored current profiler (RDI ADCP Sentinel) should be deployed continuously to provide validation for ADCP data retrieved from a submerged moving platform (Figure C.2) (Fong & Jones, 2006). Additionally the REMUS can measure basic oceanographic properties (conductivity, temperature, pressure) and biological data (chlorophyll *a* fluorescence, and turbidity). Concurrently, small surface drifters (Microstar, Pacific Gyre) equipped with temperature probes should be deployed at the southern end of Shi'b Habil (five on each side of the reef) (Figure C.2). This will help provide a snapshot of micro-scale surface currents as performed by Ohlmann (2011). The combined effort would aim to detect current patterns that could be aggregating plankton that coincides with the peak of the season but not observed prior to or after the season.

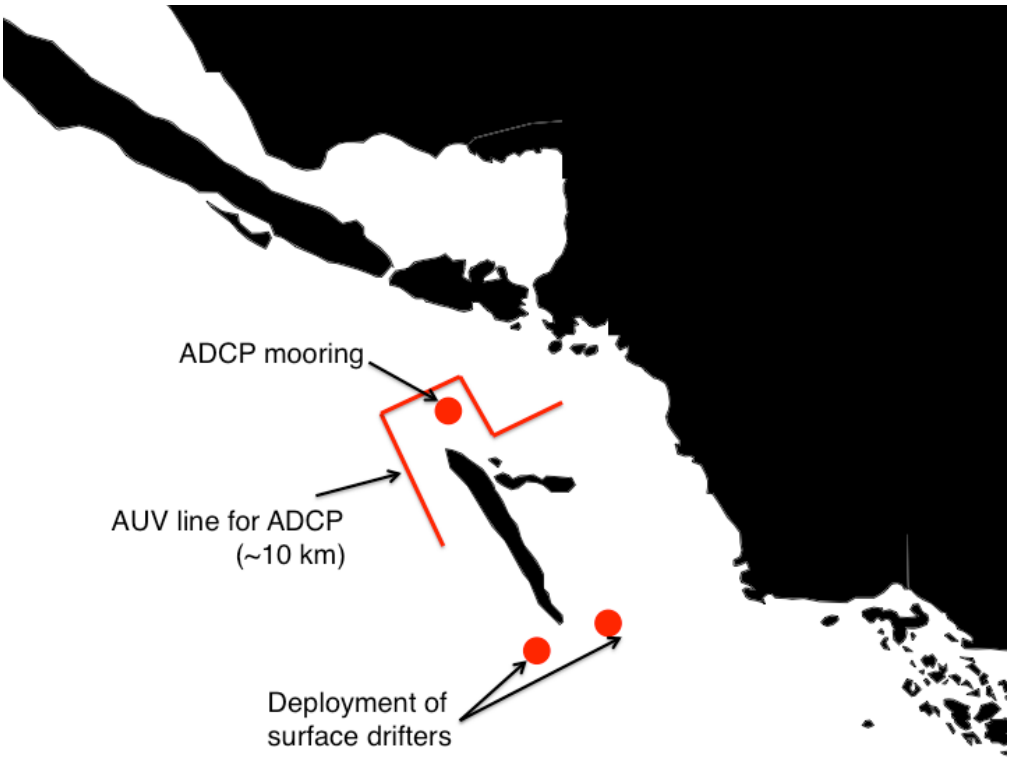

Figure C.2. Suggested locations for fieldwork to study the current patterns at this reef. The surface drifters (Microstars) should be deployed at the southern end of Shi'b Habil due to suspected northwestward currents from winter wind convergence. The REMUS line survey the northern end of the reef to capture current patterns at the site with highest whale shark detections. The ADCP mooring should be located overlapping the REMUS survey line to validate the ADCP measurements on the REMUS with the stationary moored ADCP data.

APPENDIX A: EXPECTED PUBLICATIONS

1) Hozumi, A., and Jones, B. (in prep) Spatio-temporal variability of water masses at a whale shark aggregation site in the Red Sea. *Limnology and Oceanography*
2) Hozumi, A., Røstad, A., Kaartvedt, S., and Jones, B. (in prep) Spatio-temporal variability of acoustic backscatter at a Red Sea whale shark aggregation site.
3) Hozumi, A., Hong, P., and Jones, B. (in prep) Water quality, seasonality and trajectory of an aquaculture-associated plume in the Red Sea. *Coastal, Estuarine and Shelf Science*

APPENDIX B: REMUS SPATIAL SURVEY IN 2013

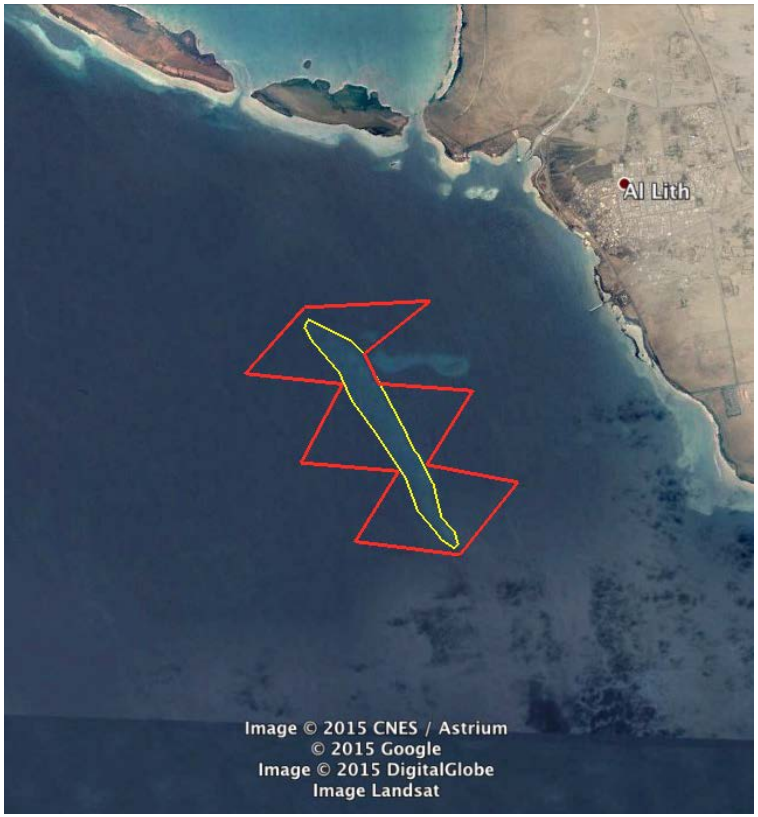

A map of the survey lines for May, June (yellow), September, October, and December (red) around Shi'b Habil is shown. The spatial variability of a) potential temperature, b) practical salinity, c) chlorophyll *a* fluorescence, and d) turbidity measurements from the REMUS survey efforts in 2013 are shown. Each column is from a different monthly survey (May to December from left to right). The color axes are inconsistent with each other to better highlight the spatial variability in each month.

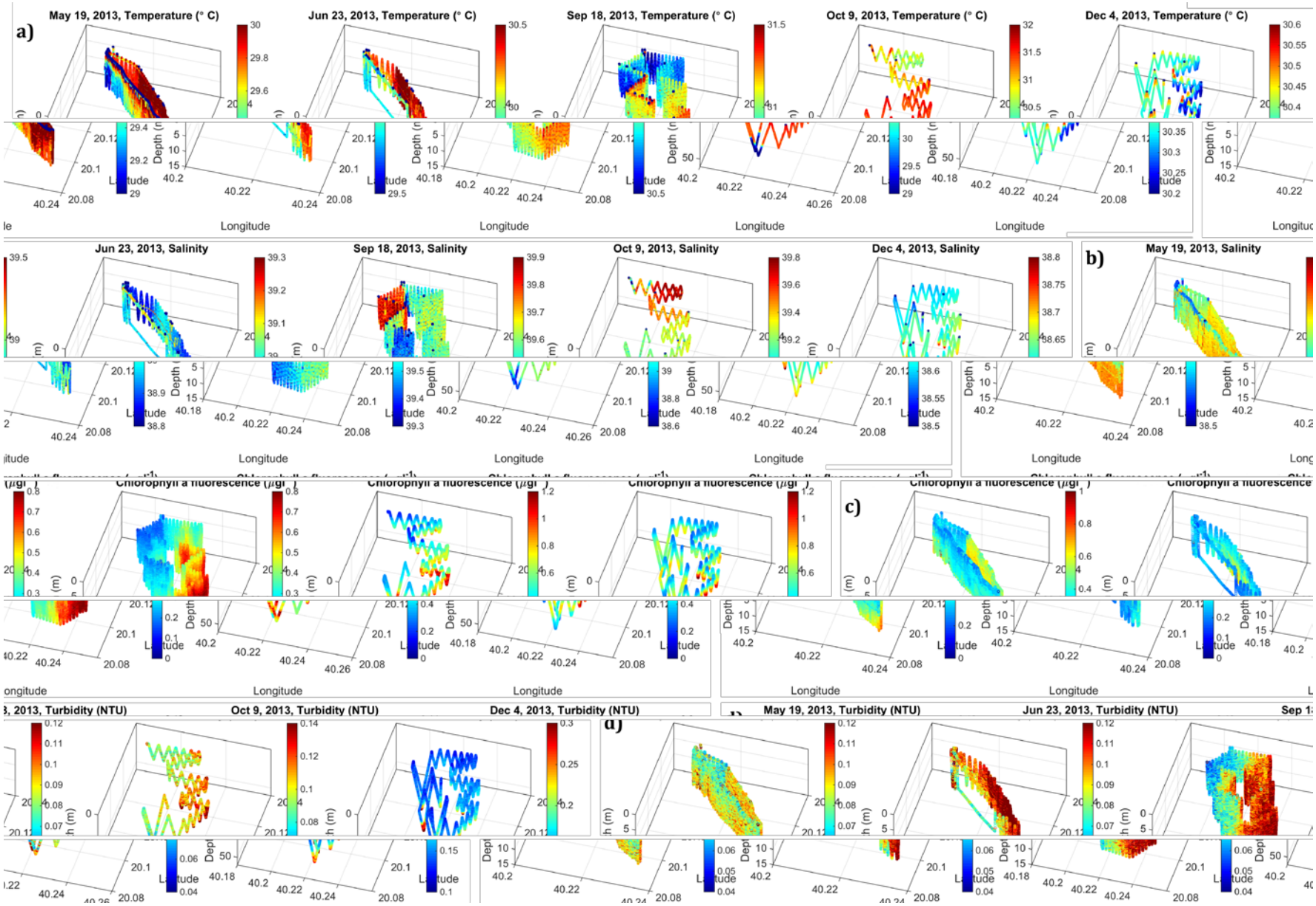
a)
May 19, 2013, Temperature (° C)
Jun 23, 2013, Temperature (° C)
Sep 18, 2013, Temperature (° C)
Oct 9, 2013, Temperature (° C)
Dec 4, 2013, Temperature (° C)
Jun 23, 2013, Salinity
Sep 18, 2013, Salinity
Oct 9, 2013, Salinity
Dec 4, 2013, Salinity
b)
May 19, 2013, Salinity
Chlorophyll a fluorescence (µgl
c)
Oct 9, 2013, Turbidity (NTU)
Dec 4, 2013, Turbidity (NTU)
May 19, 2013, Turbidity (NTU)
Jun 23, 2013, Turbidity (NTU)
Longitude
Depth (m)
Latitude

A temperature-salinity plot of all the monthly surveys is included (e) to illustrate the seasonal variability of water masses at Shi'b Habil captured by our REMUS efforts. The water gets warmer from May to October and the salinity range increases, showing stratification of the water column except in December when the water is homogenous and is colder and fresher compared to the previously sampled survey in October.

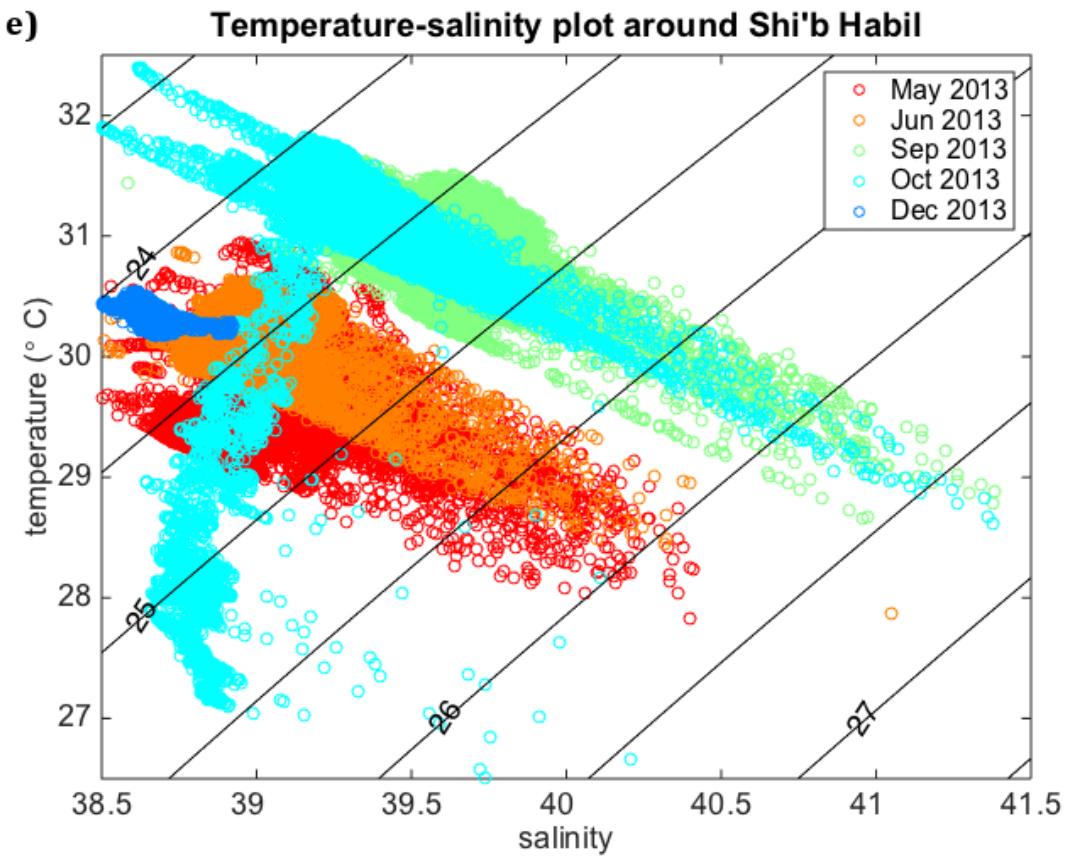

APPENDIX C: CORRECTION FOR ADCP DATA FROM REMUS

The following corrections I used were obtained from suggested corrections from Teledyne RD Instruments manuals (2010) and Haven (2012). First the speed of sound is corrected for because the given velocity uses a pre-set speed of sound instead of the actual speed of sound. Next each bin is corrected for to its real depth that compensates for the REMUS movement. Then the velocities are transformed from instrument to earth coordinates and corrected for the REMUS velocity.

Speed of sound correction

The speed of sound the REMUS uses to derive the velocity it gives us as data ($V_{uncorrected}$) is not using the actual speed of sound of the sampled water. The actual speed of sound depends on the temperature, salinity, and depth and is calculated from the CTD measurements. Thus this needs to be corrected for to obtain the actual velocity measured ($V_{corrected}$) using the formula below.

$$V_{corrected} = V_{uncorrected} \left(\frac{C_{actual}}{C_{used}}\right)$$

Then the real depth of each bin was acquired using the REMUS' depth, blanking distance, cell size, pitch, and roll.

Instrument to earth coordinate transformation

The ADCP gives the u, v, and z components of the measured velocity (X, Y, and Z) in relation to the vehicle (REMUS). Because the REMUS' heading, pitch, and roll are constantly moving during its mission, the velocity needs to be transformed from instrument to earth coordinates to have u and v components that correspond to earth's north and east coordinates. For this, the given X, Y, and Z velocity components need to be multiplied by matrix M.

$$M = \begin{bmatrix} CH & SH & 0 \\ -SH & CH & 0 \\ 0 & 0 & 1 \end{bmatrix} \begin{bmatrix} 1 & 0 & 0 \\ 0 & CP & -SP \\ 0 & SP & CP \end{bmatrix} \begin{bmatrix} CR & 0 & SR \\ 0 & 1 & 0 \\ -SR & 0 & CR \end{bmatrix}$$

$$\begin{bmatrix} N \\ E \\ U \end{bmatrix} = M \begin{bmatrix} X \\ Y \\ Z \end{bmatrix}$$

In the above equation, C= cos(), S = sin(), H= heading, P= pitch, and R= roll of the REMUS. Thus CH = cos(heading). N, E, and U give the corrected velocity components in earth coordinates for north, east, and vertical.

APPENDIX D: VERTICAL PROFILES OF ALL STATIONS

Vertical profiles taken at each station during our monthly cruises are presented. Depending on the month, combination of temperature, salinity, chlorophyll *a* fluorescence, turbidity, particulate beam attenuation coefficient, and backscattering were measured. The map below shows the locations of these stations in relation to Shi'b Habil, the Al-Lith coast, and the aquaculture outfall.

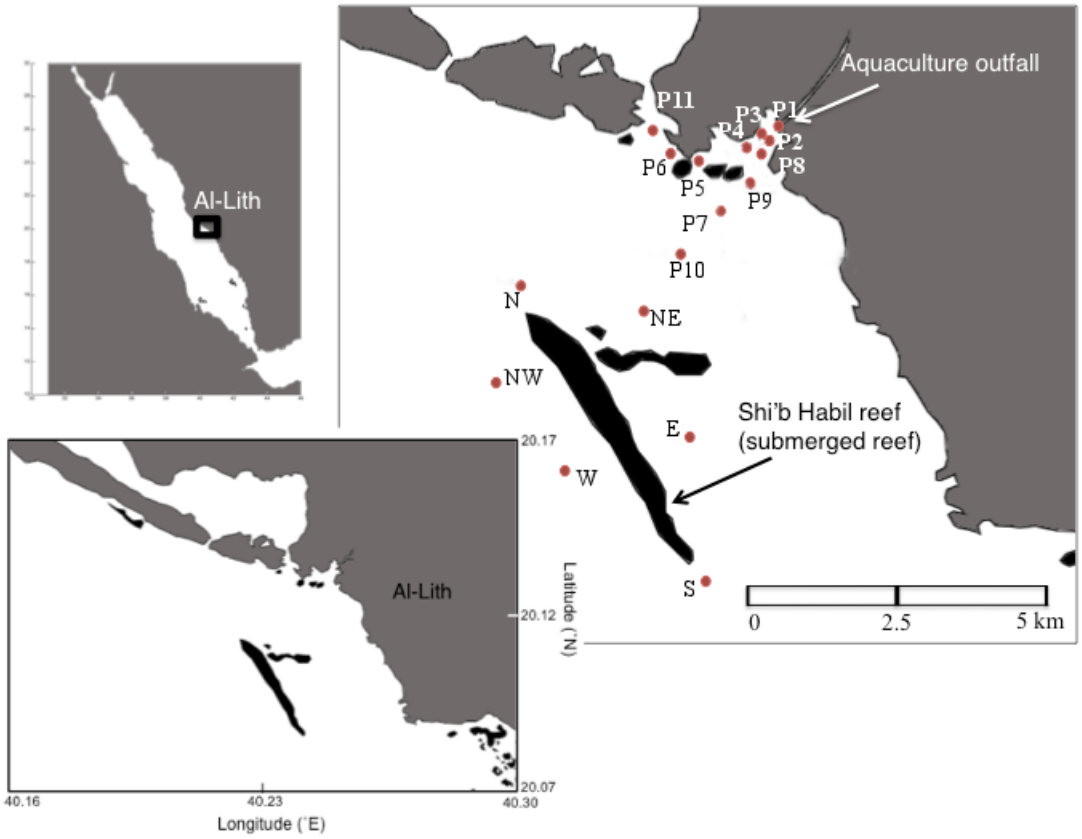

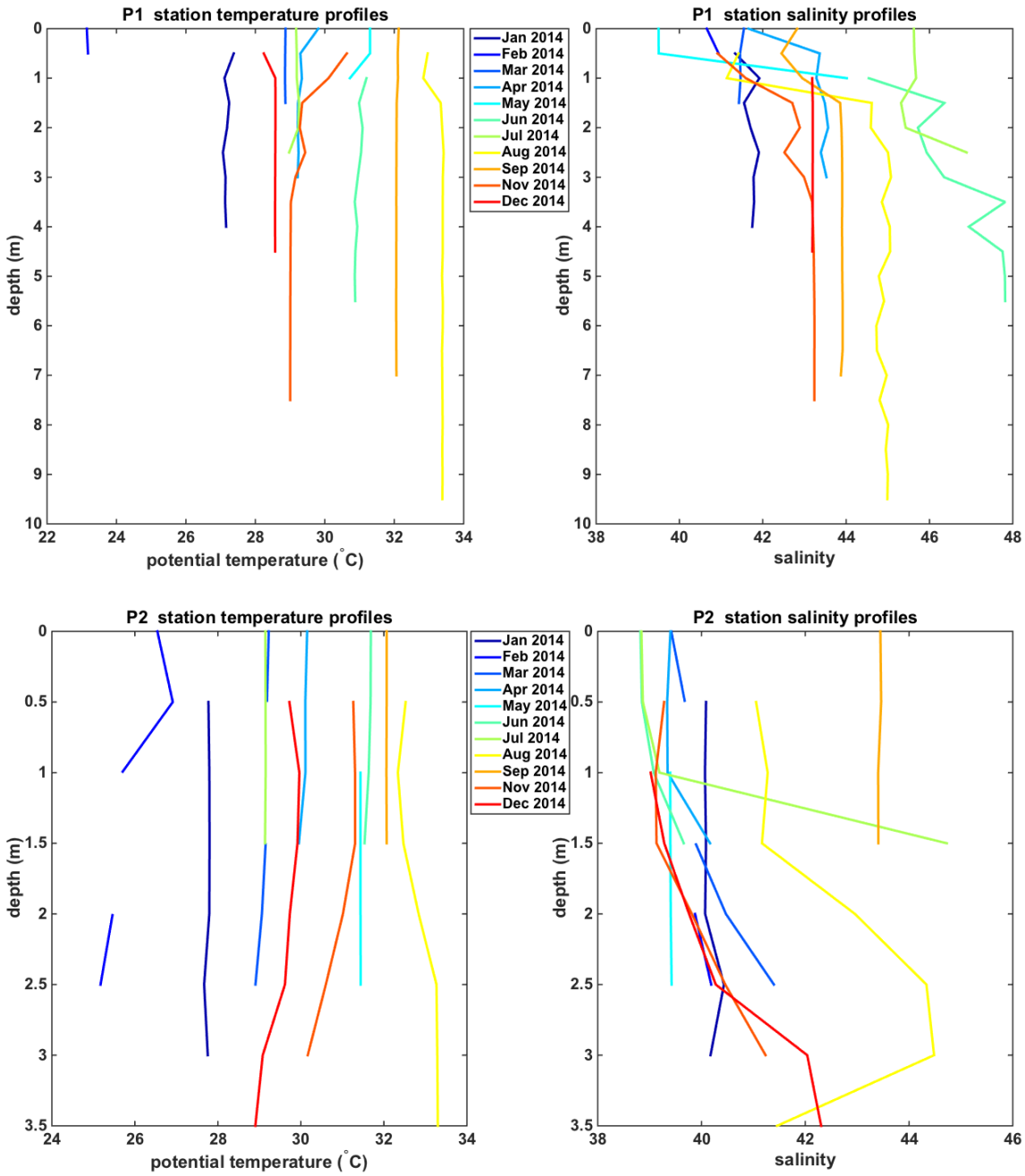
P1 station temperature profiles
depth (m)
potential temperature (°C)
Jan 2014
Feb 2014
Mar 2014
Apr 2014
May 2014
Jun 2014
Jul 2014
Aug 2014
Sep 2014
Nov 2014
Dec 2014
P1 station salinity profiles
depth (m)
salinity
P2 station temperature profiles
depth (m)
potential temperature (°C)
P2 station salinity profiles
depth (m)
salinity

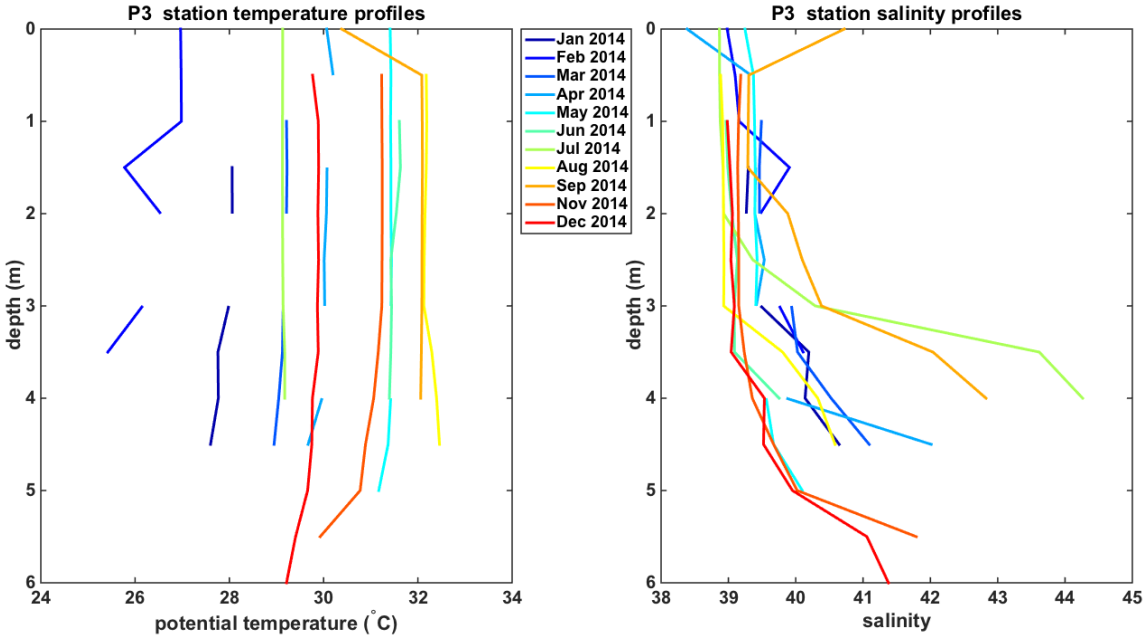
P3 station temperature profiles
depth (m)
potential temperature (˚C)
Jan 2014
Feb 2014
Mar 2014
Apr 2014
May 2014
Jun 2014
Jul 2014
Aug 2014
Sep 2014
Nov 2014
Dec 2014
P3 station salinity profiles
depth (m)
salinity

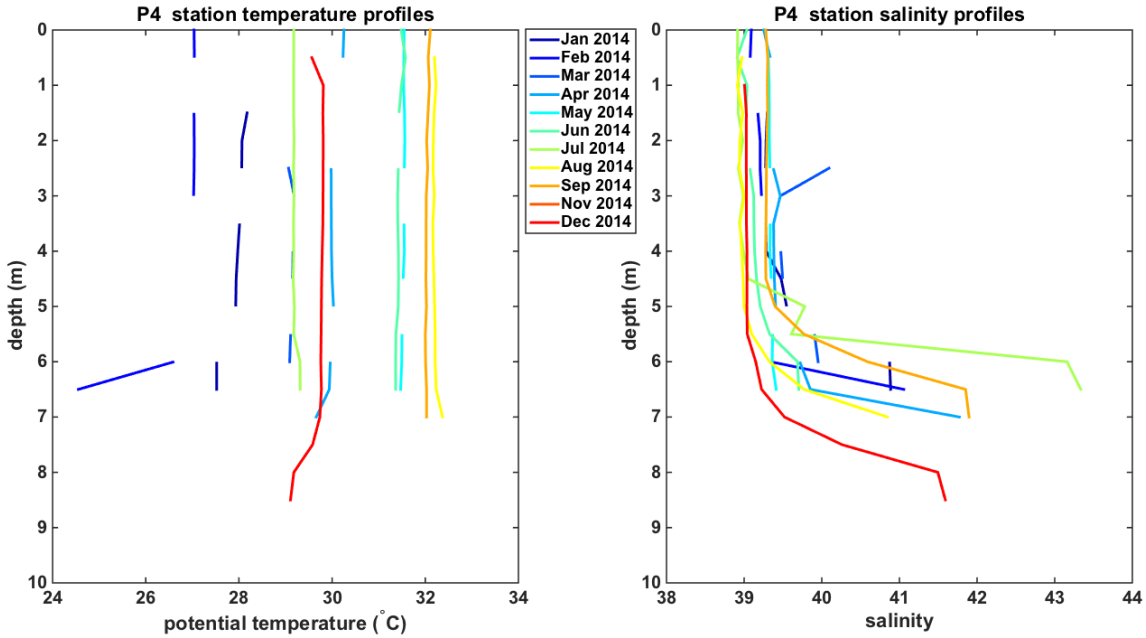
P4 station temperature profiles
depth (m)
potential temperature (˚C)
Jan 2014
Feb 2014
Mar 2014
Apr 2014
May 2014
Jun 2014
Jul 2014
Aug 2014
Sep 2014
Nov 2014
Dec 2014
P4 station salinity profiles
depth (m)
salinity

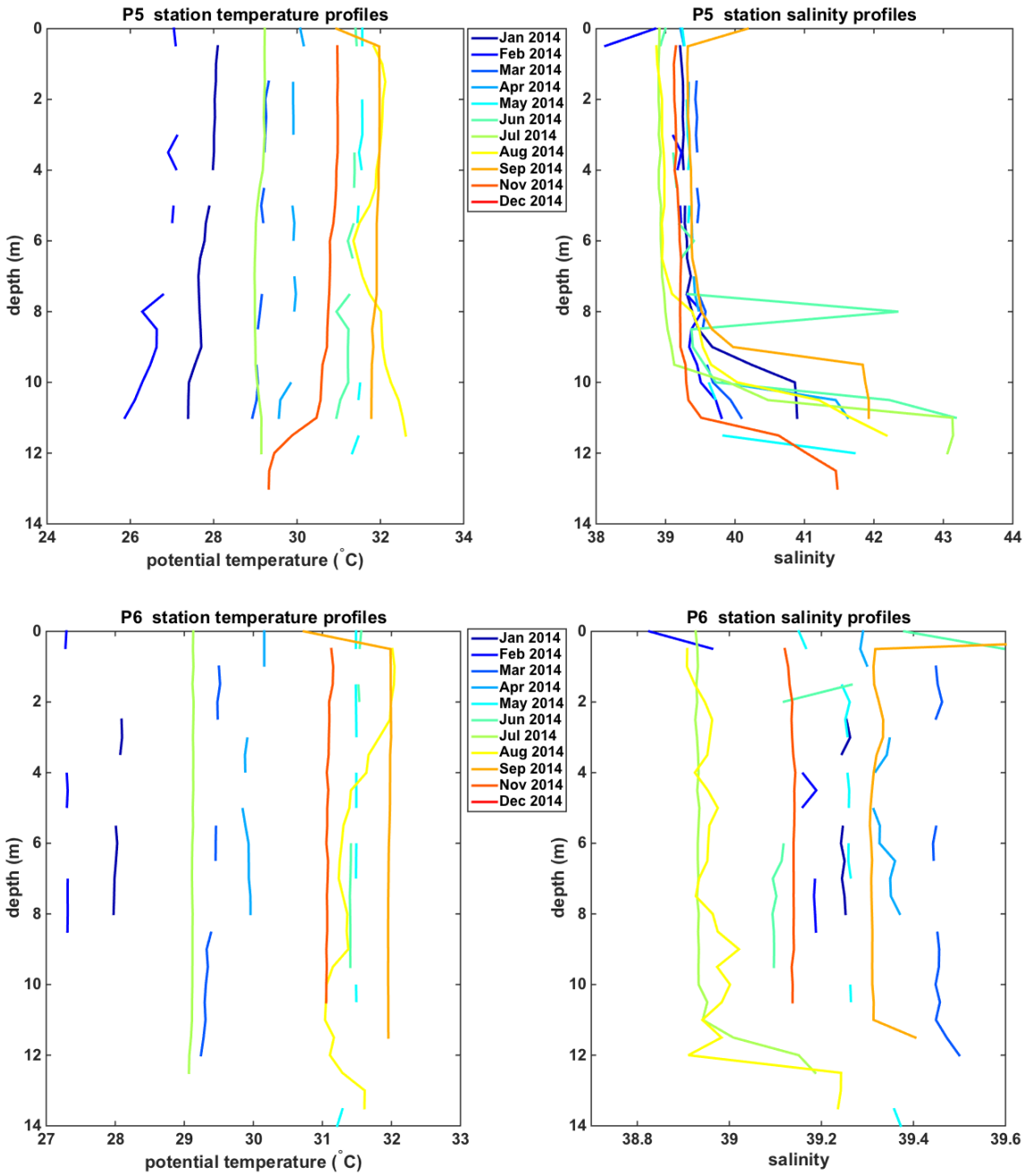
P5 station temperature profiles
depth (m)
potential temperature (˚C)
Jan 2014
Feb 2014
Mar 2014
Apr 2014
May 2014
Jun 2014
Jul 2014
Aug 2014
Sep 2014
Nov 2014
Dec 2014
P5 station salinity profiles
depth (m)
salinity
P6 station temperature profiles
depth (m)
potential temperature (˚C)
P6 station salinity profiles
depth (m)
salinity

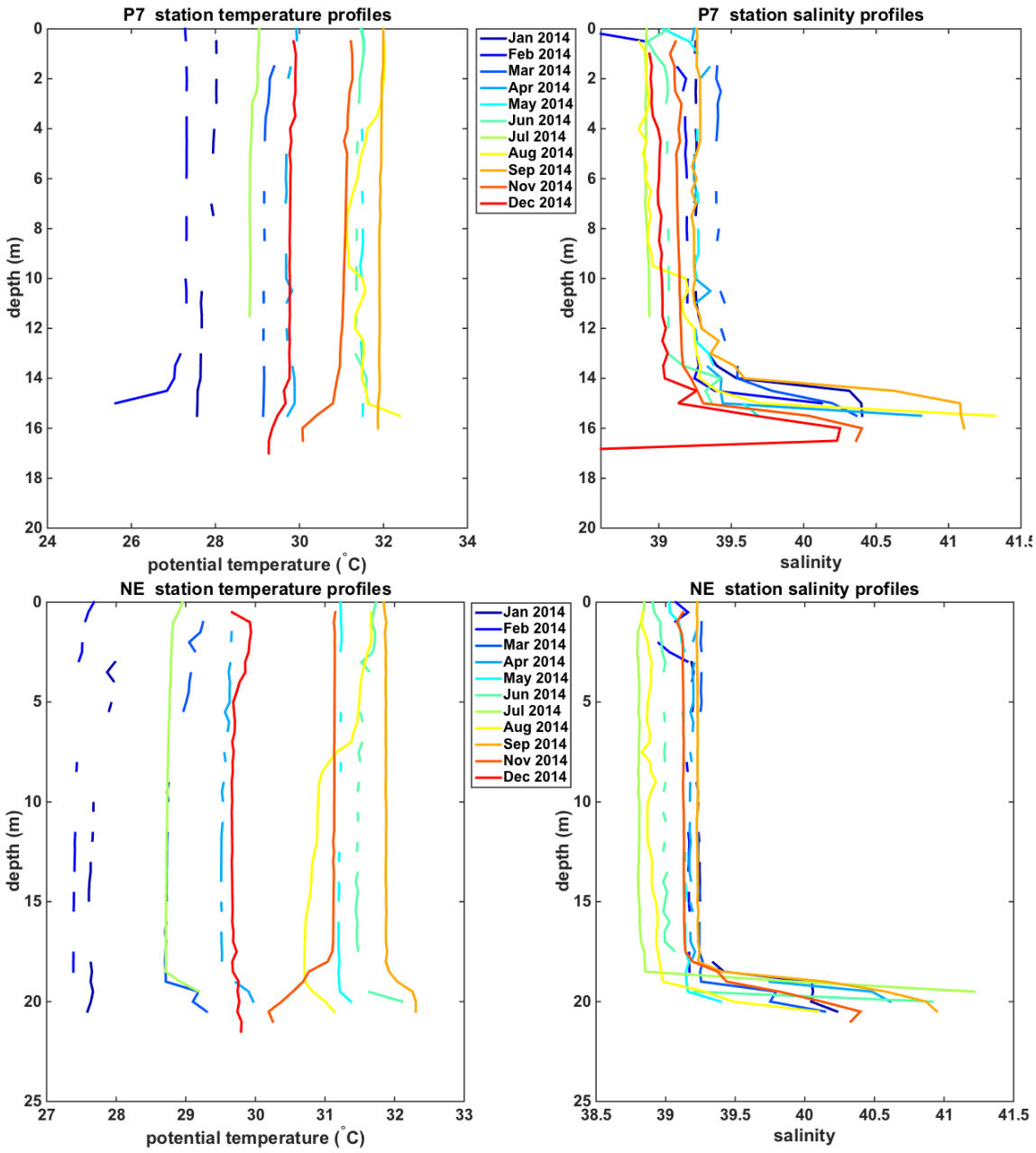
P7 station temperature profiles
depth (m)
potential temperature (°C)
Jan 2014
Feb 2014
Mar 2014
Apr 2014
May 2014
Jun 2014
Jul 2014
Aug 2014
Sep 2014
Nov 2014
Dec 2014
P7 station salinity profiles
depth (m)
salinity
NE station temperature profiles
depth (m)
potential temperature (°C)
Jan 2014
Feb 2014
Mar 2014
Apr 2014
May 2014
Jun 2014
Jul 2014
Aug 2014
Sep 2014
Nov 2014
Dec 2014
NE station salinity profiles
depth (m)
salinity

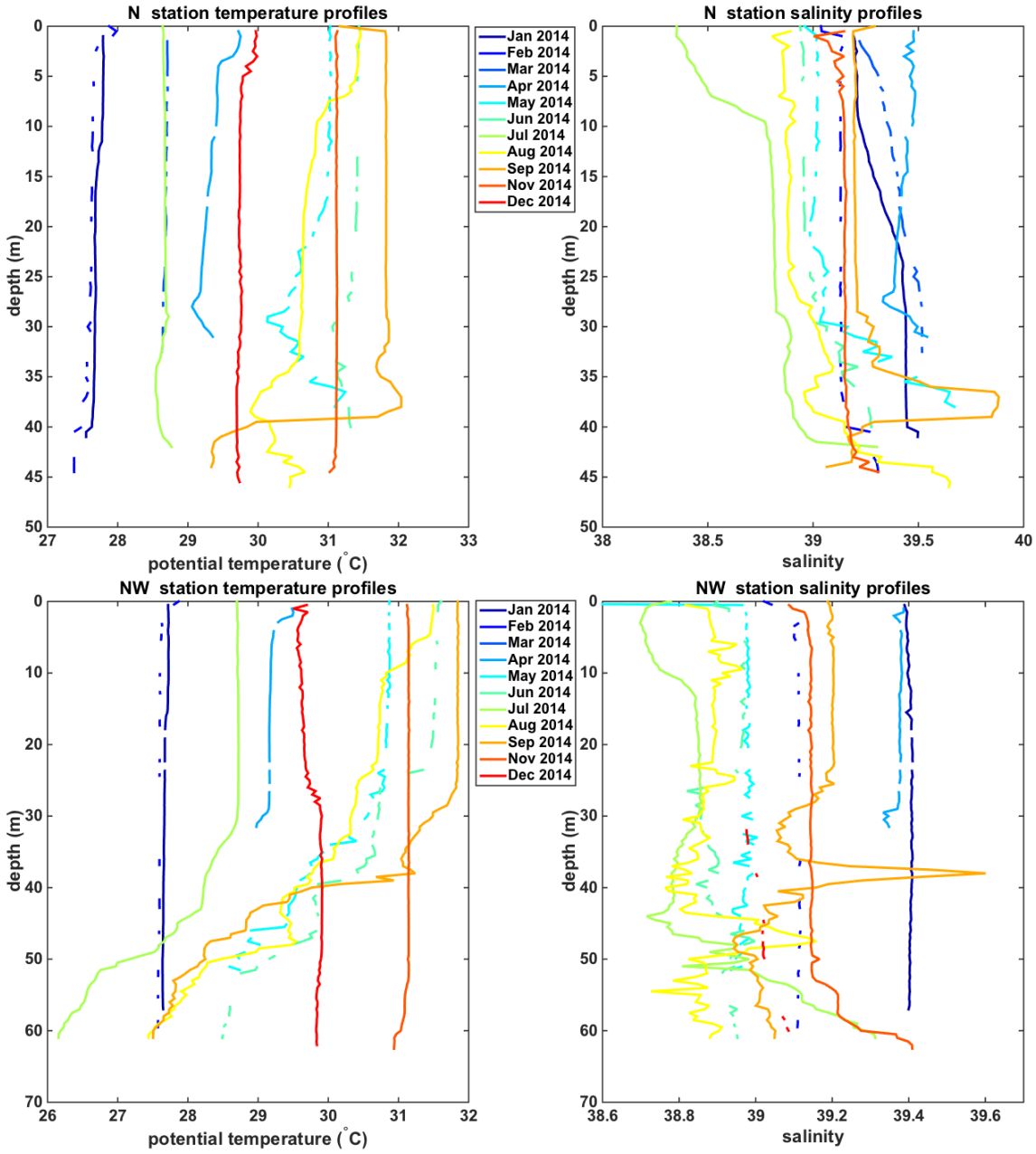
N station temperature profiles
depth (m)
potential temperature (°C)
N station salinity profiles
salinity
NW station temperature profiles
depth (m)
potential temperature (°C)
NW station salinity profiles
salinity
Jan 2014
Feb 2014
Mar 2014
Apr 2014
May 2014
Jun 2014
Jul 2014
Aug 2014
Sep 2014
Nov 2014
Dec 2014

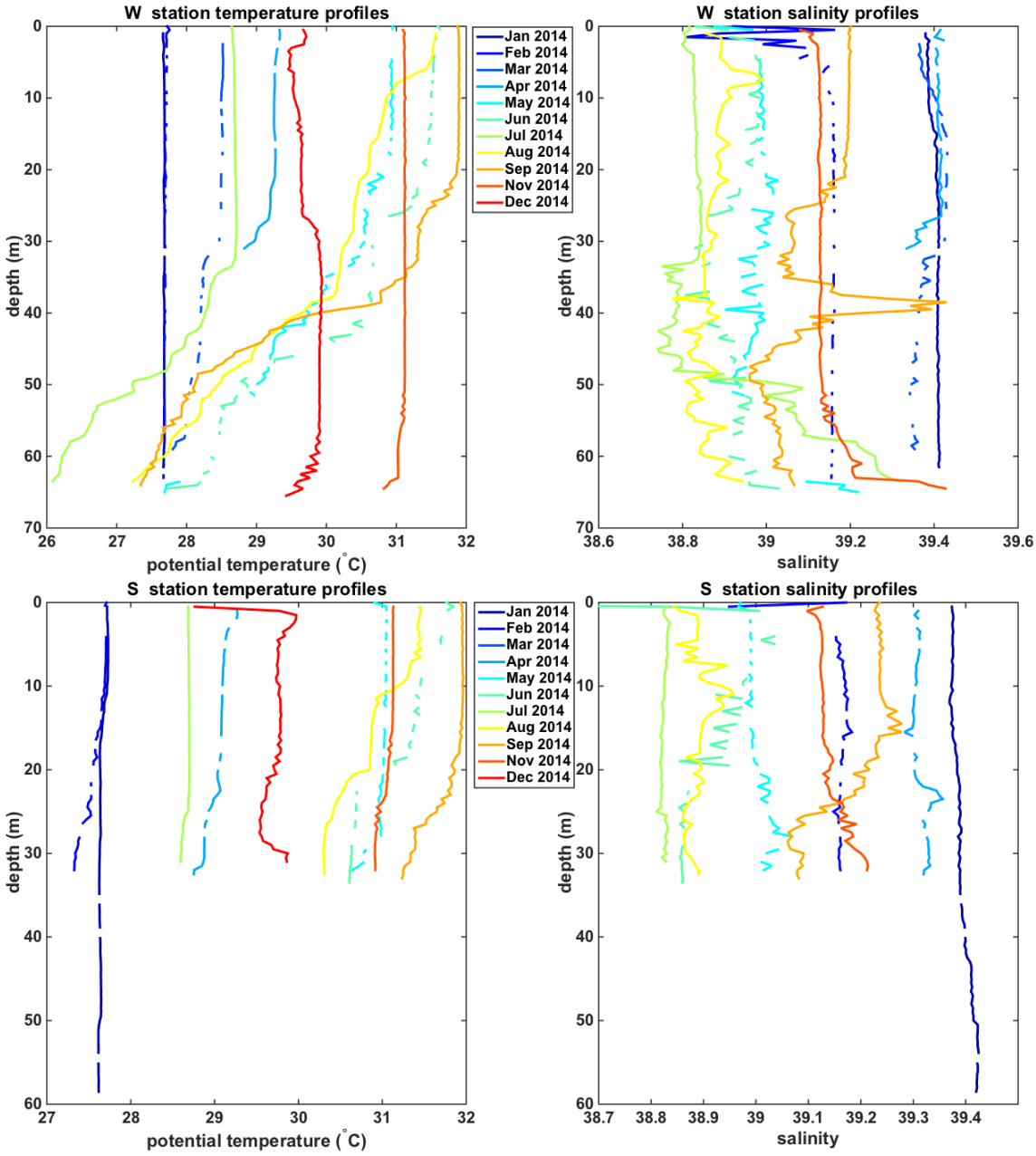
W station temperature profiles
W station salinity profiles
S station temperature profiles
S station salinity profiles
Jan 2014
Feb 2014
Mar 2014
Apr 2014
May 2014
Jun 2014
Jul 2014
Aug 2014
Sep 2014
Nov 2014
Dec 2014
depth (m)
potential temperature (˚C)
salinity

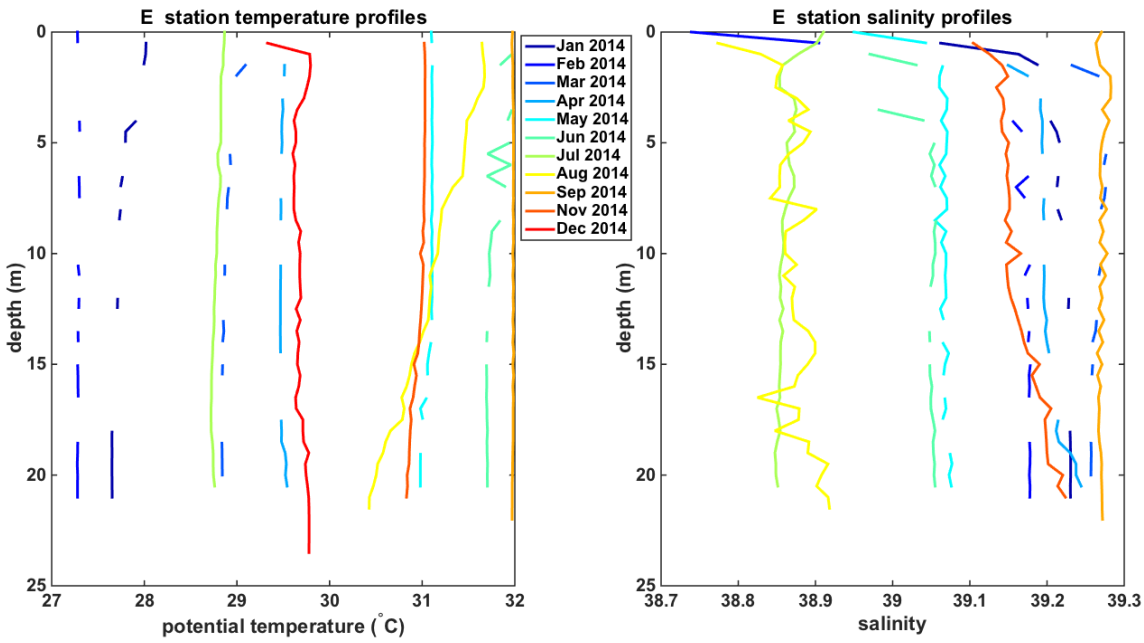
E station temperature profiles
depth (m)
potential temperature (°C)
Jan 2014
Feb 2014
Mar 2014
Apr 2014
May 2014
Jun 2014
Jul 2014
Aug 2014
Sep 2014
Nov 2014
Dec 2014
E station salinity profiles
depth (m)
salinity

APPENDIX E: ECHOSOUNDER SPATIAL SURVEY

The echosounder survey conducted on January 15, 2014, tracked the aquaculture plume from the outfall through its coastal recipient, northeast of Shi'b Habil. Real-time data was observed and used to determine the trajectory of our boat-mounted survey path (yellow). CT profiles were taken at 4 locations (diamonds) during the survey to supplement the acoustic data.

All echograms of our survey are included below. The x-axis is in time but also represents space. The y-axis is the depth of the water column with surface at the top. The color scheme represents the strength of the acoustic backscatter in dB, which is a log scale unit. The strong (dark red) signal is the strong backscatter from the seafloor. Thus acoustic backscatter above this seafloor signal to the surface is measured backscatter in the water column.

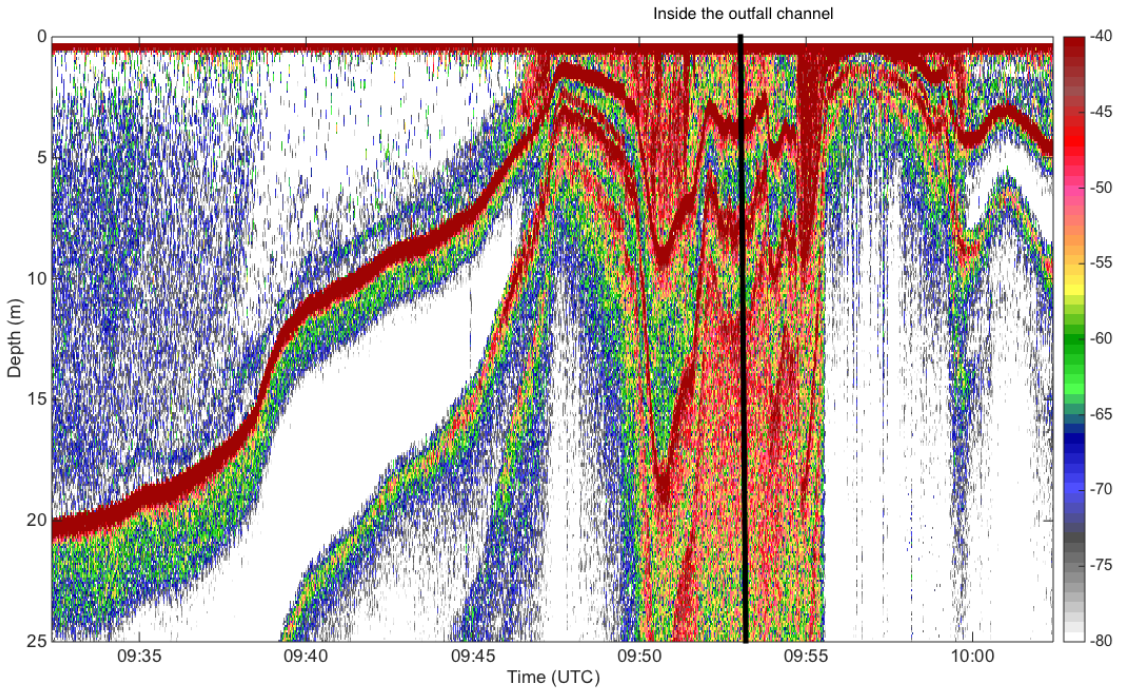
Inside the outfall channel
Depth (m)
Time (UTC)
09:35
09:40
09:45
09:50
09:55
10:00

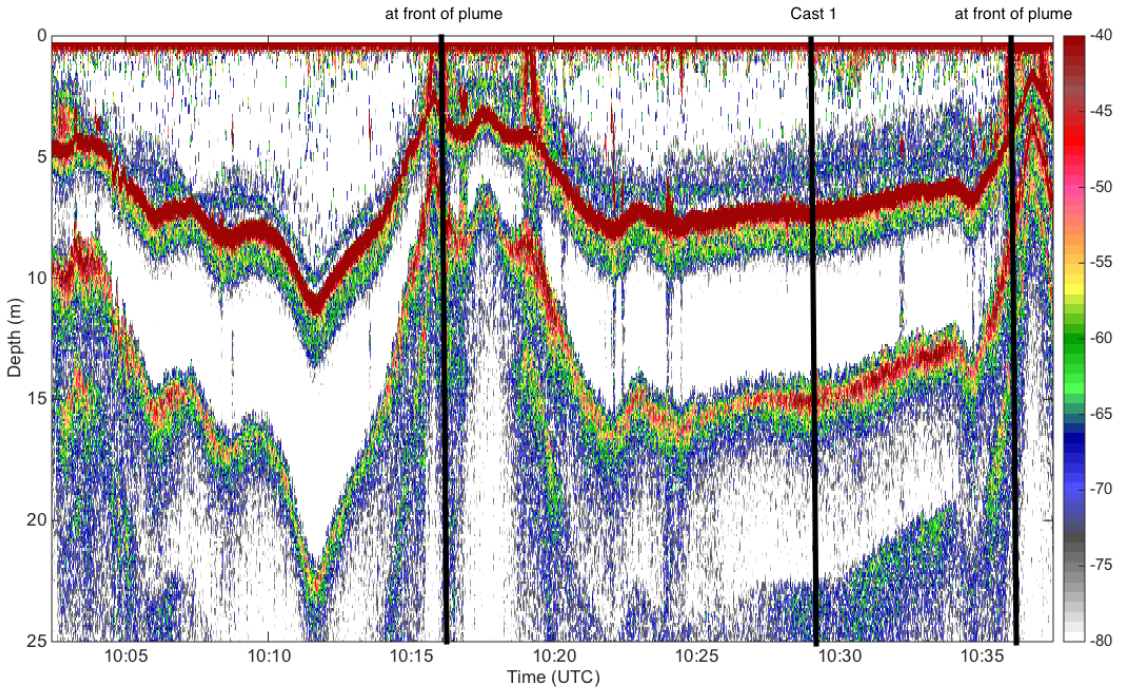
at front of plume
Cast 1
at front of plume
Depth (m)
Time (UTC)
10:05
10:10
10:15
10:20
10:25
10:30
10:35

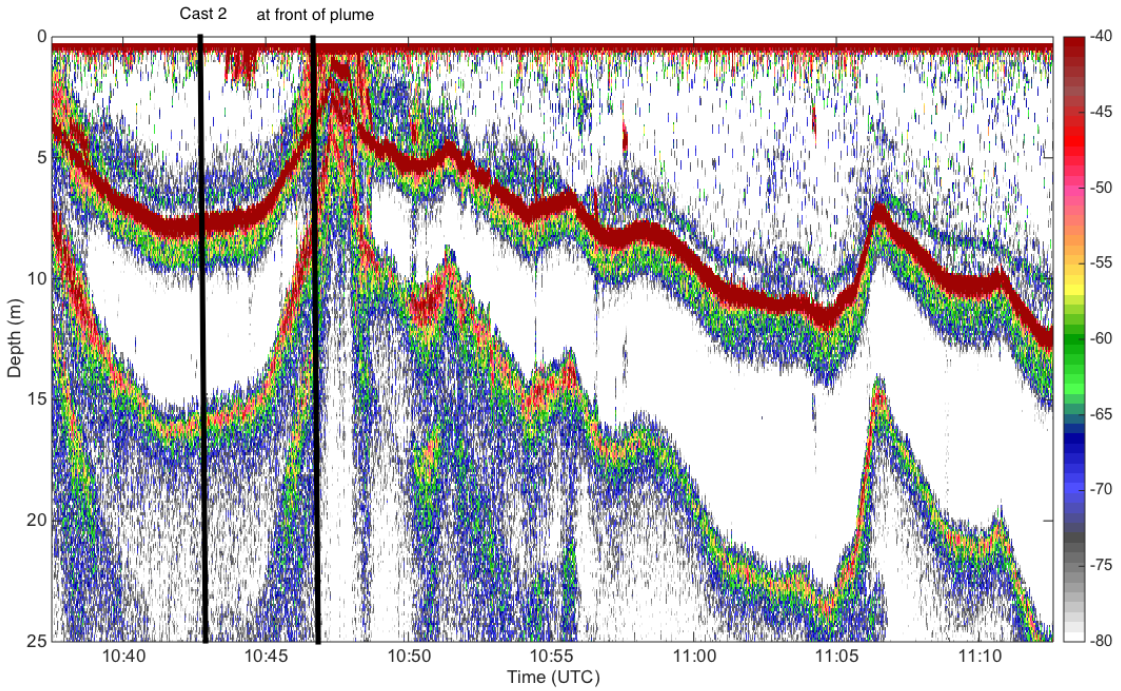
Cast 2
at front of plume
Depth (m)
Time (UTC)
10:40
10:45
10:50
10:55
11:00
11:05
11:10

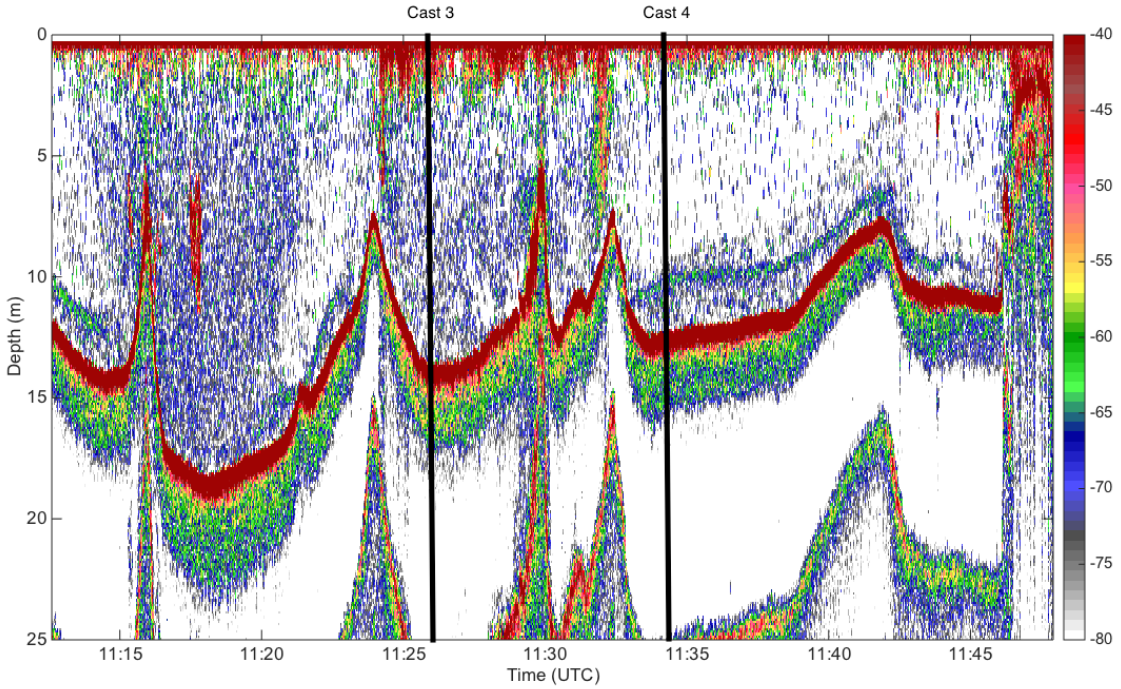
Cast 3
Cast 4
Depth (m)
Time (UTC)
11:15
11:20
11:25
11:30
11:35
11:40
11:45

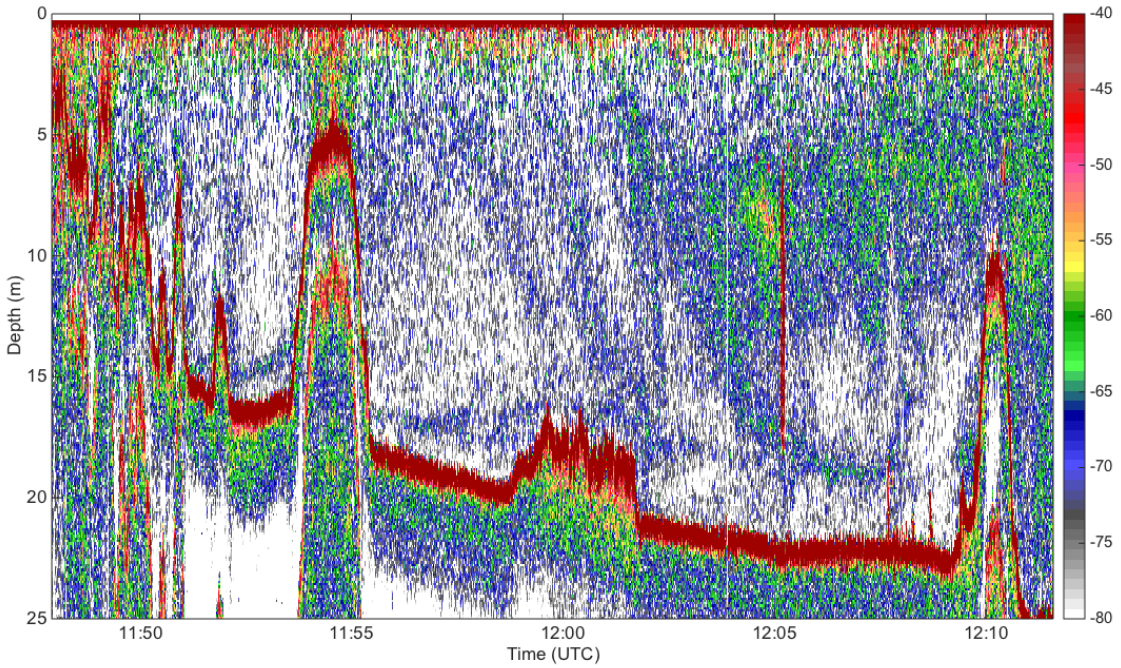

The CT cast had no pressure sensor. So the downcast of the profiles were extracted using density and are presented below. All casts except Cast 3 had a halocline near the bottom of the profile. This was consistent with our observations of the acoustic signal from the echosounder profiles (above).

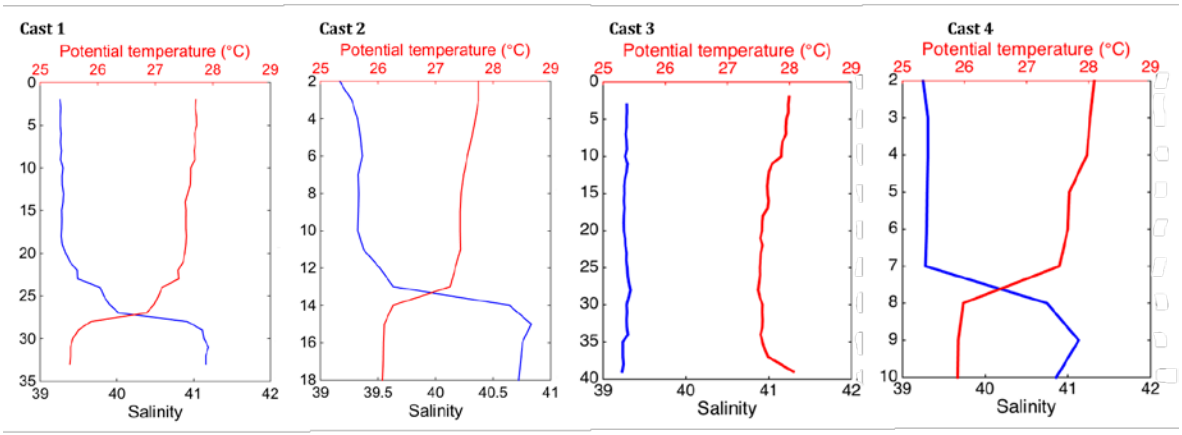

APPENDIX F: FILTERED SUSPENDED PARTICULATE MATTER

Water samples were filtered to measure the suspended particulate matter inside and near the aquaculture facility's outfall in Al-Lith. This effort was conducted on November 18, 2014, December 15, 2014, and January 31, 2015.

Date sampled	Station	Volume (L)	Depth (m)	SPM (µg/L)
11/18/14	P1	0.2	6.9	6480
11/18/14	P1	0.2	5	13050
11/18/14	P2	0.2	2.2	3905
11/18/14	P2	0.2	1	8690
11/18/14	P3	0.2	4.7	10375
11/18/14	P3	0.2	2	12670
11/18/14	P4	0.2	7	17635
11/18/14	P4	0.2	5	11600
11/18/14	P5	0.2	12.2	20000
11/18/14	P5	0.2	5	31135
11/18/14	P6	0.2	10.6	19365
11/18/14	P6	0.2	5	11275
11/18/14	P7	0.2	15.9	19525
11/18/14	P7	0.2	5	15610
11/18/14	P8	0.2	4.8	20030
11/18/14	P8	0.2	1	3225
12/15/14	P1	0.5	0.5	4246
12/15/14	P2	0.5	2	2374
12/15/14	P2	0.5	3	2168
12/15/14	P3	0.5	2	1978
12/15/14	P3	0.5	5.5	2398
12/15/14	P4	0.5	2	1908
12/15/14	P4	0.5	8	2086
12/15/14	P5	0.5	5	1864
12/15/14	P5	0.5		8000
12/15/14	P6	0.5	5	4572
12/15/14	P6	0.5		1914
12/15/14	P7	0.5	5	2262
12/15/14	P7	0.5	16.5	10198
12/15/14	P8	0.5	5	2204
12/15/14	P8	0.5	6.5	2666

12/15/14	P9	0.5	5	1382
12/15/14	P9	0.5	12.5	1302
12/15/14	P10	0.5	5	1088
12/15/14	P10	0.5	11	1832
12/15/14	P11	0.5	5	1924
12/15/14	P11	0.5	14	3394
1/31/15	NE	0.96	20.5	1271
1/31/15	P1	0.5	0.5	4604
1/31/15	P1	0.5	3.5	3394
1/31/15	P2	1	0.5	1232
1/31/15	P2	1	2.5	1470
1/31/15	P3	0.95	3	1607
1/31/15	P3	0.96	6	1706
1/31/15	P4	0.95	3	1306
1/31/15	P4	0.97	7	1099
1/31/15	P5	0.94	5	1219
1/31/15	P5	0.98	13.5	3003
1/31/15	P6	1	5	3978
1/31/15	P6	0.96	14	1451
1/31/15	P7	0.95	5	1088
1/31/15	P8	1	0.5	685
1/31/15	P8	0.9	7	1289
1/31/15	P9	1	5	1113
1/31/15	P9	1	12.5	2089
1/31/15	P10	0.99	5	675
1/31/15	P10	0.96	11	1799
1/31/15	P11	1	5	1026
1/31/15	P11	0.96	14	1503

There was no significant correlation between the filtered SPM measurements and the *in-situ* optical measurements of particulate beam attenuation coefficient (proxy for suspended particulate matter) (below). This could be due to the extremely low particle concentrations in the non-discharge waters that were on the lower limits of the instrument (LISST 100X) with 5 cm path length. In addition, the high particulate

load of the discharge saturated the upper limit of the instrument sensitivity and could have resulted in no observed correlation.

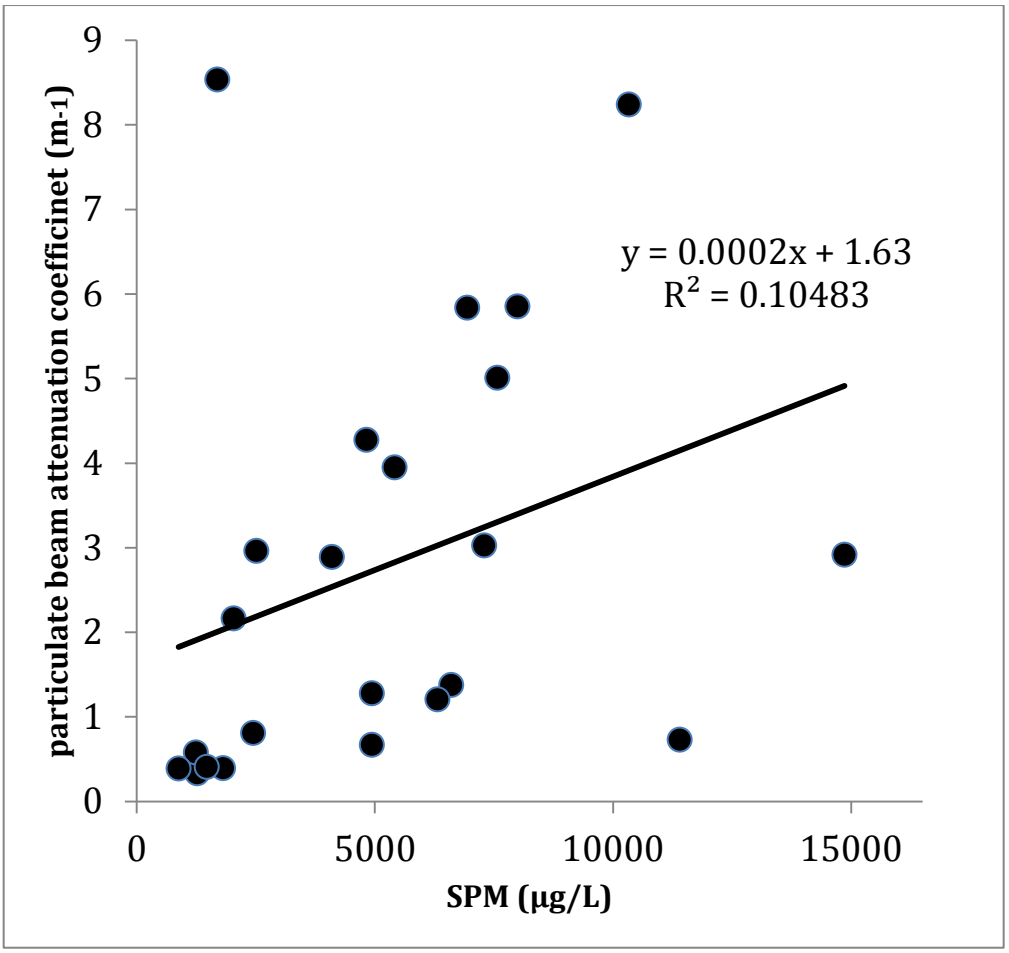

APPENDIX G: MICROBIAL ANALYSIS OTU

Cell counts from flow cytometry are presented below. The surface and bottom water at the outfall were significantly higher than the cell counts measured in other stations (*p*-value = <0.05 and <0.001, respectively).

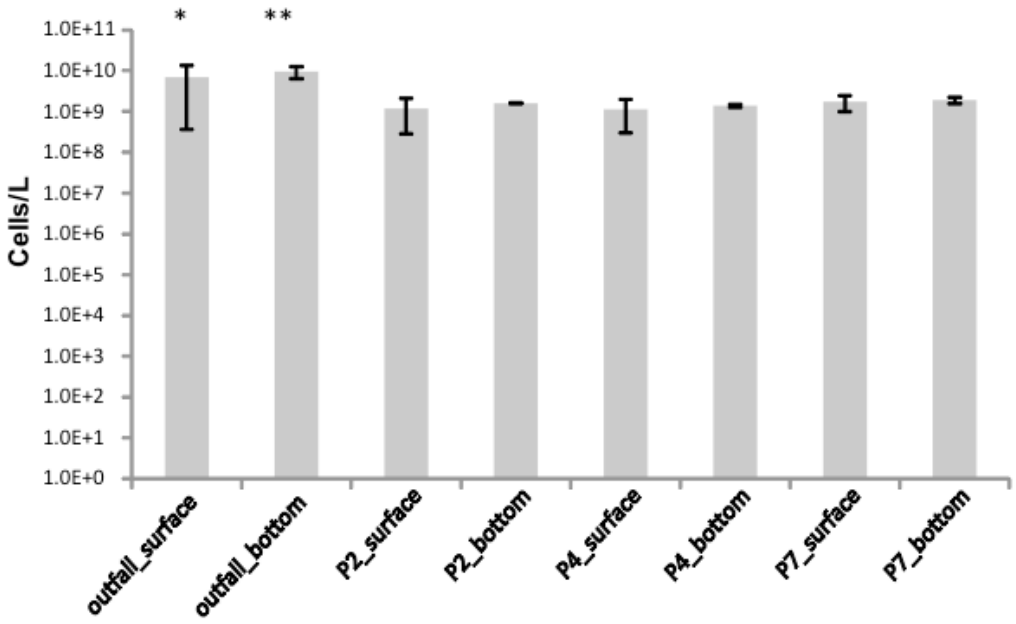

The total nitrogen measured for these samples reveal P1 had significantly higher total nitrogen than the other stations offshore from the outfall.

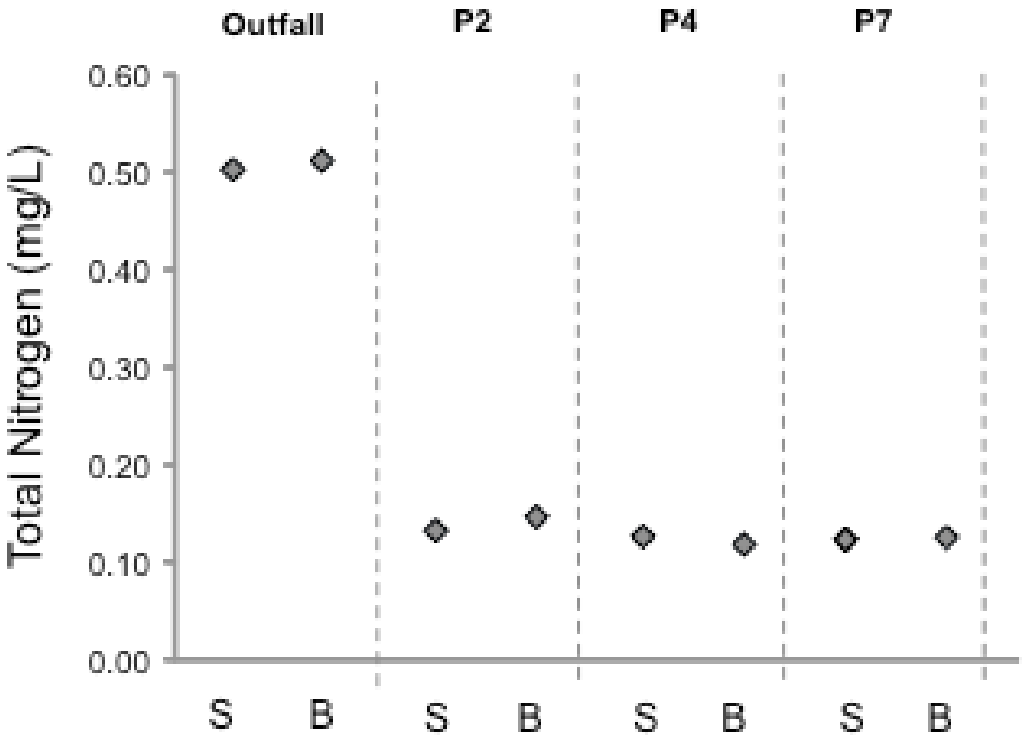
Outfall
P2
P4
P7
Total Nitrogen (mg/L)
0.60
0.50
0.40
0.30
0.20
0.10
0.00
S
B
S
B
S
B
S
B

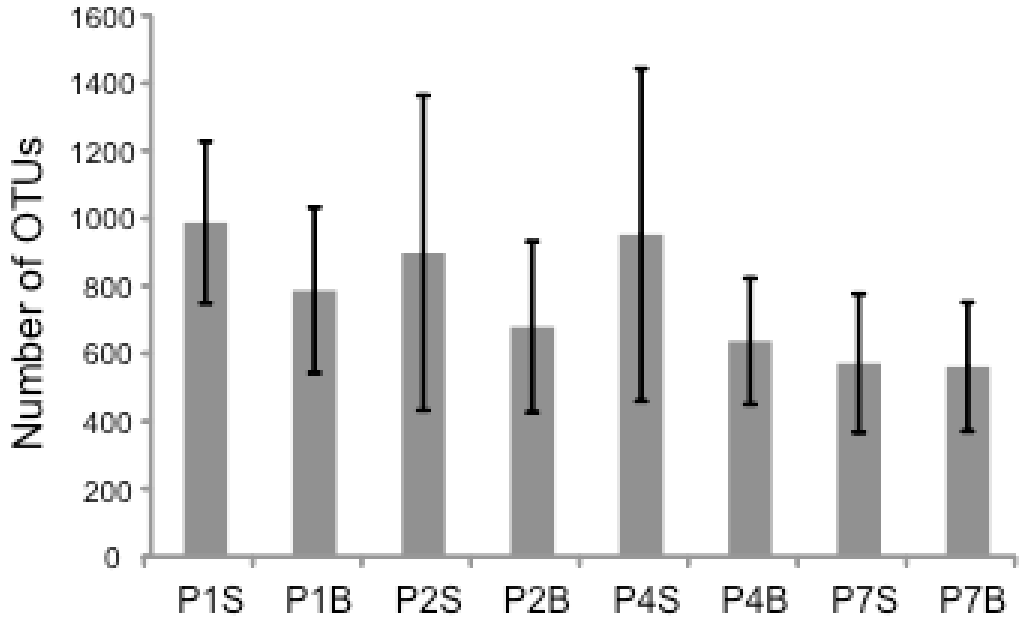
Number of OTUs
1600
1400
1200
1000
800
600
400
200
0
P1S
P1B
P2S
P2B
P4S
P4B
P7S
P7B

Tables listing OTUs present in the different stations (P1, P2, P4, P7) and the p-values for testing its relative abundance in the outfall (P1) compared to the other stations are included below. a) OTUs >29-fold relatively abundant in P1 than P7 and significantly higher than other (P2 and P4) stations are listed. b) OTUs with >0.5% relative abundance in P1 and >five-fold higher than P7 and significantly more abundant than other stations are listed. c) OTUs only present in P1 with >0.01% relative abundance are listed.

a)

OTUs present in abundance > 29-fold higher than P7, and significantly more abundant in outfall than all other locations

	P1	P2	P4	P7	*p*-value	Best-matched identities (Identity %, E-value)	
OTU1629	0.0059	0	0	0	0.04	*Gracilimonas rosea* (92%, 4e-168)	*Chitinophagaceae /Bacteroidetes*
OTU4378	0.0066	0.00067	0	0	0.03	*Candidatus Rhodoluna lacicola* (96%, 0)	*Microbacteriaceae /Actinobacteria*
OTU4936	0.013	0.00067	0.00044	0.00022	0.04	*Loktanella agnita* (96%, 3e-176)	*Proteobacteria*
OTU9436	0.0059	0	0	0	0.02	*Aquibacter zeaxanthinifaciens* or *Sediminicola luteus* (89%, 4e-136)	*Bacteroidetes*
OTU10068	0.0048	0	0	0	0.05	*Pseudomonas cremoricolorata* (93%, 4e-156)	*Proteobacteria*
OTU10308	0.0056	0	0.00020	0.00022	0.01	*Alkaliphilus sp.* (94%, 3e-170)	*Clostridiales/Firmicutes*

b)

OTUs present in > 0.5% relative abundance, and >five-fold higher abundance than P7, and significantly more abundant in P1 than other locations							
	P1	P2	P4	P7	*p*-value	Best-matched identities	
OTU133	1.0	0.21	0.11	0.14	0.0004	*Hydrotalea sandarakina* or *Solitalea koreensis* (86%, 5e-123)	*Chitinophagaceae /Bacteroidetes*
OTU2352	1.9	0.46	0.28	0.17	0.005	*Candidatus Aquiluna rubra* (98%, 0)	*Microbacteriaceae /Actinobacteria*
OTU2586	1.9	0.48	0.26	0.20	0.02	*Pontimonas salivibrio* (96%, 2e-179)	*Microbacteriaceae /Actinobacteria*
OTU2587	0.95	0.20	0.075	0.073	0.002	*Gracilimonas rosea* (90%, 4e-149)	*Chitinophagaceae /Bacteroidetes*
OTU3029	0.69	0.15	0.041	0.079	0.04	*Candidatus Aquiluna rubra* (97%, 0)	*Microbacteriaceae /Actinobacteria*
OTU3207	0.73	0.21	0.084	0.096s	0.0003	*Alteromonas sp.* (97%, 0)	*Proteobacteria*

c)

OTUs present only in P1 and > 0.01% relative abundance							
	P1	P2	P4	P7	*p*-value	Best-matched identities	
OTU252	0.020	0	0	0	0.35	*Ilumatobacter fluminis* (97%, 0)	*Acidimicrobiaceae /Actinobacteria*
OTU3886	0.014	0	0	0	0.28	*Calothrix desertica* (82%, 6e-103)	*Cyanobacteria*
OTU5565	0.036	0	0	0	0.34	*Crocinitomix catalasitica* (93%, 9e-164)	*Bacteroidetes*
OTU6285	0.012	0	0	0	0.27	*Sediminicola luteus* (89%, 1e-136)	*Bacteroidetes*
OTU7864	0.0092	0	0	0	0.19	*Lewinella persica* (84%, 3e-113)	*Bacteroidetes*

APPENDIX H: ZOOPLANKTON IDENTIFICATION FROM MULTINET VERTICAL NET SAMPLING

Zooplankton enumeration using microscopy revealed no vertical structure between the three depth cells sampled. Abundance (counts) of each identified species/genera/family is listed below. The replicate number of the cast is listed in the first column and the depth range sampled in the second column. Copepods were the most abundant in number.

Cast ID	Depth (m)	*Calanoid*	*Cyclopoid*	*Cyclopoid with eggs*	*Oithana (Cyclopoid)*	*Cyclopoid (veins)*	*Ocartie (calanoid)*	*Mollusca*	*Appendicularia (Chordata)*	*flatworm*	*Terapod*	*Chaetogonata*	*ghost shrimp*	*crab larvae*	*cirripodia*	*crustacean larvae*	*jelly*
C1	0-15	193	181	7	25	84	43	31	260	36	17	24	2	1	10	68	232
C2	0-15	487	117	3	26	210	43	26	605	21	27	28	8	8	7	170	4
C3	0-15	1648	286	3	40	503	82	73	1566	42	48	207	15	8	15	478	849
C1	15-25	681	1313	126	27	126	60	13	207	128	58	80	8	40	16	94	92
C2	15-25	293	98	2	15	18	61	13	209	18	12	15	3	2	1	27	67
C3	15-25	627	99	4	31	66	90	53	1029	25	44	84	14	12	15	159	312
C1	25-40	370	521	131	19	91	28	16	47	36	16	14	6	27	15	60	25
C2	25-40	1027	568	77	166	209	66	48	456	43	33	94	7	28	65	138	159
C3	25-40	373	122	7	26	48	61	17	345	25	11	39	3	14	36	62	51

Cast ID	Depth (m)	*protozoan radiolarlia*	*single egg*	*echinoderm*	*brachiopoda*	*polychaete*	*Ostracoda*	*fish larvae*	*Centropages (calanoid)*	*Chiridius (calanoid)*	*Microcalanus (calanoid)*	*Harpacticoid (copepod)*	*Harpacticoid (copepod)*	*Izapod*	*Megalopa (larvae)*	*Paracalanus*	*Onychocorycaeus*
C1	0-15	30	45	1	0	3	1	1	17	30	5	2	0	0	0	0	0
C2	0-15	76	69	4	6	11	10	4	18	28	2	1	2	1	0	0	8
C3	0-15	140	252	6	32	47	6	9	28	118	1	4	0	4	0	0	0
C1	15-25	72	8	2	4	5	2	5	8	22	1	0	0	0	0	0	0
C2	15-25	10	8	0	0	0	19	4	3	7	0	2	0	0	0	0	0
C3	15-25	98	48	4	0	16	44	13	5	22	4	0	0	0	0	0	0
C1	25-40	7	3	0	0	0	0	0	0	0	0	0	0	0	0	0	0
C2	25-40	171	9	0	0	3	93	6	3	96	19	2	0	1	1	0	0
C3	25-40	18	12	0	0	1	34	2	2	46	12	1	0	0	0	1	0

REFERENCES

Abal, E., & Dennison, W. (1996). Seagrass depth range and water quality in southern Moreton Bay, Queensland, Australia . *Marine and Freshwater Research*, *47*, 763. doi:10.1071/MF9960763

Acker, J., Leptoukh, G., Shen, S., Zhu, T., & Kempler, S. (2008). Remotely-sensed chlorophyll a observations of the northern Red Sea indicate seasonal variability and influence of coastal reefs. *Journal of Marine Systems*, *69*, 191–204. doi:10.1016/j.jmarsys.2005.12.006

Al-Hashmi, K. A., Sarma, Y. V. B., Claereboudt, M., Al-Azri, A. R., Piontkovski, S. A., & Al-Habsi, H. (2012). Phytoplankton Community Structure in the Bay of Bandar Khyran, Sea of Oman with Special Reference to Harmful Algae. *International Journal of Marine Science*, *2*(5), 31–42. doi:10.5376/ijms.2012.02.0005

Al Lith Monthly Climate Average, Saudi Arabia. (n.d.). Retrieved November 2, 2015, from http://www.worldweatheronline.com/Al-Lith-weather-averages/Makkah/SA.aspx

Ansari, M. I., Harb, M., Jones, B., & Hong, P.-Y. (2015). Molecular-based approaches to characterize coastal microbial community and their potential relation to the trophic state of Red Sea. *Scientific Reports*, *5*, 9001. doi:10.1038/srep09001

Aronson, R. B., & Precht, W. F. (1995). Landscape patterns of reef coral diversity: a test of the intermediate disturbance hypothesis. *Journal of Experimental Marine Biology and Ecology*, *192*(1), 1–14. doi:10.1016/0022-0981(95)00052-S

Axenrot, T., Didrikas, T., Danielsson, C., & Hansson, S. (2004). Diel patterns in pelagic fish behaviour and distribution observed from a stationary, bottom-mounted, and upward-facing transducer. *ICES Journal of Marine Science*, *61*, 1100–1104. doi:10.1016/j.icesjms.2004.07.006

Baria, M. V. B., Kurihara, H., & Harii, S. (2015). Tolerance to Elevated Temperature and Ocean Acidification of the Larvae of the Solitary Corals Fungia fungites (Linnaues, 1758) and Lithophyllon repanda (Dana, 1846). Zoological science, 32(5), 447-454.

Basaham, a., Rifaat, a., El-Mamoney, M., & El-Sayed, M. (2009). Re-Evaluation of the Impact of Sewage Disposal on Coastal Sediments of the Southern Corniche, Jeddah, Saudi Arabia. *Journal of King Abdulaziz University-Marine Sciences*, *20*(1), 109–126. doi:10.4197/Mar.20-1.8

Berrendero, E., Perona, E., & Mateo, P. (2011). Phenotypic variability and phylogenetic relationships of the genera Tolypothrix and Calothrix (Nostocales, Cyanobacteria) from running water. *International Journal of Systematic and Evolutionary Microbiology*, *61*(12), 3039–3051. doi:10.1099/ijs.0.027581-0

Berumen, M. L., Braun, C. D., Cochran, J. E. M., Skomal, G. B., & Thorrold, S. R. (2014). Movement patterns of juvenile whale sharks tagged at an aggregation site in the Red Sea. *PloS One*, *9*(7), e103536. doi:10.1371/journal.pone.0103536

Berumen, M. L., Hoey, A. S., Bass, W. H., Bouwmeester, J., Catania, D., Cochran, J. E. M., … Saenz-Agudelo, P. (2013). The status of coral reef ecology research in the Red Sea. *Coral Reefs*. doi:10.1007/s00338-013-1055-8

Boss, E., Guidi, L., Richardson, M. J., Stemmann, L., Gardner, W., Bishop, J. K. B., … Sherrell, R. M. (2015). Optical techniques for remote and in-situ characterization of particles pertinent to GEOTRACES. *Progress in Oceanography*, *133*, 43–54. doi:10.1016/j.pocean.2014.09.007

Bosworth, W., Huchon, P., & McClay, K. (2005). The Red Sea and Gulf of Aden Basins. *Journal of African Earth Sciences*, *43*, 334–378. doi:10.1016/j.jafrearsci.2005.07.020

Bowman, J. P., Nichols, C. M., & Gibson, J. a E. (2003). Algoriphagus ratkowskyi gen. nov., sp. nov., Brumimicrobium glaciale gen. nov., sp. nov., Cryomorpha ignava gen. nov., sp. nov. and Crocinitomix catalasitica gen. nov., sp. nov., novel flavobacteria isolated from various polar habitats. *International Journal of Systematic and Evolutionary Microbiology*, *53*(5), 1343–1355. doi:10.1099/ijs.0.02553-0

Braun, C. D. (2013). *Movement Ecology of the Reef Manta Ray Manta alfredi in the Eastern Red Sea*.

Braun, C. D., Skomal, G. B., Thorrold, S. R., & Berumen, M. L. (2014). Diving Behavior of the Reef Manta Ray Links Coral Reefs with Adjacent Deep Pelagic Habitats. *PLoS ONE*, *9*(2), e88170. doi:10.1371/journal.pone.0088170

Braun, C. D., G.B. Skomal, S. R. Thorrold, & Berumen, M. L. (in press) Movements of the reef manta ray (Manta alfredi) in the Red Sea using satellite and acoustic telemetry. Accepted to Marine Biology Oct 2015.

Brügmann, L., & Kremling, K. (2007). Sampling. *Methods of Seawater Analysis*, 1–25. doi:10.1002/9783527613984.ch1

Brunnschweiler, J., & Sims, D. (2011). Diel oscillations in whale shark vertical movements associated with meso-and bathypelagic diving. *American Fisheries Society Symposium*, *76*, 457–469. Retrieved from http://www.pescecane.ch/Projects/Publications/2011-Brunnschweiler-Sims.pdf

Burford, M. a., Costanzo, S. D., Dennison, W. C., Jackson, C. J., Jones, a. B., McKinnon, a. D., … Trott, L. a. (2003). A synthesis of dominant ecological processes in intensive shrimp ponds and adjacent coastal environments in NE Australia. *Marine Pollution Bulletin*, *46*, 1456–1469. doi:10.1016/S0025-326X(03)00282-0

Burks, C. M., & Mullin, K. D. (2006). Abundance and distribution of whale sharks (Rhincodon typus) in the northern Gulf of Mexico. *Fishery Bulletin*, *104*, 579–584. Retrieved from http://scholar.google.com/scholar?hl=en&btnG=Search&q=intitle:Abundance+and+distribution+of+whale+sharks+(Rhincodon+typus)+in+the+northern+Gulf+of+Mexico#3

Cagua, E. F., Berumen, M. L., & Tyler, E. H. M. (2013). Topography and biological noise determine acoustic detectability on coral reefs. *Coral Reefs*, *32*(4), 1123–1134. doi:10.1007/s00338-013-1069-2

Cagua, E. F., Cochran, J. E. M., Rohner, C. a, Prebble, C. E. M., Sinclair-Taylor, T. H., Pierce, S. J., & Berumen, M. L. (2015). Acoustic telemetry reveals cryptic residency of whale sharks. *Biology Letters*, *11*(4), 20150092–. doi:10.1098/rsbl.2015.0092

Cantin, N. E., Cohen, A. L., Karnauskas, K. B., Tarrant, A. M., & McCorkle, D. C. (2010). Ocean warming slows coral growth in the central Red Sea. *Science (New York, N.Y.)*, *329*(2010), 322–325. doi:10.1126/science.1190182

Cárdenas-Palomo, N., Herrera-Silveira, J., Velázquez-Abunader, I., Reyes, O., & Ordoñez, U. (2014). Distribution and feeding habitat characterization of whale sharks Rhincodon typus in a protected area in the north Caribbean Sea. *Journal of Fish Biology*, 1–19. doi:10.1111/jfb.12589

Cetinić, I., Toro-Farmer, G., Ragan, M., Oberg, C., & Jones, B. H. (2009). Calibration procedure for Slocum glider deployed optical instruments. *Optics Express*, *17*(18), 15420–15430. doi:10.1364/OE.17.015420

Chen, C., Li, R., Pratt, L., Limeburner, R., Beardsley, R. C., Bower, A., … Kim, T. (2014). Process modeling studies of physical mechanisms of the formation of an anticyclonic eddy in the central Red Sea. *Journal of Geophysical Research: Oceans*, *119*(2), 1445–1464. doi:10.1002/2013JC009351

Chen, V. Y., & Phipps, M. J. (2002). *Management and Trade of Whale Sharks in Taiwan*. *Traffic East Asia Report*.

Chen, Y., Mills, S., Street, J., Golan, D., Post, A., Jacobson, M., & Paytan, A. (2007). Estimates of atmospheric dry deposition and associated input of nutrients to Gulf of Aqaba seawater. *Journal of Geophysical Research*, *112*(D4), D04309. doi:10.1029/2006JD007858

Cho, Y., Chung, H., Jang, G. Il, Choi, D. H., Noh, J. H., & Cho, B. C. (2013). Gracilimonas rosea sp. nov., isolated from tropical seawater, and emended description of the genus Gracilimonas. *International Journal of Systematic and Evolutionary Microbiology*, *63*(PART 11), 4006–4011. doi:10.1099/ijs.0.052340-0

Christen, R., & Ivanova, E. P. (2004). Phylogenetic relationships among marine Alteromonas -like proteobacteria : emended description of the family Alteromonadaceae and proposal of Pseudoalteromonadaceae fam . nov ., Colwelliaceae fam . nov ., Shewanellaceae fam ., 1773–1788.

doi:10.1099/ijs.0.02997-0

Churchill, J. H., Bower, A. S., Mccorkle, D. C., & Abualnaja, Y. (2014). The transport of nutrient-rich Indian Ocean water through the Red Sea and into coastal reef systems. *Journal of Marine Research*, *72*, 165–181.

Clark, E., & Nelson, D. R. (1997). Young whale sharks, Rhincodon typus, feeding on a copepod bloom near La Paz, Mexico. *Environmental Biology of Fishes*, *50*, 63–73. doi:10.1023/A:1007312310127

Claustre, H., Hooker, S. B., Van Heukelem, L., Berthon, J.-F., Barlow, R., Ras, J., … Marty, J.-C. (2004). An intercomparison of HPLC phytoplankton pigment methods using in situ samples: application to remote sensing and database activities. *Marine Chemistry*, *85*(1-2), 41–61. doi:10.1016/j.marchem.2003.09.002

Clifford, M., Horton, C., & Schmitz, J. (1997). An oceanographic nowcast / forecast system for the Red Sea Depth ", m, *102*(Cll).

Cochran, J. E. M. (2014). *Characterization of Novel Whale Shark Aggregations at Shib Habil, Saudi Arabia and Mafia Island, Tanzania*.

Coles, S. L. (1988). Limitations on Reef Coral Development in the Arabian Gulf: Temperature or Algal Competition? *Proceedings of the 6th International CoralReef Symposium, Australia, 1988, Vol. 3*, *3*, 211–216.

Coles, S. L. (2003). Coral species diversity and environmental factors in the Arabian Gulf and the Gulf of Oman: A comparison to the Indo-Pacific region. *Atoll Research Bulletin*, (497-508), 1–19. doi:10.5479/si.00775630.507.1

Colman, J. G. (1997). A review of the biology and ecology of the whale shark. *Journal of Fish Biology*, *51*, 1219–1234.

Compagno, L. J. V. (1984). FAO Species Catalogue. Vol. 4, Sharks of the world. An annotated and illustrated catalogue of shark species known to date. Part 1—Hexanchiformes to Lamniformes. *FAO Fisheries Synopsis*, *125*, 209–211.

Compagno, L. J. V. (2001). Sharks of the World. An annotated and illustrated catalogue of Shark species known to date - Volume 2. Bullhead, mackerel and carpet sharks (Heterodontformes, Lamniformes and Orectolobiformes). *FAO Species Catalogue for Fishery Purposes*, *2*(1), 269. doi:10.1071/MF9920109

Cromwell, D., & Smeed, D. A. (1998). Altimetric observations of sea level cycles near the Strait of Bab al Mandab. *International Journal of Remote Sensing*, *19*(8), 1561–1578.

Dandonneau, Y., Menkes, C., Duteil, O., & Gorgues, T. (2008). Concentration of floating biogenic material in convergence zones. *Journal of Marine Systems*, *69*, 226–232. doi:10.1016/j.jmarsys.2006.02.016

DiBattista, J. D., Berumen, M. L., Gaither, M. R., Rocha, L. A., Eble, J. A., Choat, J. H., … Bowen, B. W. (2013). After continents divide: comparative phylogeography of

reef fishes from the Red Sea and Indian Ocean. *Journal of Biogeography*, *40*(6), 1170–1181. doi:10.1111/jbi.12068

DiBattista, J.D., Choat, J.H., Gaither, M.R., Hobbs, J.P., Lozano-Cortés, D.F., Myers, R.F., Paulay, G., Rocha, L.A., Toonen, R.J., Westneat, M., and Berumen, M.L. (2015a) On the origin of endemic species in the Red Sea. Journal of Biogeography. doi:10.1111/JBI.12631.

DiBattista, J.D., Roberts, M., Bouwmeester, J., Bowen, B.W., Coker, D.F., Lozano-Cortés, D.F., Choat, J.H., Gaither, M.R., Hobbs, J.P., Khalil, M., Kochzius, M., Myers, R., Paulay, G., Robitzch, V., Saenz-Agudelo, P., Salas, E., Sinclair-Taylor, T.H., Toonen, R.J., Westneat, M., Williams, S., and Berumen, M.L. (2015b) A review of contemporary patterns of endemism for shallow water reef fauna in the Red Sea. Journal of Biogeography. doi:10.1111/JBI.12649.

Dove, A. D. M. (2015). Foraging and Ingestive Behaviors of Whale Sharks , Rhincodon typus , in Response to Chemical Stimulus Cues. *Biological Bulletin*, (228), 65–74.

Duffy, C. A. J. (2002). New Zealand Journal of Marine and Freshwater Research feeding behaviour of whale sharks (Rhincodon typus) observed in New Zealand waters. *New Zealand Journal of Marine and Freshwater Research*, *36*(3), 565–570.

Fong, D. a, & Jones, N. L. (2006). Evaluation of AUV-based ADCP measurements. *Limnology and Oceanography: Methods*, *4*(2005), 58–67. doi:10.4319/lom.2006.4.58

Foote, K. G. (1980). Importance of the swimbladder in acoustic scattering by fish: A comparison of gadoid and mackerel target strengths. *Journal of Acoustical Society of America*, *67*(6), 2084–2089.

Foote, K. G., Everson, I., Watkins, J. L., & Bone, D. G. (1990). Target strengths of Antarctic krill (Euphausia superba) at 38 and 120 kHz. *The Journal of the Acoustical Society of America*, *87*(1), 16–24. doi:10.1121/1.2027195

Franks, P. (1992). Sink or swim: accumulation of biomass at fronts. *Marine Ecology Progress Series*, *82*, 1–12. doi:10.3354/meps082001

Freedman, J. a, & Noakes, D. L. G. (2002). Why are there no really big bony fishes? A point-of-view on maximum body size in teleosts and elasmobranchs. *Reviews in Fish Biology and Fisheries*, *12*(4), 403–416. doi:10.1023/A:1025365210414

Froukh, T., & Kochzius, M. (2007). Genetic population structure of the endemic fourline wrasse (Larabicus quadrilineatus) suggests limited larval dispersal distances in the Red Sea. *Molecular Ecology*, *16*(7), 1359–1367. doi:10.1111/j.1365-294X.2007.03236.x

Frouzova, J., & Kubecka, J. (2004). Changes of acoustic target strength during juvenile perch development. *Fisheries Research*, *66*(2-3), 355–361.

doi:10.1016/S0165-7836(03)00182-6

Furby, K. a., Apprill, a., Cervino, J. M., Ossolinski, J. E., & Hughen, K. a. (2014). Incidence of lesions on fungiidae corals in the eastern Red Sea is related to water temperature and coastal pollution. *Marine Environmental Research*, *98*, 29–38. doi:10.1016/j.marenvres.2014.04.002

Genin, A., Jaffe, J. S., Reef, R., Richter, C., & Franks, P. J. S. (2005). Swimming Against the Flow : A Mechanism of Zooplankton Aggregation. *Science*, *308*, 860–862.

Giles, E. C., Saenz-Agudelo, P., Hussey, N. E., Ravasi, T., & Berumen, M. L. (2015). Exploring seascape genetics and kinship in the reef sponge *Stylissa carteri* in the Red Sea. *Ecology and Evolution*, n/a–n/a. doi:10.1002/ece3.1511

Gladstone, W., Tawfiq, N., Nasr, D., Andersen, I., Cheung, C., Drammeh, H., … Lintner, S. (1999). Sustainable use of renewable resources and conservation in the Red Sea and Gulf of Aden: Issues, needs and strategic actions. *Ocean and Coastal Management*, *42*(8), 671–697. doi:10.1016/S0964-5691(99)00040-X

Glibert, P. M., Trice, T. M., Michael, B., & Lane, L. (2005). Urea in the tributaries of the Chesapeake and coastal Bays of Maryland. *Water, Air, and Soil Pollution*, *160*(1-4), 229–243. doi:10.1007/s11270-005-2546-1

Godø, O. R., Samuelsen, A., Macaulay, G. J., Patel, R., Hjøllo, S. S., Horne, J., … Johannessen, J. a. (2012). Mesoscale eddies are oases for higher trophic marine life. *PloS One*, *7*(1), e30161. doi:10.1371/journal.pone.0030161

Graham, R. T., Roberts, C. M., & Smart, J. C. R. (2006). Diving behaviour of whale sharks in relation to a predictable food pulse. *Journal of the Royal Society, Interface / the Royal Society*, *3*(April 2005), 109–116. doi:10.1098/rsif.2005.0082

Gudger, E. W. (1940). Whale sharks rammed by ocean vessels: How these sluggish leviathans aid in their own destruction. *The New England Naturalist*, *7*, 1–10.

Hahn, M. W. (2009). Description of seven candidate species affiliated with the phylum Actinobacteria, representing planktonic freshwater bacteria. *International Journal of Systematic and Evolutionary Microbiology*, *59*(1), 112–117. doi:10.1099/ijs.0.001743-0

Hahn, M. W., Schmidt, J., Taipale, S. J., Doolittle, W. F., & Koll, U. (2014). Rhodoluna lacicola gen. nov., sp. nov., a planktonic freshwater bacterium with stream-lined genome. *International Journal of Systematic and Evolutionary Microbiology*, 3254–3263. doi:10.1099/ijs.0.065292-0

Hay, M. E. (2009). Marine Chemical Ecology: Chemical Signals and Cues Structure Marine Populations, Communities, and Ecosystems. *Annual Review of Marine Science*, *1*, 193–212. doi:10.1016/j.biotechadv.2011.08.021.Secreted

Heyman, W. D., Graham, R. T., Kjerfve, B., & Johannes, R. E. (2001). Whale sharks Rhincodon typus aggregate to feed on fish spawn in Belize. *Marine Ecology Progress Series*, *215*, 275–282. doi:10.3354/meps215275

Hoffmayer, E., & Franks, J. (2007). Observations of a feeding aggregation of whale sharks, Rhincodon typus, in the north central Gulf of Mexico. *Gulf and Caribbean Research*, *19*(June 2006), 69–73.

Hughes, T. P., Graham, N. A. J., Jackson, J. B. C., Mumby, P. J., & Steneck, R. S. (2010). Rising to the challenge of sustaining coral reef resilience. *Trends in Ecology & Evolution*, *25*(11), 633–642. doi:10.1016/j.tree.2010.07.011

Ivanova, E. P., Zhukova, N. V., Lysenko, A. M., Gorshkova, N. M., Sergeev, A. F., Mikhailov, V. V., & Bowman, J. P. (2005). Loktanella agnita sp. nov. and Loktanella rosea sp. nov., from the north-west Pacific Ocean. *International Journal of Systematic and Evolutionary Microbiology*, *55*(5), 2203–2207. doi:10.1099/ijs.0.63461-0

Iwasaki, Y. (1970). On the distribution and environment of the whale shark, Rhincodon typus, in skipjack fishing grounds in the western Pacific Ocean. *Journal of the College of Marine Science and Technology, Tokai University*, *4*, 37–51. Retrieved from http://scholar.google.com/scholar?hl=en&btnG=Search&q=intitle:On+the+Distribution+and+Environment+of+the+Whale+Shark,+Rhincodon+typus,+in+Skipjack+Fishing+Grounds+in+the+Western+Pacific+Ocean#0

Jackson, C., Preston, N., & Thompson, P. J. (2004). Intake and discharge nutrient loads at three intensive shrimp farms. *Aquaculture Research*, *35*(11), 1053–1061. doi:10.1111/j.1365-2109.2004.01115.x

Jang, G. I., Cho, Y., & Cho, B. C. (2013). Pontimonas salivibrio gen. nov., sp. nov., a new member of the family Microbacteriaceae isolated from a seawater reservoir of a solar saltern. *International Journal of Systematic and Evolutionary Microbiology*, *63*(PART6), 2124–2131. doi:10.1099/ijs.0.043661-0

Jiang, H., Farrar, J. T., Beardsley, R. C., Chen, R., & Chen, C. (2009). Zonal surface wind jets across the Red Sea due to mountain gap forcing along both sides of the Red Sea. *Geophysical Research Letters*, *36*(19), L19605. doi:10.1029/2009GL040008

Joung, S., Chen, C., Clark, E., Uchida, S., & Huang, W. Y. P. (1996). The whale shark, Rhincodon typus, is a livebearer: 300 embryos found in one ?megamamma? supreme. *Environmental Biology of Fishes*, *46*(3), 219–223. doi:10.1007/BF00004997

Khan, S. T., Fukunaga, Y., Nakagawa, Y., & Harayama, S. (2007). Emended descriptions of the genus Lewinella and of Lewinella cohaerens, Lewinella nigricans and Lewinella persica, and description of Lewinella lutea sp. nov. and Lewinella marina sp. nov. *International Journal of Systematic and Evolutionary Microbiology*, *57*(12), 2946–2951. doi:10.1099/ijs.0.65308-0

Kheireddine, M., & Antoine, D. (2014). Diel variability of the beamattenuation and backscattering coefficients in the northwestern Mediterranean Sea (BOUSSOLE site). *Journal of Geophysical Research: Oceans*, *119*(doi:10.1002/2014JC010007.). doi:10.1002/2014JC010007.Received

Kotb, M., Abdulaziz, M., Al-Agwan, Z., Al-Shaikh, K., Al-Yami, H., Banajah, A., … Zajonz, U. (2004). Status of coral reefs in the Red Sea and Gulf of Aden in 2004. In *Status of Coral Reefs of the World: 2004* (pp. 137–154). Retrieved from http://www.researchgate.net/publication/230751435_Status_of_coral_reefs_in_the_Red_Sea_and_Gulf_of_Aden_in_2004/file/79e415083e0f9c5658.pdf

Kringel, K., Jumars, P. a., & Holliday, D. V. (2003). A shallow scattering layer: High-resolution acoustic analysis of nocturnal vertical migration from the seabed. *Limnology and Oceanography*, *48*(3), 1223–1234. doi:10.4319/lo.2003.48.3.1223

Kürten, B., Al-Aidaroos, A. M., Struck, U., Khomayis, H. S., Gharbawi, W. Y., & Sommer, U. (2014). Influence of environmental gradients on C and N stable isotope ratios in coral reef biota of the Red Sea, Saudi Arabia. *Journal of Sea Research*, *85*, 379–394. doi:10.1016/j.seares.2013.07.008

Kürten, B., Khomayis, H. S., Devassy, R., Audritz, S., Sommer, U., Struck, U., … Al-Aidaroos, A. M. (2014). Ecohydrographic constraints on biodiversity and distribution of phytoplankton and zooplankton in coral reefs of the Red Sea , Saudi Arabia. *Marine Ecology*, 1–20. doi:10.1111/maec.12224

Levik, A., & Hovem, J. M. (1979). An experimental investigation of swimbladder resonance in fishes. *Journal of Acoustical Society of America*, *66*(3), 850–854.

Levitus, S., 1982: Climatological Atlas of the World Ocean. NOAA Professional Paper No. 13, U.S. GPO, Washington, D.C.

Maillard, C., & Soliman, G. (1986). Hydrography of the Red-Sea and exchanges with the Indian-Ocean in summer. *Oceanologica Acta*, *9*, 249–269. Retrieved from http://archimer.ifremer.fr/doc/00110/22113/19751.pdf

Martin, R. A. (2007). A review of behavioural ecology of whale sharks (Rhincodon typus). *Fisheries Research*, *84*, 10–16. doi:10.1016/j.fishres.2006.11.010

McClatchie, S., Alsop, J., & Coombs, R. F. (1996). A re-evaluation of relationships between fish size, acoustic frequency, and target strength. *ICES Journal of Marine Science*, *53*, 780–791. doi:10.1006/jmsc.1996.0099

McCook, L., Jompa, J., & Diaz-Pulido, G. (2001). Competition between corals and algae on coral reefs: a review of evidence and mechanisms. *Coral Reefs*, *19*(4), 400–417. doi:10.1007/s003380000129

McDougall, T. J. & Barker, P. M.. (2011). Getting started with TEOS-10 and the Gibbs Seawater (GSW) Oceanographic Toolbox, 28pp., SCOR/IAPSO WG127, ISBN 978-0-646-55621-5.

Motta, P. J., Maslanka, M., Hueter, R. E., Davis, R. L., de la Parra, R., Mulvany, S. L., … Zeigler, L. D. (2010). Feeding anatomy, filter-feeding rate, and diet of whale sharks Rhincodon typus during surface ram filter feeding off the Yucatan

Peninsula, Mexico. *Zoology*, *113*(4), 199–212. doi:10.1016/j.zool.2009.12.001

Nagelkerken, I., Roberts, C. M., Velde, G. Van Der, Dorenbosch, M., Riel, M. C. Van, Cocheret de la Moriniere, E., & Nienhuis, P. H. (2002). How important are mangroves and seagrass beds for coral-reef fish? The nursery hypothesis tested on an island scale. *Marine Ecology Progress Series*, *244*, 299–305.

Nanninga, G. B., Saenz-Agudelo, P., Manica, A., & Berumen, M. L. (2014). Environmental gradients predict the genetic population structure of a coral reef fish in the Red Sea. *Molecular Ecology*, *23*(3), 591–602. doi:10.1111/mec.12623

NASA Ocean Biology (OB). Sea-viewing Wide Field-of-view Sensor (SeaWiFS) Ocean Color Data, 2014.0 Reprocessing. NASA OB.DAAC, Greenbelt, MD, USA. doi: 10.5067/ORBVIEW-2/SEAWIFS_OC.2014.0. Accessed 2015/07/09. Maintained by NASA Ocean Biology Distibuted Active Archive Center (OB.DAAC), Goddard Space Flight Center, Greenbelt MD.

Ohlmann, J. C. (2011). Drifter Observations of Small-scale Flows in the Philippine Archipelago. *Oceanography*, *24*(1), 122–129.

Ohman, M. D., Frost, B. W., & Cohen, E. B. (1983). Reverse diel vertical migration: an escape from invertebrate predators. *Science (New York, N.Y.)*. doi:10.1126/science.220.4604.1404

Pade, N. G., Queiroz, N., Humphries, N. E., Witt, M. J., Jones, C. S., Noble, L. R., & Sims, D. W. (2009). First results from satellite-linked archival tagging of porbeagle shark, Lamna nasus: Area fidelity, wider-scale movements and plasticity in diel depth changes. *Journal of Experimental Marine Biology and Ecology*, *370*, 64–74. doi:10.1016/j.jembe.2008.12.002

PÁez-Osuna, F. (2001). The environmental impact of shrimp aquaculture: Causes, effects, and mitigating alternatives. *Environmental Management*, *28*(1), 131–140. doi:10.1007/s002670010212

Pastorok, R., & Bilyard, G. (1985). Effects of sewage pollution on coral-reef communities. *Marine Ecology Progress Series*, *21*, 175–189. doi:10.3354/meps021175

Patzert, W. C. (1974). Wind-induced reversal in Red Sea circulation. *Deep Sea Research and Oceanographic Abstracts*, *21*(September 1973), 109–121. doi:10.1016/0011-7471(74)90068-0

Pedgley, D. E. (1972). Desert depression over north-east Africa. *Meteorological Magazine*, *101*, 228–244.

Quadfasel, D., & Baudner, H. (1993). Gyre-scale circulation cells in the Red Sea. *Oceanologica Acta*, *16*(3), 221–229.

Racault, M., Raitsos, D. E., Berumen, M. L., Brewin, R. J. W., Platt, T., Sathyendranath, S., & Hoteit, I. (2015). Phytoplankton phenology indices in coral reef ecosystems: Application to ocean-color observations in the Red Sea. *Remote*

Sensing of Environment, *160*, 222–234. doi:10.1016/j.rse.2015.01.019

Raitsos, D. E., Pradhan, Y., Brewin, R. J. W., Stenchikov, G., & Hoteit, I. (2013). Remote Sensing the Phytoplankton Seasonal Succession of the Red Sea. *PLoS ONE*, *8*(6). doi:10.1371/journal.pone.0064909

Risk, M., Sherwood, O., Nairn, R., & Gibbons, C. (2009). Tracking the record of sewage discharge off Jeddah, Saudi Arabia, since 1950, using stable isotope records from antipatharians. *Marine Ecology Progress Series*, *397*, 219–226. doi:10.3354/meps08414

Roberts, C. M., Shepherd, A. R. D., & Ormond, R. F. G. (1992). Large-scale variation in assemblage structure of Red Sea butterflyfishes and angelfishes. *Journal of Biogeography*, *19*(3), 239–250. doi:10.2307/2845449

Roberts, D. a., Johnston, E. L., & Knott, N. a. (2010). Impacts of desalination plant discharges on the marine environment: A critical review of published studies. *Water Research*, *44*(18), 5117–5128. doi:10.1016/j.watres.2010.04.036

Robinson, D. P., Jaidah, M. Y., Jabado, R. W., Lee-Brooks, K., Nour El-Din, N. M., Al Malki, A. a, … Ormond, R. F. G. (2013). Whale sharks, Rhincodon typus, aggregate around offshore platforms in Qatari waters of the Arabian Gulf to feed on fish spawn. *PloS One*, *8*(3), e58255. doi:10.1371/journal.pone.0058255

Roesler, C. S. (2011). Calibration and Correction of the Chlorophyll Fluorometer on GoMOOS Buoy A01: Nov 2005 - Apr 2011. Boston: Massachusetts Water Resources Authority. Report 2011 - 15. 8 p.

Rohner, C. a, Armstrong, A. J., Pierce, S. J., Prebble, C. E. M., & Cagua, E. F. (2015). Whale sharks target dense prey patches of sergestid shrimp off Tanzania, *37*, 1–11. doi:10.1093/plankt/fbv010

Rowat, D., & Brooks, K. S. (2012). A review of the biology, fisheries and conservation of the whale shark Rhincodon typus. *Journal of Fish Biology*, *80*(5), 1019–56. doi:10.1111/j.1095-8649.2012.03252.x

Ryu, J. H., Choi, J. K., Eom, J., Ahn, J. H., & Samples, F. (2011). Temporal variation in Korean coastal waters using Geostationary Ocean Color Imager, (64), 1731–1735.

Savoca, M. S., & Nevitt, G. a. (2014). Evidence that dimethyl sulfide facilitates a tritrophic mutualism between marine primary producers and top predators. *Proceedings of the National Academy of Sciences of the United States of America*, *111*(11), 4157–61. doi:10.1073/pnas.1317120111

Sawall, Y., Al-sofyani, A., Kuerten, B., Al-Aidaroos, a. M., Hoang, B. X., Marimuthu, N., … Wahl, M. (2014). Coral Communities, in Contrast to Fish Communities, Maintain a High Assembly Similarity along the Large Latitudinal Gradient along the Saudi Red Sea Coast. *Journal of Ecosystem and Ecography*, *3*(4). doi:10.4172/2157-7625.S4-003

Scales, K. L., Miller, P. I., Embling, C. B., Ingram, S. N., Pirotta, E., Stephen, C., & Votier, S. C. (2014). Mesoscale fronts as foraging habitats : composite front mapping reveals oceanographic drivers of habitat use for a pelagic seabird Mesoscale fronts as foraging habitats : composite front mapping reveals oceanographic drivers of habitat use for a pelagic s.

Schaffelke, B., Mellors, J., & Duke, N. C. (2005). Water quality in the Great Barrier Reef region: Responses of mangrove, seagrass and macroalgal communities. *Marine Pollution Bulletin*, *51*(1-4), 279–296. doi:10.1016/j.marpolbul.2004.10.025

Schmidt, J. V., Chen, C. C., Sheikh, S. I., Meekan, M. G., Norman, B. M., & Joung, S. J. (2010). Paternity analysis in a litter of whale shark embryos. *Endangered Species Research*, *12*(2), 117–124. doi:10.3354/esr00300

Sequeira, A., Mellin, C., Rowat, D., Meekan, M. G., & Bradshaw, C. J. A. (2012). Ocean-scale prediction of whale shark distribution. *Diversity and Distributions*, *18*(5), 504–518. doi:10.1111/j.1472-4642.2011.00853.x

Sharif, A. (2008). Sewage lake threatens Jeddah. *The National*, p. www.thenational.ae/news/uae‐ news/environment/sewag.

Shepard, E. L. C., Wilson, R. P., Quintana, F., Gómez Laich, A., Liebsch, N., Albareda, D. A., … McDonald, D. W. (2008). Identification of animal movement patterns using tri-axial accelerometry. *Endangered Species Research*, *10*, 47–60. doi:10.3354/esr00084

Sheppard, C. R. C. (1988). Similar trends, different causes: Responses of Corals to Stressed Environments in Arabian Seas. *Proceedings of the 6th International CoralReef Symposium, Australia, 1988, Vol. 3*, 297–302.

Sims, D. W., Southall, E. J., Tarling, G. a., & Metcalfe, J. D. (2005). Habitat-specific normal and reverse diel vertical migration in the plankton-feeding basking shark. *Journal of Animal Ecology*, *74*, 755–761. doi:10.1111/j.1365-2656.2005.00971.x

Smeed, D. (1997). Seasonal variation of the flow in the strait of Bab al Mandab. *Oceanologica Acta*, *20*, 773–781. Retrieved from /home/siccha/Documents/Library/Smeed 1997.pdf

Smeed, D. A. (2004). Exchange through the Bab el Mandab. In *Deep-Sea Research Part II: Topical Studies in Oceanography* (Vol. 51, pp. 455–474). doi:10.1016/j.dsr2.2003.11.002

Smith, P. T. (1996). Physical and chemical characteristics of sediments from prawn farms and mangrove habitats on the Clarence River, Australia. *Aquaculture*, *146*, 47–83. doi:10.1016/S0044-8486(96)01361-0

Snider, D. M., & Andrews, M. J. (1994). Rayleigh-Taylor and shear driven mixing with an unstable thermal stratification. *Physics of Fluids*, *6*(10), 3324. doi:10.1063/1.868065

Sofianos, S. S., & Johns, W. E. (2001). Wind induced sea level variability in the Red Sea. *Geophysical Research Letters*, *28*(16), 3175–3178. doi:10.1029/2000GL012442

Sofianos, S. S., & Johns, W. E. (2003). An Oceanic General Circulation Model (OGCM) investigation of the Red Sea circulation: 2. Three-dimensional circulation in the Red Sea. *Journal of Geophysical Research*, *108*(C3), 3066. doi:10.1029/2001JC001185

Sofianos, S. S., & Johns, W. E. (2007). Observations of the summer Red Sea circulation. *Journal of Geophysical Research*, *112*(C6), C06025. doi:10.1029/2006JC003886

Sofianos, S. S., Johns, W. E., & Murray, S. P. (2002). Heat and freshwater budgets in the Red Sea from direct observations at Bab el Mandeb. *Deep-Sea Research Part II: Topical Studies in Oceanography*, *49*, 1323–1340. doi:10.1016/S0967-0645(01)00164-3

Spaet, J. L. Y., Jabado, R. W., Henderson, A. C., Moore, A. B. M., & Berumen, M. L. (2015). Population genetics of four heavily exploited shark species around the Arabian Peninsula. *Ecology and Evolution*, *5*(12), 2317–32. doi:10.1002/ece3.1515

Stevens, J. D. (2007). Whale shark (Rhincodon typus) biology and ecology: A review of the primary literature. *Fisheries Research*, *84*(1), 4–9. doi:10.1016/j.fishres.2006.11.008

Szmant, A. M. (2002). Nutrient enrichment on coral reefs: Is it a major cause of coral reef decline? *Estuaries*, *25*(4), 743–766. doi:10.1007/BF02804903

Takai, K., Moser, D. P., Onstott, T. C., Spoelstra, N., Pfiffner, S. M., Dohnalkova, A., & Fredrickson, J. K. (2001). an extremely alkaliphilic bacterium isolated from a deep South African gold mine, 1245–1256.

Taylor, J. G. (1996). Seasonal occurrence, distribution and movements of the whale shark, Rhincodon typus, at Ningaloo reef, western Australia. *Marine and Freshwater Research*, *47*(4), 637–642. doi:10.1071/MF9960637

Taylor, J. G. (2007). Ram filter-feeding and nocturnal feeding of whale sharks (Rhincodon typus) at Ningaloo Reef, Western Australia. *Fisheries Research*, *84*(1), 65–70. doi:10.1016/j.fishres.2006.11.014

Teledyne RD Instruments. (2010) ADCP Coordinate Transformation Formulas and Calculations. P/N 951-6079-00.

Tesfamichael, D., & Pitcher, T. (2007). Estimating the unreported catch of Eritrean Red Sea fisheries. *African Journal of Marine Science*, *29*(1), 55–63. doi:10.2989/AJMS.2007.29.1.5.70

Trauth, M. H. (2010). *MATLAB® Recipes for Earth Sciences* (3rd ed.). Springer-Verlag Berlin Heidelberg. doi:10.1007/978-3-642-12762-5

Triantafyllou, G., Yao, F., Petihakis, G., Tsiaras, K. P., Raitsos, D. E., & Hoteit, I. (2014). Exploring the Red Sea seasonal ecosystem functioning using a three-dimensional biophysical model. *Journal of Geophysical Research: Oceans*, *119*, 1791–1811. doi:10.1002/2013JC009641

Turner, R. E., Qureshi, N., Rabalais, N. N., Dortch, Q., Justic, D., Shaw, R. ., & Cope, J. (1998). Fluctuating silicate : nitrate ratios and coastal plankton food webs. *Proceedings of the National Academy of Sciences of the United States of America*, *95*(22), 13048–13051.

van der Merwe, R., Röthig, T., Voolstra, C. R., Ochsenkühn, M. A., Lattemann, S., & Amy, G. L. (2014). High salinity tolerance of the Red Sea coral Fungia granulosa under desalination concentrate discharge conditions: an in situ photophysiology experiment. *Frontiers in Marine Science*, *1*(November), 1–8. doi:10.3389/fmars.2014.00058

Van Trappen, S., Tan, T. L., Yang, J., Mergaert, J., & Swings, J. (2004). Alteromonas stellipolaris sp. nov., a novel, budding, prosthecate bacterium from Antarctic seas, and emended description of the genus Alteromonas. *International Journal of Systematic and Evolutionary Microbiology*, *54*(4), 1157–1163. doi:10.1099/ijs.0.02862-0

Vargas, C. a., Martinez, R. a., Cuevas, L. A., Pavez, M. a., Cartes, C., González, H. E., … Daneri, G. (2007). The relative importance of microbial and classical food webs in a highly productive coastal upwelling area. *Limnology and Oceanography*, *52*(4), 1495–1510. doi:10.4319/lo.2007.52.4.1495

Voolstra, C. R., Miller, D. J., Ragan, M. A., Hoffmann, A., Hoegh-Guldberg, O., Bourne, D., … Berumen, M. L. (2015). The ReFuGe 2020 Consortium--using “omics” approaches to explore the adaptability and resilience of coral holobionts to environmental change. *Frontiers in Marine Science*, *2*(68). doi:10.3389/fmars.2015.00068

Weon, H. Y., Kim, B. Y., Lee, C. M., Hong, S. B., Jeon, Y. A., Koo, B. S., & Kwon, S. W. (2009). Solitalea koreensis gen. nov., sp. nov. and the reclassification of [Flexibacter] canadensis as Solitalea canadensis comb. nov. *International Journal of Systematic and Evolutionary Microbiology*, *59*(8), 1969–1975. doi:10.1099/ijs.0.007278-0

Wilson, S. G., Pauly, T., & Meekan, M. G. (2002). Distribution of zooplankton inferred from hydroacoustic backscatter data in coastal waters off Ningaloo Reef, Western Australia. *Marine and Freshwater Research*, *53*(6), 1005–1015. doi:10.1071/MF01229

Wilson, S. G., Polovina, J. J., Stewart, B. S., & Meekan, M. G. (2006). Movements of whale sharks (Rhincodon typus) tagged at Ningaloo Reef, Western Australia. *Marine Biology*, *148*(5), 1157–1166. doi:10.1007/s00227-005-0153-8

Wilson, S. G., Taylor, J. G., & Pearce, A. F. (2001). The seasonal aggregation of whale sharks at Ningaloo Reef,Western Australia: currents, migrations and the El

Nino/ Southern Oscillation. *Environmental Biology of Fishes*, *61*(1), 1–11.

Winters, H., Isquith, I. R., & Bakish, R. (1979). Influence of desalination effluents on marine ecosystems. *Desalination*, *30*, 403–410.

Yao, F., Hoteit, I., Pratt, L. J., Bower, A. S., Kohl, A., Gopalakrishnan, G., & Rivas, D. (2014). Seasonal overturning circulation in the Red Sea: 2. Winter circulation. *Journal of Geophysical Research : Oceans*, *119*, 2263–2289. doi:10.1002/2013JC009004.Key

Yao, F., Hoteit , I., Pratt, L. J., Bower, A. S., Zhai, P., Kohl, A., & Gopalakrishnan, G. (2014). Seasonal overturning circulation in the Red Sea: 1. Model validation and summer circulation. *Journal of Geophysical Research : Oceans*, *119*, 2238–2262. doi:10.1002/2013JC009331.Key

Zhai, P. (2011). *The response of the Red Sea to a strong wind jet near the Tokar Gap in summer*.

Zhai, P., & Bower, A. (2013). The response of the Red Sea to a strong wind jet near the Tokar Gap in summer. *Journal of Geophysical Research: Oceans*, *118*(November 2012), 422–434. doi:10.1029/2012JC008444

Zhan, P. (2013). *Sea Surface Height Variability and Eddy Statistical Properties in the Red Sea*.

Zhan, P., Subramanian, A. C., Yao, F., & Hoteit, I. (2014). Eddies in the Red Sea: A statistical and dynamical study. *Journal of Geophysical Research : Oceans*, *119*, 3909–3925. doi:10.1002/2013JC009563.Received

Zubkov, M. V, Fuchs, B. M., Tarran, G. A., Burkill, P. H., & Amann, R. (2003). High Rate of Uptake of Organic Nitrogen Compounds by Prochlorococcus Cyanobacteria as a Key to Their Dominance in Oligotrophic Oceanic Waters High Rate of Uptake of Organic Nitrogen Compounds by Prochlorococcus Cyanobacteria as a Key to Their Dominance in. doi:10.1128/AEM.69.2.1299